(NASA-CR-150641) TWO-DIMENSIONAL COMPUTER CODE FOR DESIGN ASSESSMENT OF SRM AFT CLOSURE ENVIRONMENT Final Report (Lockheed Missiles and Space Co.) 82 p HC A05/MF A01 CSCL 21B G3/20

N78-24276

Unclas 16740

NASA CONTRACTOR REPORT

NASA CR-150641

TWO-DIMENSIONAL COMPUTER CODE FOR DESIGN ASSESSMENT OF SRM AFT CLOSURE ENVIRONMENT

By J. A. Freeman
Lockheed Missiles & Space Company, Inc.
Huntsville Research & Engineering Center
4800 Bradford Drive
Huntsville, Alabama 35807

March 1978

Final Report

Prepared for

NASA - GEORGE C. MARSHALL SPACE FLIGHT CENTER
Marshall Space Flight Center, Alabama 35812

TECHNICAL REPORT STANDARD TITLE PAGE

1. REPORT NO.	2. GOVERNMENT ACCESSION NO.	3. RECIPIENT'S CATALOG NO.
NASA CR-150641		

4. TITLE AND SUBTITLE	5. REPORT DATE
Two-Dimensional Computer Code for Design Assessment of SRM Aft Closure Environment	March 1978
	6. PERFORMING ORGANIZATION CODE
7. AUTHOR(S)	8. PERFORMING ORGANIZATION REPORT #
J. A. Freeman	LMSC-HREC TM D568246
9. PERFORMING ORGANIZATION NAME AND ADDRESS	10. WORK UNIT NO.
Lockheed Missiles & Space Company, Inc. 4800 Bradford Drive Huntsville, Alabama 35807	11. CONTRACT OR GRANT NO. Purch Order H30540B
	13. TYPE OF REPORT & PERIOD COVERED Contractor Report Final
12. SPONSORING AGENCY NAME AND ADDRESS National Aeronautics and Space Administration Washington, D. C. 20546	14. SPONSORING AGENCY CODE

15. SUPPLEMENTARY NOTES

This work was done under the technical monitorship of Mr. H. R. Blevins, George C. Marshall Space Flight Center, Alabama.

16. ABSTRACT

This document was prepared by personnel of the Lockheed-Huntsville Research & Engineering Center, Huntsville, Alabama, for NASA-Marshall Space Flight Center, and is the final report for Purchase Order H30540B. The report presents the results of a Space Shuttle Solid Rocket Motor Aft Closure Gasdynamic Environment Analysis. This final report, the associated card decks, computer code listings, and informal orientation sessions satisfy the delivery requirements of the purchase order. The NASA technical monitor for this effort is H. R. Blevins, Solid Motor Branch, Structures and Propulsion Laboratory.

17. KEY WORDS	18. DISTRIBUTION STATEMENT
	Unclassified-Unlimited A. A. McCool Director, Structures & Propulsion Lab.

19. SECURITY CLASSIF. (of this report)	20. SECURITY CLASSIF. (of this page)	21. NO. OF PAGES	22. PRICE
Unclassified	Unclassified	81	NTIS

CONTENTS

Chapter 1. INTRODUCTION

Solid rocket motor performance and internal flow characteristics of preliminary and final design configurations can be assessed using the appropriate analytical design tools. Of particular interest to the Space Shuttle program is the prediction of the gasdynamic environment in the SRM aft closure and adjacent to the submerged SRM nozzle. To provide the capability to accomplish this objective, Lockheed-Huntsville has developed and delivered to NASA-MSFC a two-dimensional computer code which will enable the calculation of the aforementioned gasdynamic environment for the special axisymmetric flow case. The code contains optional capability for either fully three-dimensional or two-dimensional axisymmetric analyses.

To demonstrate two-dimensional axisymmetric gasdynamic analysis capability the aft closure region of the SRM has been analyzed. This report presents a brief discussion of the numerical technique, the results of an SRM aft closure gasdynamic analysis, and conclusions and recommendations concerning the analysis.

Chapter 2. SPACE SHUTTLE SOLID ROCKET MOTOR (SRM) AFT CLOSURE GASDYNAMIC ENVIRONMENT ANALYSIS

I. TWO-DIMENSIONAL UNSTEADY SRM AFT CLOSURE REGION FLOWFIELD SOLUTION TECHNIQUE

A. Introduction

The Space Shuttle SRM design configuration which includes a large propellant grain port length to diameter ratio (approximately 22) and a highly submerged nozzle presents the nozzle designer with a unique set of problems. One such problem is the calculation of the flow field in the region of the submerged nozzle. As a first step in the calculation of the low subsonic to transonic SRM aft closure flow field, Lockheed-Huntsville has adapted its unique General Interpolants Method (GIM) to the solution of this complex flowfield problem.

The GIM numerical technique employed for this solution is derived from the fully three-dimensional GIM methodology which was developed for the analysis of three-dimensional plug nozzle flow fields for the U.S. Army Missile Command (Ref. 1). An optional two-dimensional planar or axisymmetric analysis capability has been added to the code described in Ref. 1. Also a plot capability for velocity vector maps, non-dimensional pressure, temperature and Mach number contours has been added to the code consistent with the Marshall Space Flight Center (MSFC) Univac 1108 computer operating system.

The GIM numerical technique is briefly described in the following paragraphs. The solution presented is for a two-dimensional axisymmetric SRM configuration and the flow of an ideal equivalent perfect gas.

B. The General Interpolants Method

1. Introduction to the General Interpolants Method. The system of equations considered are various subsets of the Navier-Stokes equations plus an appropriate energy equation. Lagrangian coordinates or mixed Eulerian-Lagrangian frames are not considered. The equations are cast in unsteady form to pose the problem as initial valued in time. With appropriate spatial boundary values, the equations can be integrated forard in time in a parabolic/hyperbolic sense. The use of the unsteady formulation has a number of advantages: (1) the transient portion of a flow can be obtained as well as a steady state; (2) the asymptotic approach to a steady flow proceeds in much the same manner as nature; (3) subsonic, transonic and supersonic flows can be calculated with same methodology; (4) multi-dimensional flows can be handled more conveniently; (5) with a proper form of the differential equations, integration can automatically proceed through shock waves or other discontinuities without undue complication; and (6) computation of viscous flows with time-fluctuating turbulence can be performed more naturally.

The General Interpolants Method (GIM) is a new methodology for constructing numerical analogs of the partial differential equations of continuum mechanics. A general formulation is provided which permits classical finite element methods and many of the finite difference methods to be derived directly. The GIM approach is new in the sense that it can combine the best features of finite element and finite difference methods. The technique allows complex geometries to be handled in the finite element manner and operates on the integral form of the conservation laws. Solutions can be generated implicitly with the finite element analogs or by explicit finite difference analogs, which do not require a reduction of large systems of linear algebraic equations (no matrix inverse). A quasi-variational procedure is used to introduce boundary conditions into the method and to provide a natural assembly sequence for combining the element equations into the full domain equations. Attempts have been made in the literature to relate finite difference and finite element methods but have achieved limited success, and apparently no one has combined the two approaches in any way.

The domain of interest is first discretized by appropriate subdivision into an assemblage of interconnected finite elements. A mesh generation is used in the GIM approach which incorporates general curvilinear coordinates stretching transformations and bivariate blending to produce an automated mesh/element generation. Shape functions based on a set of generalized interpolants are then chosen to describe the behavior over each element. We then proceed, as in the Method of Weighted Residuals, by multiplying the discretized equations by a set of weight functions and integrating over the volume of the element. A quasi-variational procedure is then used to construct the assembled system of equations from the element equations, and to introduce boundary conditions into the method. By choosing the weight functions equal to the shape functions, we reproduce via Galerkin. the classical finite element nodal analogs. It is at this point that we introduce one of the important concepts of GIM: orthogonal weight/shape functions. By appropriately choosing the weight functions to be orthogonal to the shape functions, we can obtain explicit nodal analogs. Further, by choice of arbitrary constants in the orthogonal weight functions, we can reproduce known finite difference nodal analogs, such as centered difference, upwind/downwind differences and the two-step MacCormack algorithm. As a result of this spatial discretization, we have reduced the partial differential equations to ordinary differential equations where techniques such as Euler, Runge-Kutta or predictor-corrector can be used to advance the solution profiles in time.

The following points summarize GIM and its advantages over previous approaches:

- GIM is a higher order procedure for constructing computational analogs of the conservation laws of continuum mechanics.
- GIM is a total calculational procedure in that arbitrary geometries, expandable equation sets, different nodal analogs, general curvilinear coordinate systems and multi-constraint boundary values are handled.
- Non-orthogonal sets of weight/shape functions give rise to analogs which have generally been classified as finite element methods.
- Orthogonal sets of weight/shape functions give rise to explicit finite difference nodal analogs.

- A single analysis can be generated which selectively employs either of several finite element approaches or either or several finite difference techniques according to the wishes of the analyst.
- Finite element discussions in the literature have mentioned quasi-variational methods, but none have consistently applied these ideas to boundary conditions as we have in GIM.
- The classical finite element analogs, derived via Galerkin, are unconditionally unstable for solution of the strong conservation form of the Euler equations for shock capturing. Several authors have presented formulations entitled Finite Element with automatic shock capturing, but no solutions are reported. We have found by numerical experiment, that the nodal analogs they derive are unstable. The only solutions presented make use of the theory of "weak solutions," which destroys the strong conservation form of the equations.
- The GIM approach allows the flexibility and generality of finite element techniques to be effectively married with proven successful finite difference techniques to produce a superior higher order methodology.

2. The Structure of the GIM Code. The following paragraphs briefly describe the theory and structure of the GIM code.

1) Summary. The GIM code is divided into four modules: (1) mesh generation or geometry; (2) nodal analog or matrix assembly; (3) unsteady integration; and (4) data display. The mesh generation module accepts boundary geometry data, curve or line formula flags, and number of cuts in each coordinate direction. A set of general curvilinear coordinate maps is then used to subdivide each region into finite elements. Each region which is input is processed and then blended together. The output is a set of coordinates for each element along with the element coefficient matrices. The nodal analog assembly module takes the mesh data from a stored external file and performs, via quasi-variational procedure, the assembly of the element equations into the full domain equations. At this point, the dynamic storage allocation is set up so that the unsteady integration module can integrate with virtually unlimited problem size.

The unsteady integration module performs the actual computation of the flow by employing the boundary conditions selected by the user. The

nodal analog at this point is arbitrary and any one of a number of schemes can be selected depending on the problem being analyzed. The solution is marched forward in time for a specified number of steps or until a steady state is reached. The data display module reads the solution profiles from external storage (drum, tape) and prints, plots and maps the flow parameters. Figure 1 is a block diagram illustrating the modular construction of the GIM code.

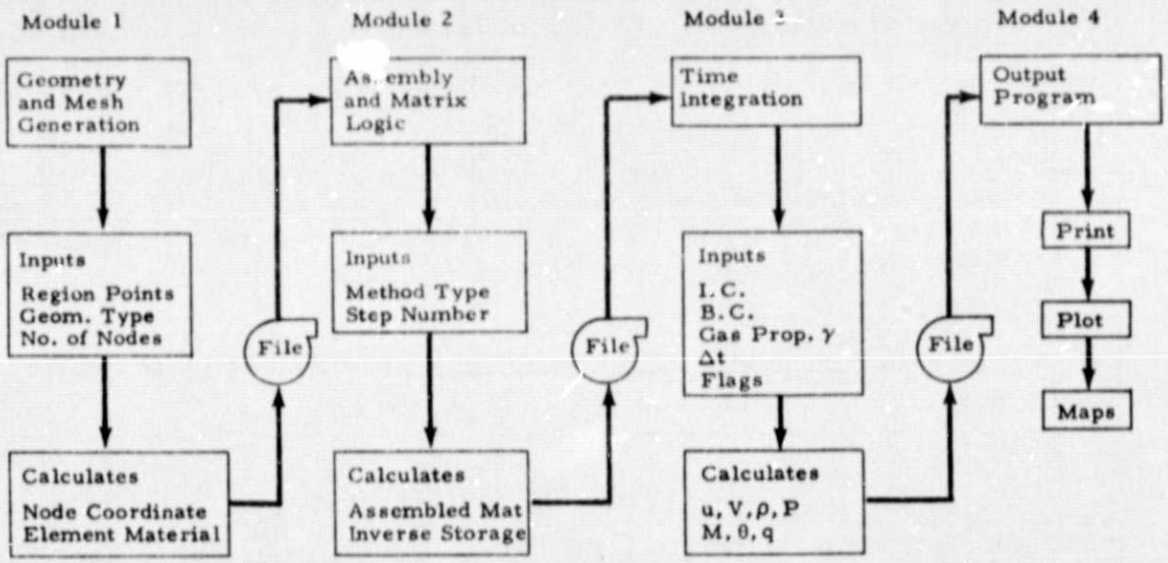

Fig. 1 - GIM Computer Code Structure

The current version of GIM can compute two- or three-dimensional flows of an ideal gas in arbitrary geometric domains. The unsteady integration module is coded such that additional capability can be readily adapted such as different equation sets (two-phase flow, non-equilibrium chemistry), other boundary values, virtually unlimited nodal points and time marching schemes.

2) Geometry Module. The domain of interest is considered to be geometrically arbitrary in that any shape is represented as a bivariate blend of regular subdomains. Figure 2 shows an example of a full geometric

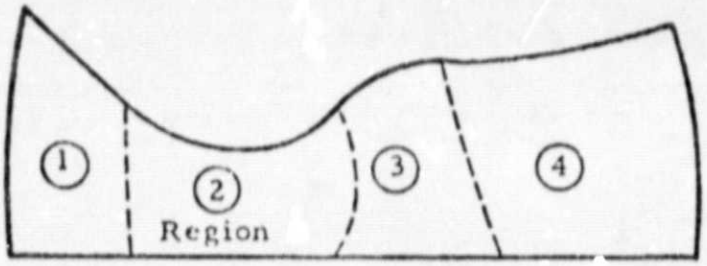

Fig. 2 - Flow Domain Example Subdivided into Regions

domain in which flow is to be computed. The domain is subdivided into four regions as shown. In general this division is made such that analytical functions describe the shape of each side but it can, of course, be made by point specification and piecewise linear sides. Attention can then be focused on each region with global coordinates (x, y) and local region coordinates (ξ, η). The regions are blended together at the junctions to provide the continuous full domain geometry.

We then proceed by considering each region separately as depicted in Fig. 3. Gordon and Hall (Ref. 2) show that the general relationship between physical space and local curvilinear coordinates is given by the transformation noted in Eq. (1).

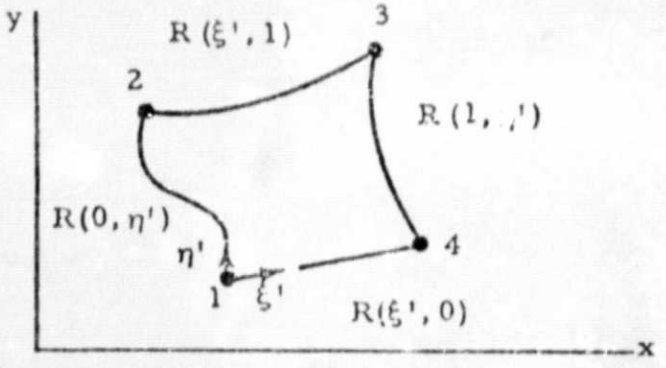

Fig. 3 - Global and Local Coordinate Systems for a Region

$$R(\xi',\eta') = (1-\xi')\,R(0,\eta') + \xi' R(1,\eta') + (1-\eta')\,R(\xi',0) + \eta' R(\xi',1)$$
$$- (1-\xi')(1-\eta')\,R_1 - (1-\xi')\,\eta' R_2 - \xi'\,R_3 - \xi'(1-\eta')\,R_4 \qquad (1)$$

Where

$$R(\xi',\eta') = \begin{Bmatrix} x(\xi',\eta') \\ y(\xi',\eta') \end{Bmatrix}$$

is a two-component vector function and ξ', η' range from 0 to 1 along the contour of the region. A similar equation is used in three-dimensional space. The quantities R_1, R_2, R_3 and R_4 are the x, y coordinates of the corners of the region and $R(0,\eta')$, $R(1,\eta')$, $R(\xi',0)$, $R(\xi',1)$, are geometric functions which describe the shape of the sides of the region (Fig. 3). To describe the geometry of a region thus requires input of four (x, y) coordinate pairs and four sets of functions to describe the sides. The GIM code contains a library of common analytical functions and input flags are used to retrieve them.

After determining the coordinates and geometries functions, we can then transform to (ξ',η') space and develop the equations in local coordinates. The next step is to subdivide each region into an assemblage of interconnected elements as depicted in Fig. 4. This is accomplished by simply

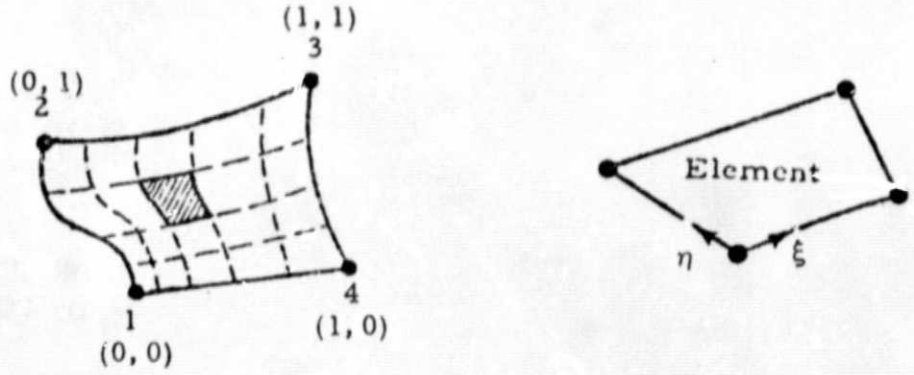

Fig. 4 - Element Breakdown for a Region

specifying the number of node points in each direction. Each element is developed in its own local coordinates (ξ, η) in the same manner as the full domain was transformed into regions. All types of stretching transformations are possible with Eq. (1) so that irregular grid patterns can be used to enhance resolution. The elements are considered isoparametric in that the same functions will be used to approximate the flow variables and the element geometry. For example, if linear interpolants are used for velocity, pressure, etc., then a typical element shown in Fig. 4 will have linear sides.

3) Matrix Assembly Module. Module 2 of the GIM code reads the geometric mesh and element integral functions from a stored external file (drum, disk, tape). The functions of this module are to assemble the element equations into the full flow domain equations and set up the storage arrays and tape blocking in an optimum manner. The assembly is performed by invoking the so-called quasi-variational procedure (Ref. 3). This essentially combines the components of the element matrices which share a common nodal point. The results of the assembly are sets of coefficient matrices which act as "derivative takers" for the differential equations. Setting up the storage of these large arrays of numbers is a primary function of this program module. A dynamic dimensioning capability is used to allow for virtually unlimited nodal points and hence, problem size capability. The coefficient matrices are stored on external files for use by module 3 of the GIM code.

4) Unsteady Integration Module. Module 3 of the GIM code performs the actual integration of the differential equations. The "derivative taker" matrices from module 2 provide the type of finite difference/finite element scheme such that the integration module can be considered a general purpose equation solver. Boundary conditions are treated in this module via input flags specified by the user. The output is a tape containing the flow field at user specified time increments. This tape can then be printed, plotted or contour maps obtained.

Module 3 solves differential equations of the form:

$$\frac{\partial U}{\partial t} + \frac{\partial E}{\partial x} + \frac{\partial F}{\partial y} + \frac{\partial G}{\partial z} + H = 0 \qquad (2)$$

where U is a column vector of dependent flow variables and E, F, G and H are functions (nonlinear in general) of the vector U. This form is termed Strong Conservation Law equations and has definite advantages in terms of numerical conservation and in computing through shock waves or other steep gradients. The length of each column vector is a variable such that expanded equation sets of a variety of flow fields can be used. Examples are multi-dimensional flows, multi-species reacting flows, single phase or multi-phase flows and laminar or turbulent viscous flows. The subprograms that define the specific equations to be used can be modified or flagged by the user.

The GIM numerical analog of Eq. (2) has the form:

$$[A_{MN}] (\dot{U}_N + H_N) + [B_{MN}]E_N + [C_{MN}]F_N + [D_{MN}]G_N = 0 \qquad (3)$$

where the matrices $[A_{MN}]$, etc., are obtained from the output tape of module 2. It is these coefficients which determine the finite difference scheme to be used. Schemes which have been tried to date include Galerkin, MacCormack and Hopscotch algorithms. The MacCormack finite difference scheme has yielded the best results for the solution of the SRM aft closure transonic flowfield.

Boundary conditions for specified nodal points in the mesh are treated via the quasi-variational technique (Ref. 3). A set of input flags are used to define a point as either:

- Known or fixed inflow/outflow
- Symmetry condition
- Stagnation point
- Corner flow condition
- Wall tangency (slip)
- Downstream (one-side difference)

- Interior point, and
- Others as specified or modified by the user.

The calculation can start at time = 0 with initial conditions as input or it can be restarted from the output solution of previous iterations. The solution proceeds for a specified number of time integration steps or can be run until a steady state is produced.

II. SRM AFT CLOSURE GEOMETRY, PROBLEM BOUNDARY CONDITIONS, AND INITIAL CONDITIONS

A. SRM Aft Closure Geometry

The SRM aft closure/nozzle region configuration which was analyzed is shown in Fig. 5. This solution is for the axisymmetric case and the nozzle is in the null gimbal angle position. The propellant grain burning surface forms one of the problem boundaries. In this case the propellant surface has burned back to the position it would occupy after 20 sec of motor burn time. This analysis is intended to simulate the aft closure gasdynamic environment of the SRM DM-1 firing (28 September 1977) after 20 sec of motor burn. Both the t = 0 and t = 20 sec propellant surfaces are indicated in Fig. 5.

The problem upstream boundary is a plane normal to the motor longitudinal centerline residing at the end of the aft segment cylindrical port of the propellant grain after 20 sec of motor burn. The downstream boundary is a plane normal to the motor longitudinal centerline downstream of the throat which assures supersonic flow for the initiation of a forward marching supersonic analysis if this were desired. A pictorial view of the SRM aft closure and nozzle configuration is shown in Fig. 6.

The fixed grid construction for the solution of the flow field is shown in Figs. 7 and 8. Figure 7 presents the entire 1728 node mesh. Figure 8 is an exploded view of the 528 nodes that comprise the boot, fixed housing, and aft dome region. Selected mesh points are indicated in these two figures

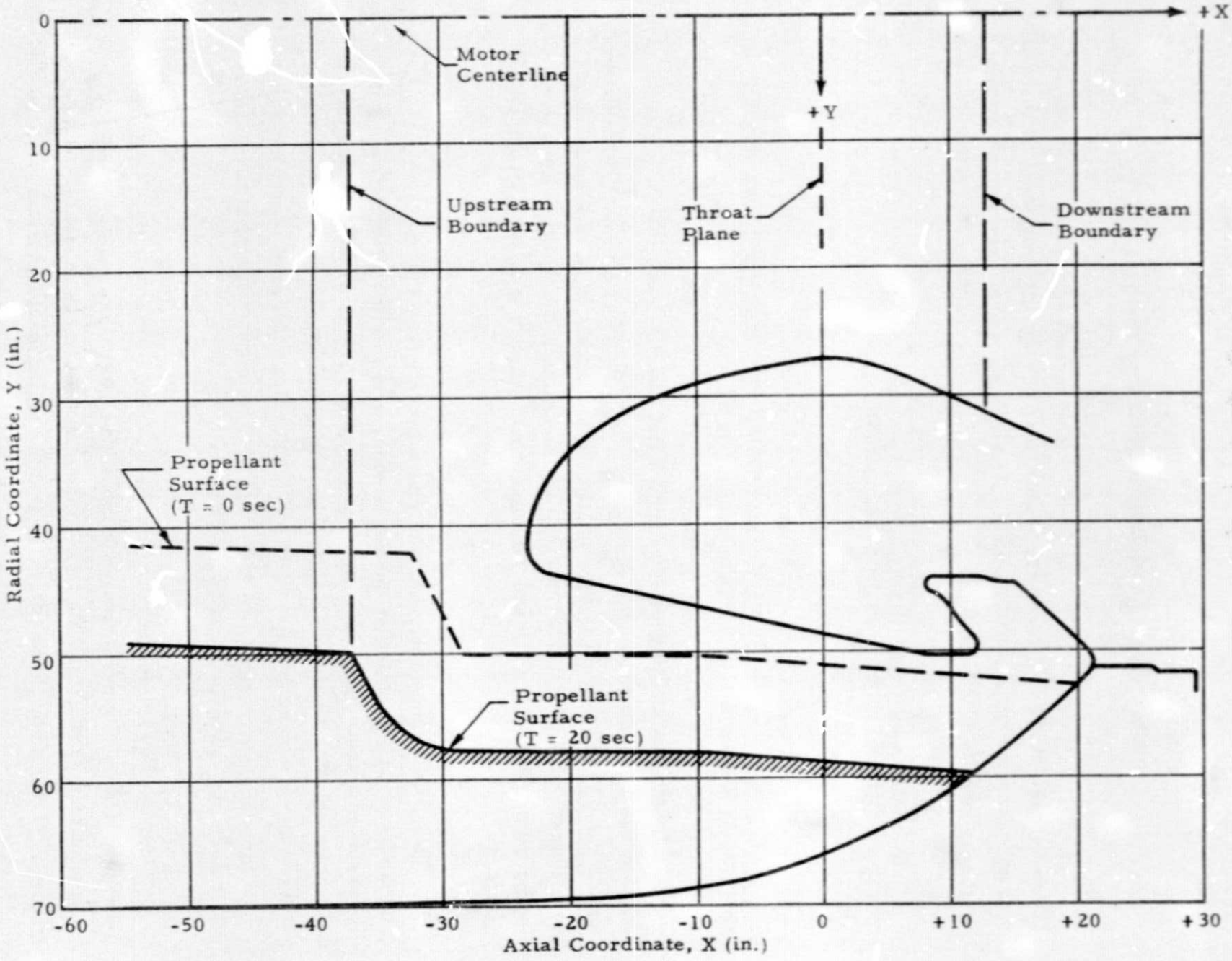

Fig. 5 - SRM Aft Closure Gasdynamic Analysis Geometry

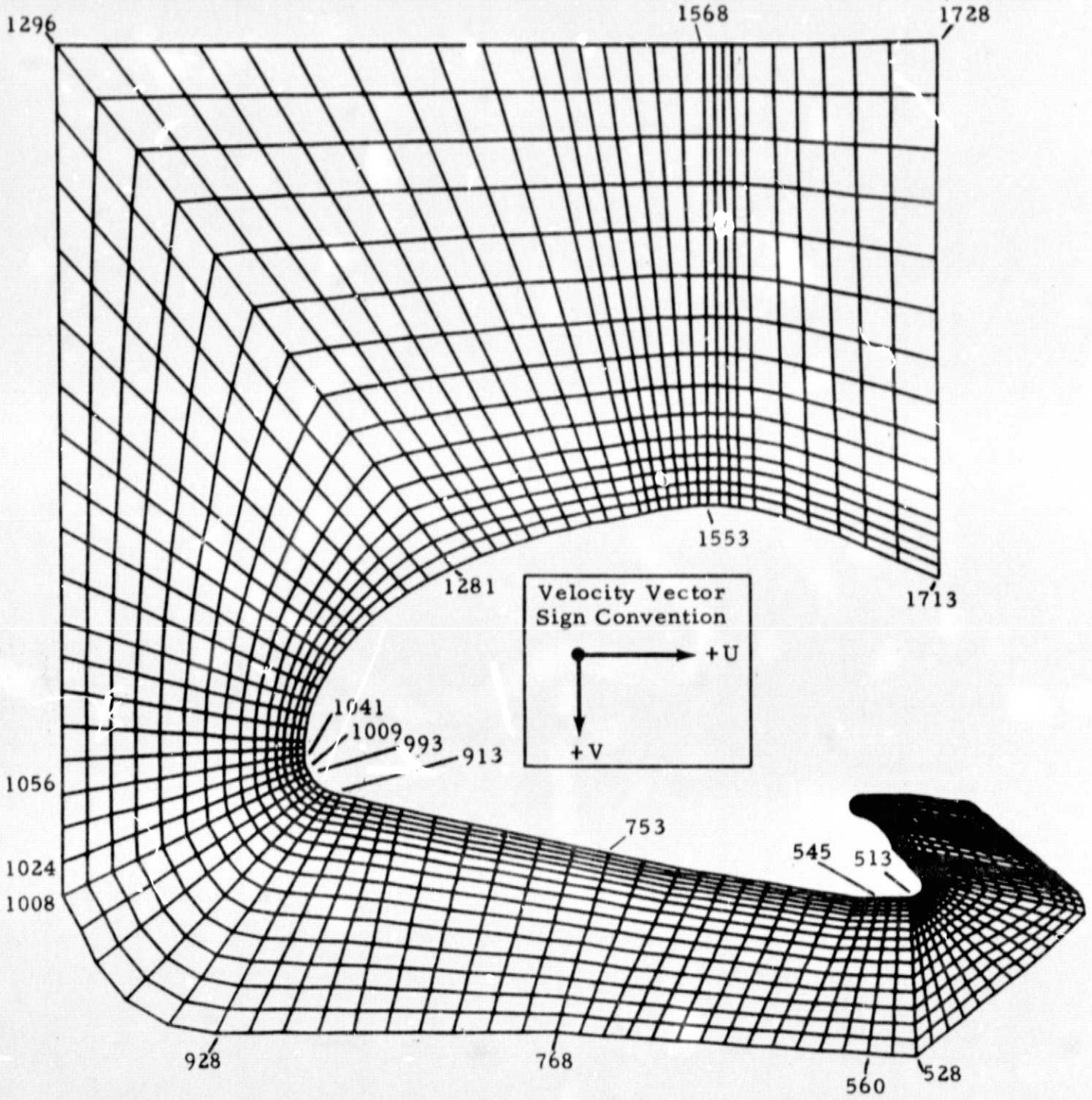

Fig. 7 - SRM Aft Closure Gasdynamic Analysis, Mesh Construction

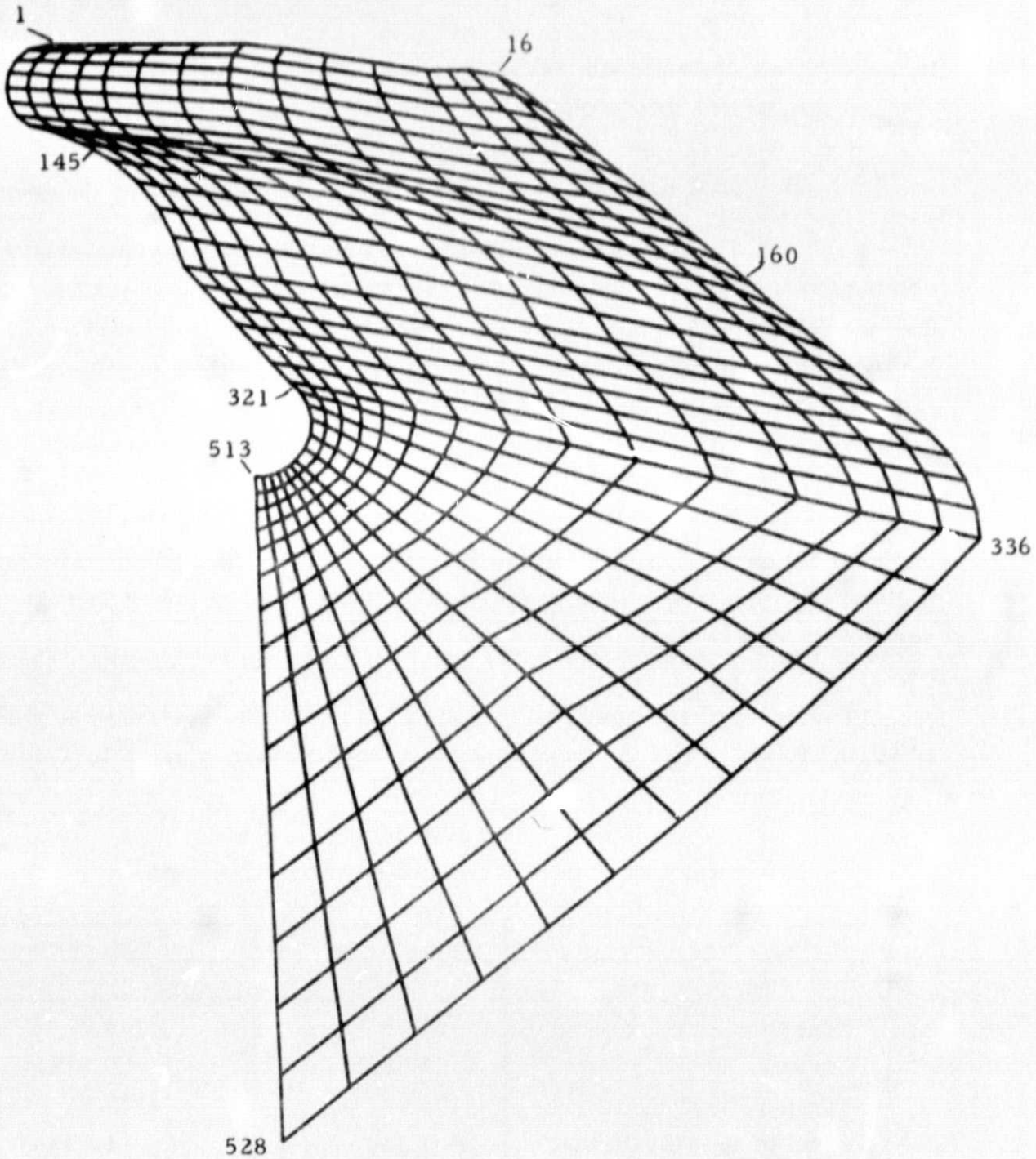

Fig. 8 - SRM Aft Closure Gasdynamic Analysis, Mesh Construction (Boot/Fixed Housing/Aft Dome Region)

to demonstrate the node numbering system. The velocity vector sign convention adopted for this problem is also noted in Fig. 7.

B. SRM Aft Closure Gasdynamic Analysis Boundary Conditions

The gas property boundary conditions for this analysis were obtained from a one-dimensional internal ballistics post-test analysis of the DM-1 SRM firing (Ref. 4). These data were provided by NASA-MSFC. From the NASA-MSFC internal ballistics analysis the gas stagnation pressure, density, temperature, and gas velocity at the end of the cylindrical port (which is the upstream boundary for this analysis) were determined. A head end chamber pressure trace from the DM-1 static firing is shown in Fig. 9. This analysis provides a solution for the gasdynamic environment in the aft closure region of the SRM for the DM-1 configuration at the 20 sec time slice. The solution is unsteady in nature so that numerous iterations are required to relax the solution to steady state.

The one-dimensional gas velocity at the problem upstream boundary is 607.63 ft/sec. The upstream boundary conditions are given in Table 1.

Table 1

SRM AFT CLOSURE GASDYNAMIC ANALYSIS,
UPSTREAM BOUNDARY CONDITIONS

Gas Property	Stagnation Value	Static Value
Pressure, psi	798.35	784.37
Density, lbm/ft^3	0.353591	0.34814
Temperature, R	6150.6	6137.5
Ratio of Specific Heats, γ	1.138	1.138
Gas Constant, ft^2/sec^2-R	1700.75	1700.75
Velocity, ft/sec	0.0	607.63
Mach number	0.0	0.1763
Flow Rate, lbm/sec	11,484.46	

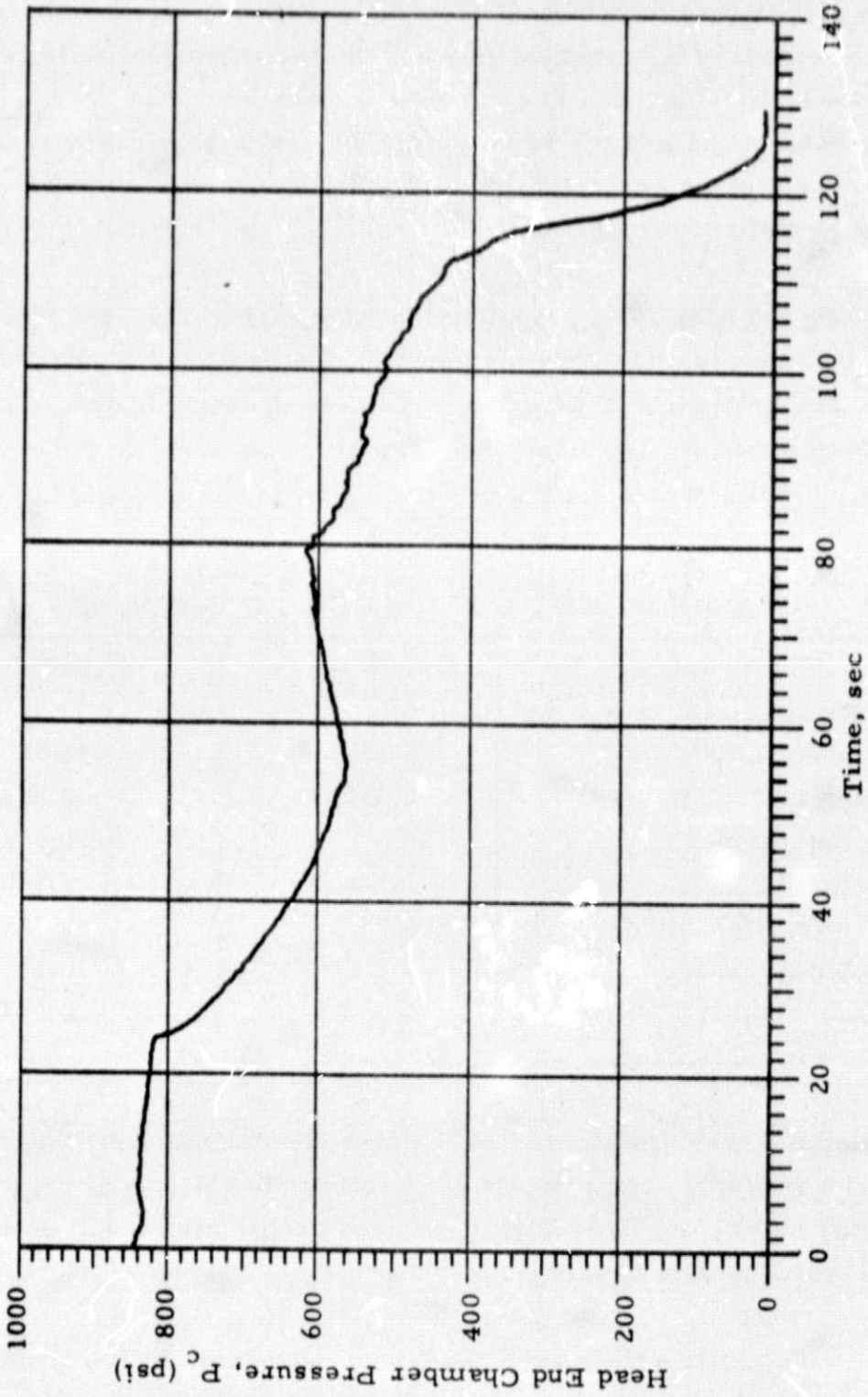

Fig. 9 - SRM DM-1 Static Firing Measured Head End Chamber Pressure vs Time

The gas properties noted in Table 1 are identical at each node along the upstream boundary, i.e., nodes 1024 to 1296 in increments of 16 (see Fig. 7). The gas velocity along this line of nodes is parallel to the X axis. Also the gas is a perfect gas and the ratio of specific heats (gamma) is representative of the gamma for an equivalent perfect gas for a gas and particle mixture for the SRM propellant composition.

Along the remaining propellant burning surface boundary (nodes 528 to 1008 in increments of 16) the gas velocity is normal to the burning surface and has a magnitude of 10.14 ft/sec. The gas property boundary conditions along the propellant burning surface boundary are listed in Table 2. Along

Table 2

SRM AFT CLOSURE GASDYNAMIC ANALYSIS, PROPELLANT BURNING SURFACE BOUNDARY CONDITIONS

Gas Property	Stagnation Value	Static Value
Pressure, psi	798.35	798.34
Density, lbm/ft^3	0.353591	0.353589
Temperature, R	6150.6	6150.6
Ratio of Specific Heats, γ	1.138	1.138
Gas Constant, ft^2/sec^2-R	1700.75	1700.75
Velocity, ft/sec	0.0	10.14
Mach number	0.0	0.00294
Flow Rate, lbm/sec	459.49	

the remaining problem boundaries the flow is required to be tangent to the wall and a free slip condition was imposed on the velocity at the wall. These conditions will be modified slightly and the modifications will be discussed in the results section of this chapter.

C. SRM Aft Closure Gasdynamic Analysis Initial Conditions

To facilitate the solution of this problem due to the complex geometry involved, a procedure was devised to solve the problem in regions.

The solution technique then is to relax the least complicated flow region to steady state then restart the next region using the results for the preceeding regional solution as input and so on until the entire problem has reached a steady state solution. The division of the mesh into regions for the SRM aft closure problem is shown in Fig. 10. Region 1 extends from nodes 1009 to 1728, region 2 from nodes 561 to 1008, and region 3 from nodes 1 to 560. The solution technique is to solve region 1 hold this region fixed then solve region 2, and then solve region 3 holding regions 1 and 2 fixed.

The initial conditions for the solution of SRM aft closure flow field are shown in Figs. 11, 12 and 13. These figures are the Mach number, non-dimensional pressure, and non-dimensional temperature contours for the zero or initial iteration of the solution. For the top half of the problem, i.e., nodes 1009 to 1728, region 1 has been subdivided into two subregions. For nodes 1009 to 1296 the velocity is set to 607.63 ft/sec and is tangent to the mesh flowing in the positive X direction. The remainder of the gas property initial conditions in this subregion are as noted in Table 1. In the second subregion of region 1 (Nodes 1297 to 1728) the gas Mach number is linearly distributed between 0.1763 and 1.5 based on the node axial position relative to the throat plane. The remaining gas properties in this subregion are calculated using a one-dimensional isentropic expansion consistent with the Mach number determination just described.

In regions 2 and 3 the gas Mach number is set to 0.00294, the gas velocity is tangent to the mesh flowing in the positive X direction, and the remaining gas properties are as shown in Table 2.

III. SRM AFT CLOSURE GASDYNAMIC ANALYSIS RESULTS

A. Introduction

This section of the report presents the results of SRM Aft Closure Gasdynamic Analysis. The flowfield solution is presented in two parts: The solution excluding the boot region, and the complete solution

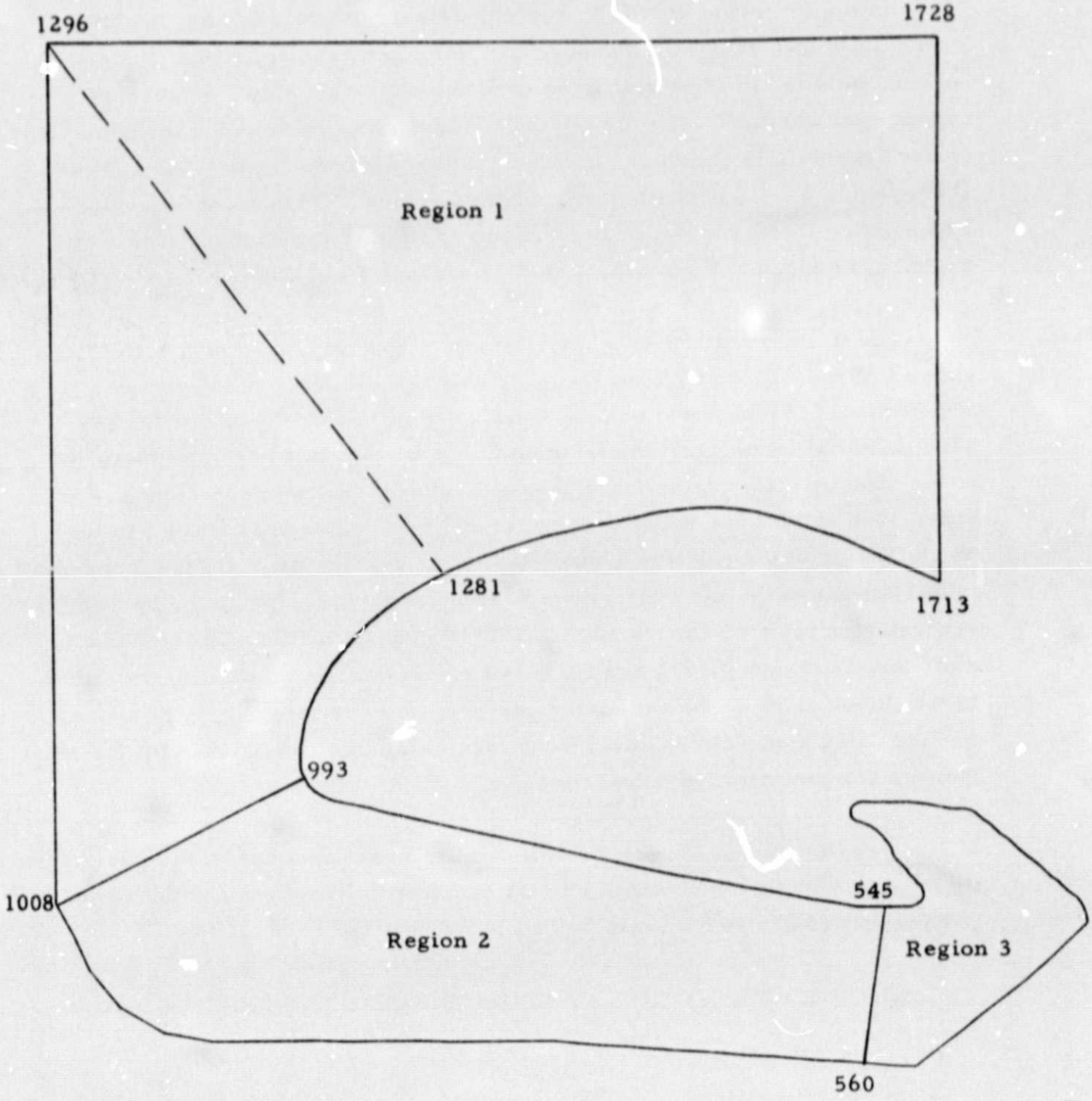

Fig. 10 - SI M Aft Closure Gasdynamic Analysis, Division of Mesh Into Regions

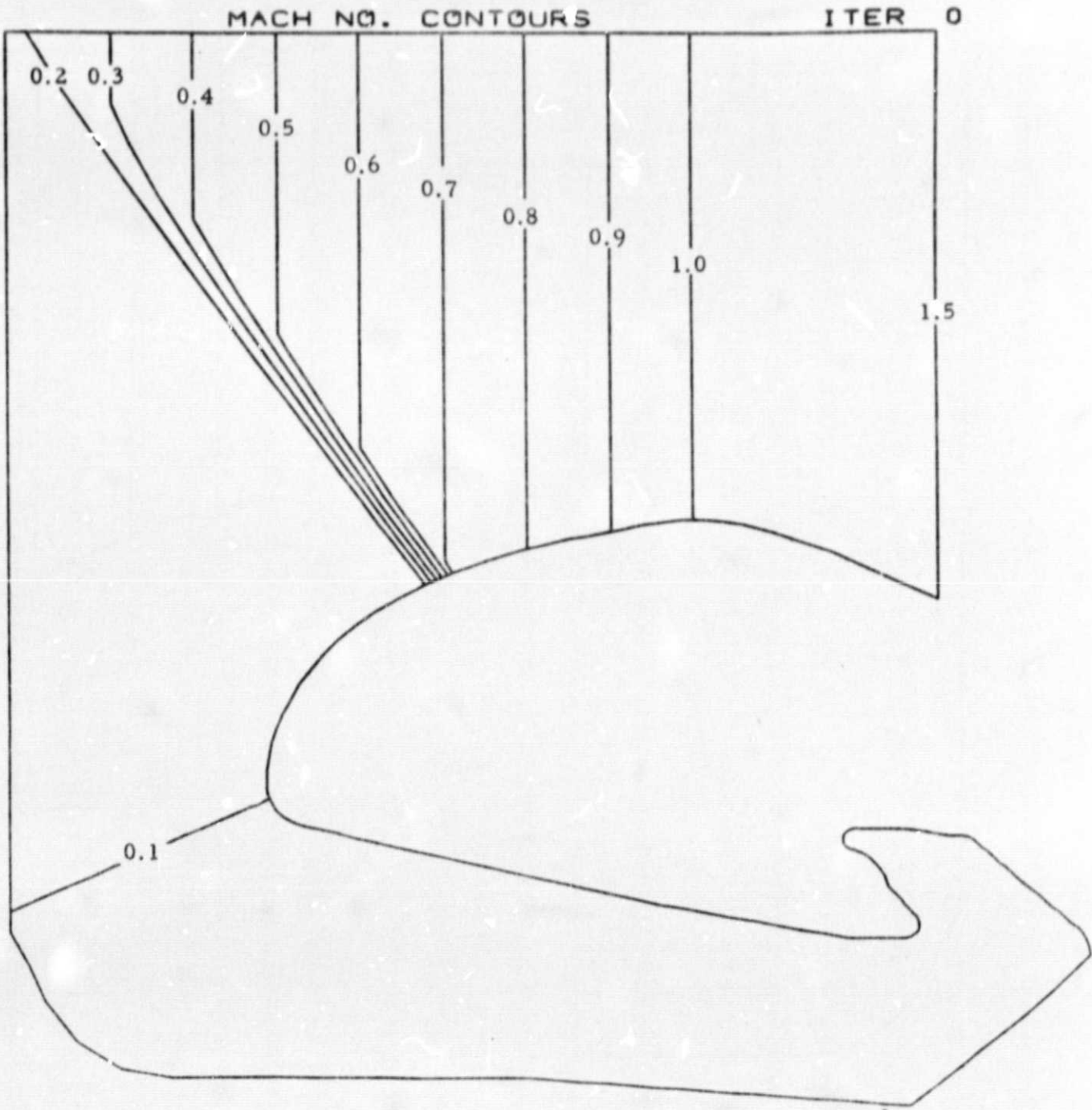

Fig. 11 - SRM Aft Closure Gasdynamic Analysis Initial Conditions, Mach Number Contours

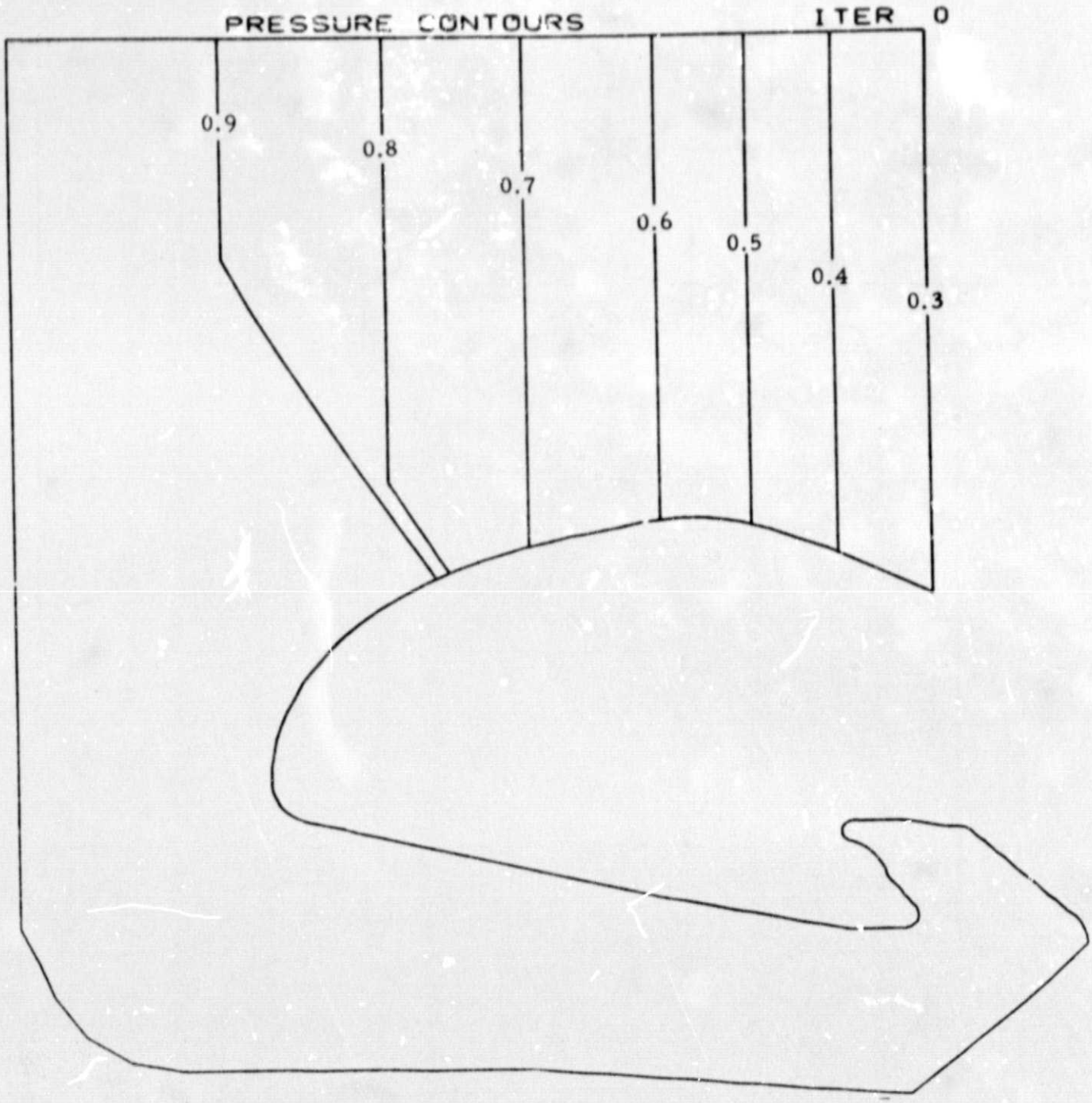

Fig. 12 - SRM Aft Closure Gasdynamic Analysis Initial Conditions, Non-Dimensional Pressure Contours, P/P_o

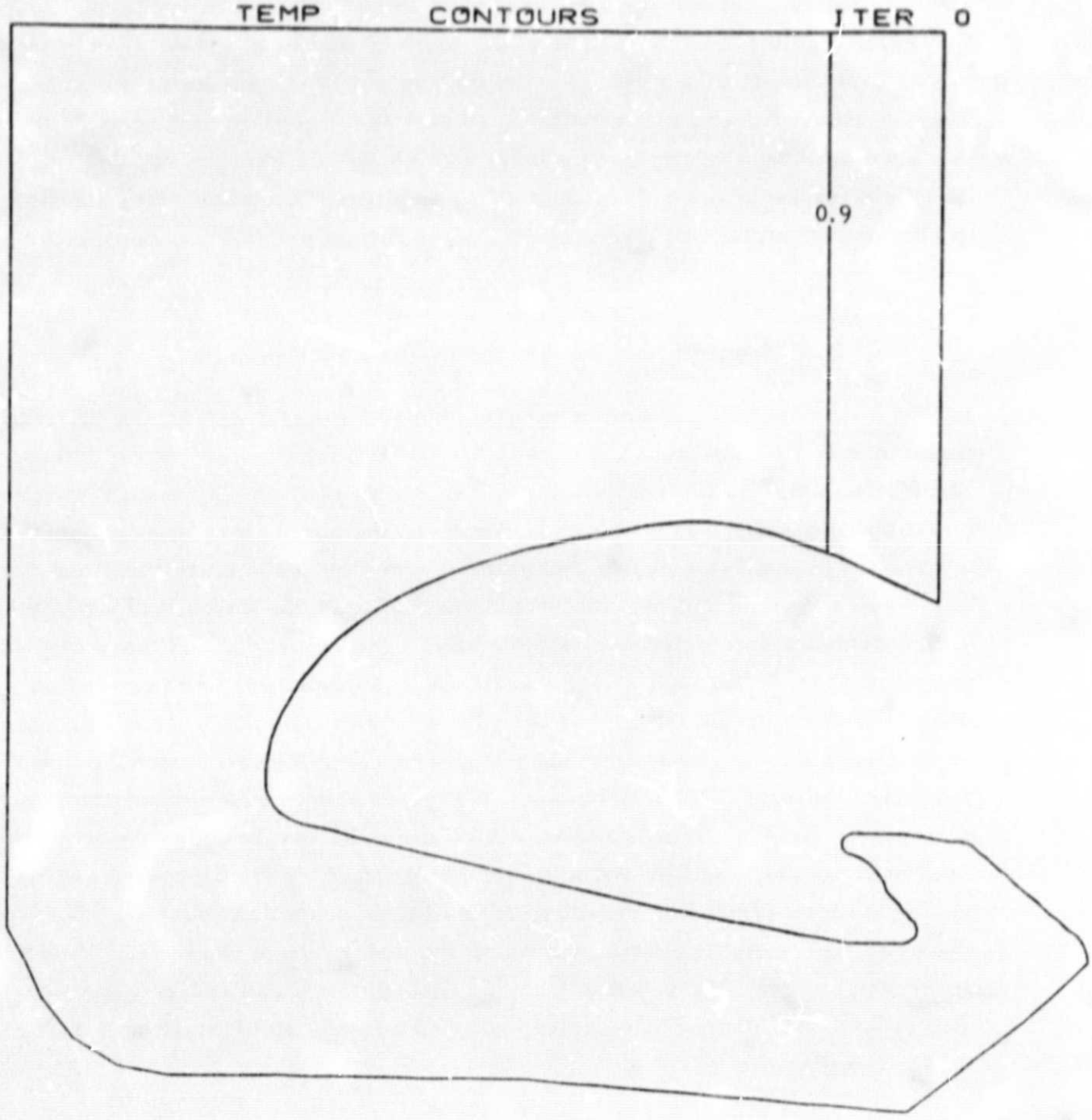

Fig. 13 - SRM Aft Closure Gasdynamic Analysis Initial Conditions, Non-Dimensional Temperature Contours, T/T_o

which includes the boot regior The first part of the solution is for regions 1 and 2 (see Fig. 10) and the second part of the solution is for regions 1, 2 and 3. The solution is presented in the form of flowfield velocity vector plots in which the length of the vector is indicative of the magnitude of the velocity. The direction of the velocity vector indicates the direction of flow at each mesh point. The velocity vector maps are shown for various regions of the flow field for successive iterations of the solution. A steady state solution is obtained when the velocity vectors do not change greatly for successive iterations.

B. Flowfield Solution Excluding the Boot Region

In this portion of the flow field (regions 1 and 2), an inviscid analysis was utilized and a steady state solution was obtained in 800 iterations. The solution for regions 1 and 2 is shown in Figs. 14 through 24 for iterations 0 through 800. The nose region of the nozzle was of particular interest in the analysis due to higher than predicted erosion in this area for the DM-1 static firing. To provide better resolution of the calculated flow field in this region the velocity vector plots have been enlarged, and these are presented in Figs. 25 through 35 for iterations 0 through 800. An interesting feature of the solution is the way the flow splits in the nose region with most of the flow going up and toward the throat and a small portion flowing down and under the nose. This is obvious in Figs. 25 through 29. After the flow has split at the nose, then mass starts to enter the cavity under the nose by flowing along the lower propellant surface boundary. The flow then begins to develop a recirculation region near the lower propellant surface boundary and exits the cavity by flowing out along the underside of the nose. These developments are illustrated in Figs. 30 through 35. The recirculation pattern is well established by iteration 800 and appears to be stationary for successive iterations.

The velocity vector maps presented here are intended to illustrate the trends in the development of a steady state solution for this problem. Contour plots of gas Mach number, pressure and temperature were generated as a result of the study but the velocity vectors best tell the story.

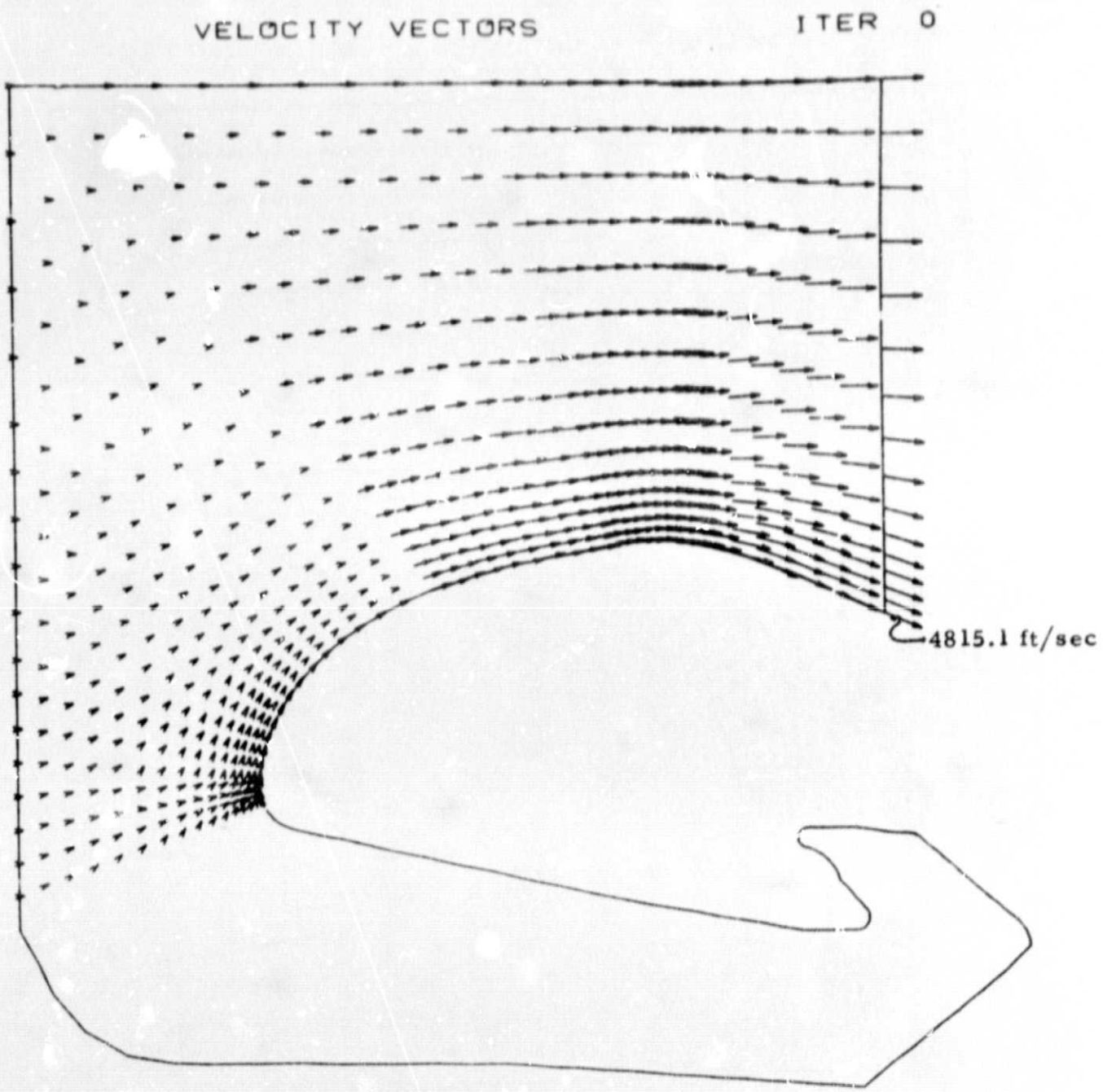

Fig. 14 - SRM Aft Closure Gasdynamic Analysis, Velocity Vector Map (Iteration 0)

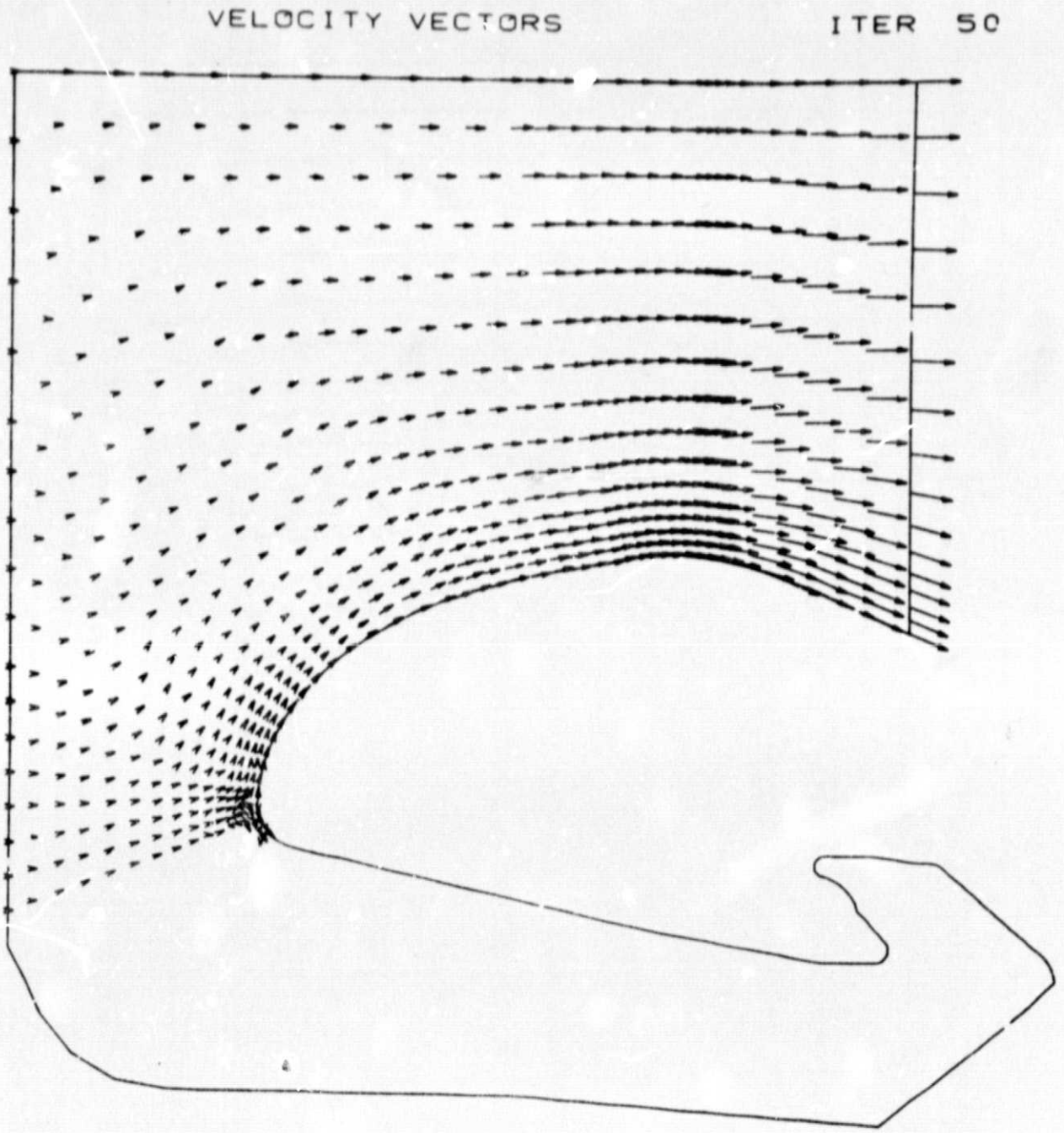

Fig. 15 - SRM Aft Closure Gasdynamic Analysis, Velocity Vector Map (Iteration 50)

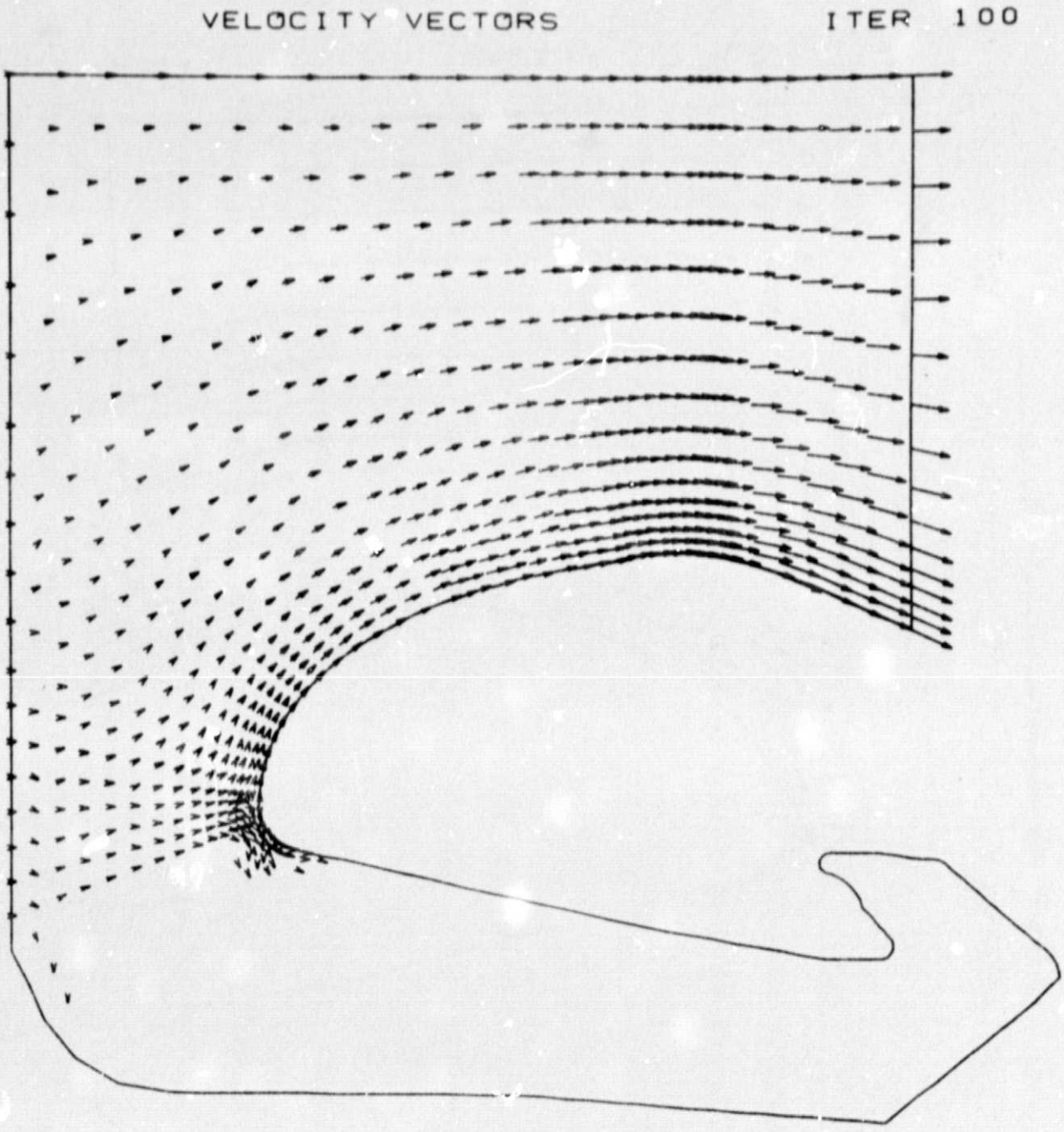

Fig. 16 - SRM Aft Closure Gasdynamic Analysis, Velocity Vector Map (Iteration 100)

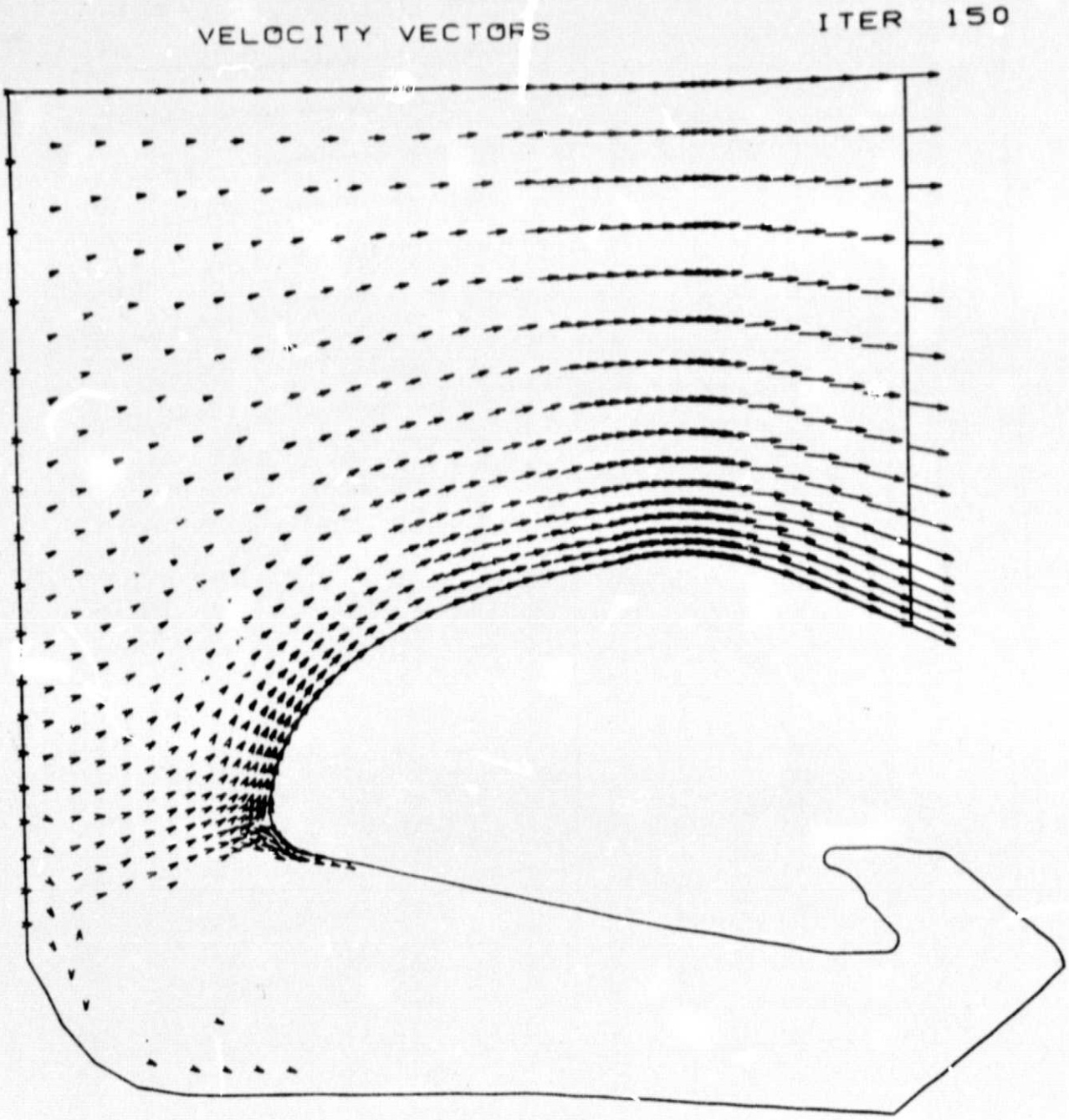

Fig. 17 - SRM Aft Closure Gasdynamic Analysis, Velocity Vector Map (Iteration 150)

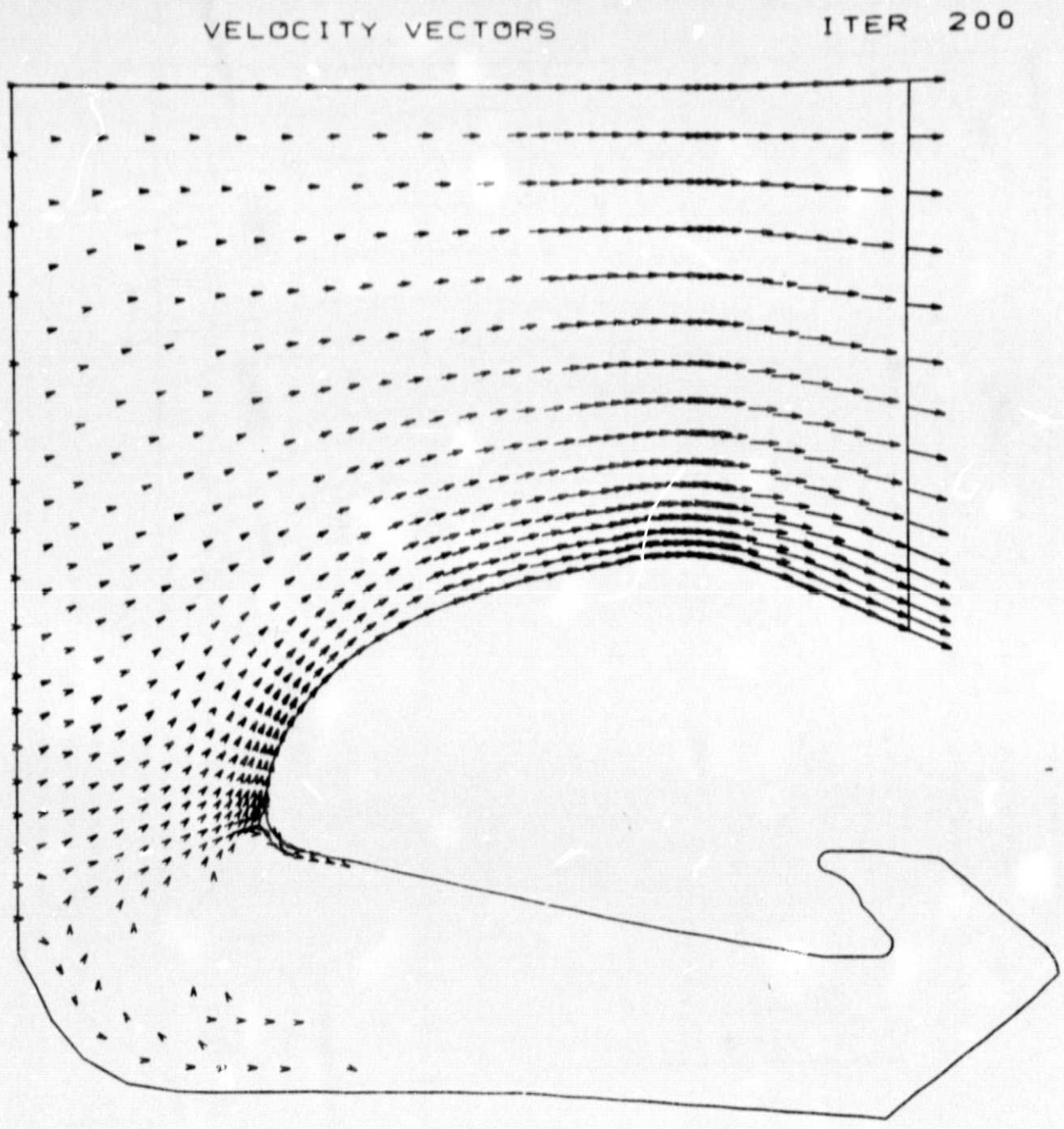

Fig. 18 - SRM Aft Closure Gasdynamic Analysis, Velocity Vector Map (Iteration 200)

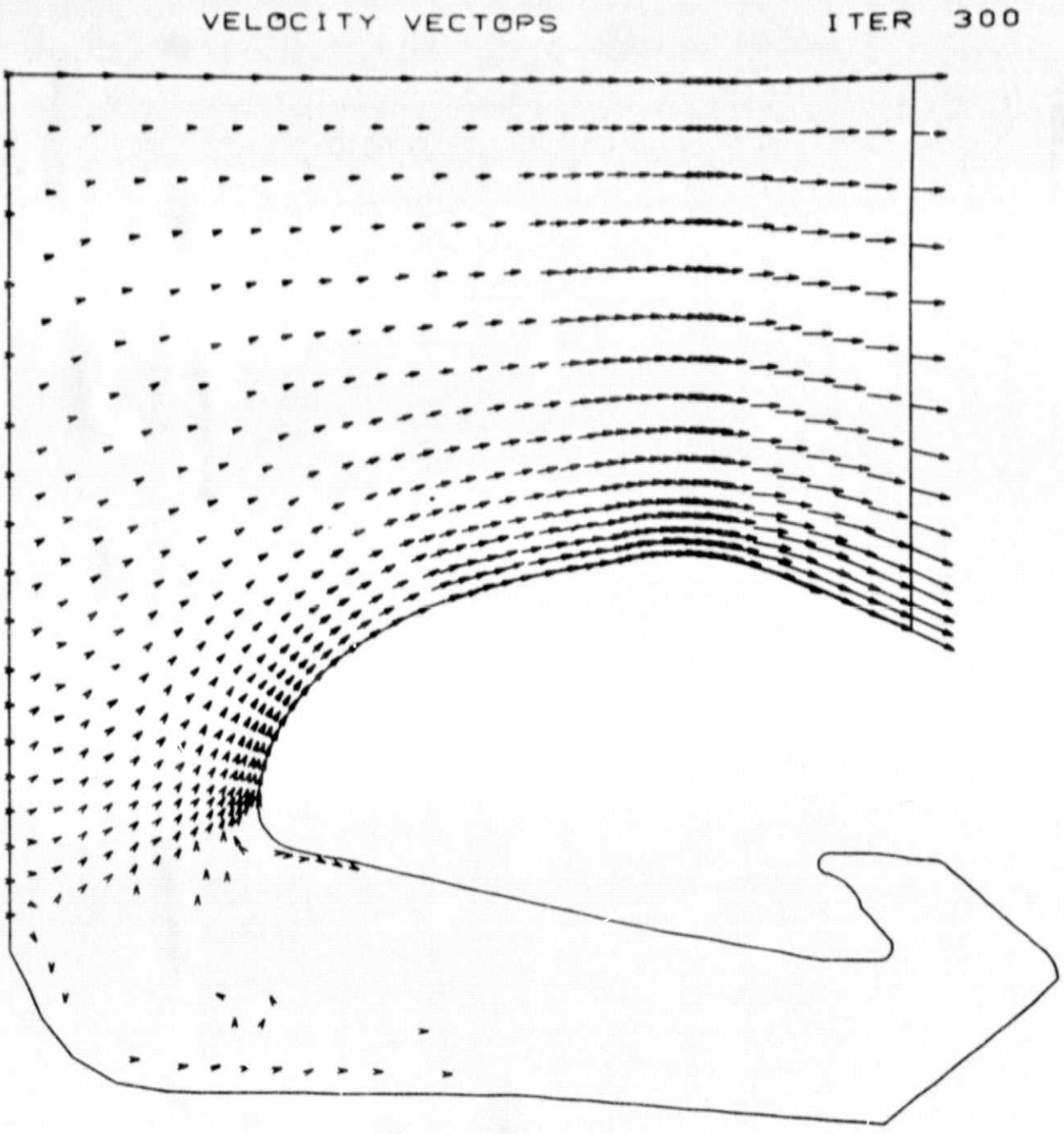

Fig. 19 - SRM Aft Closure Gasdynamic Analysis, Velocity Vector Map (Iteration 300)

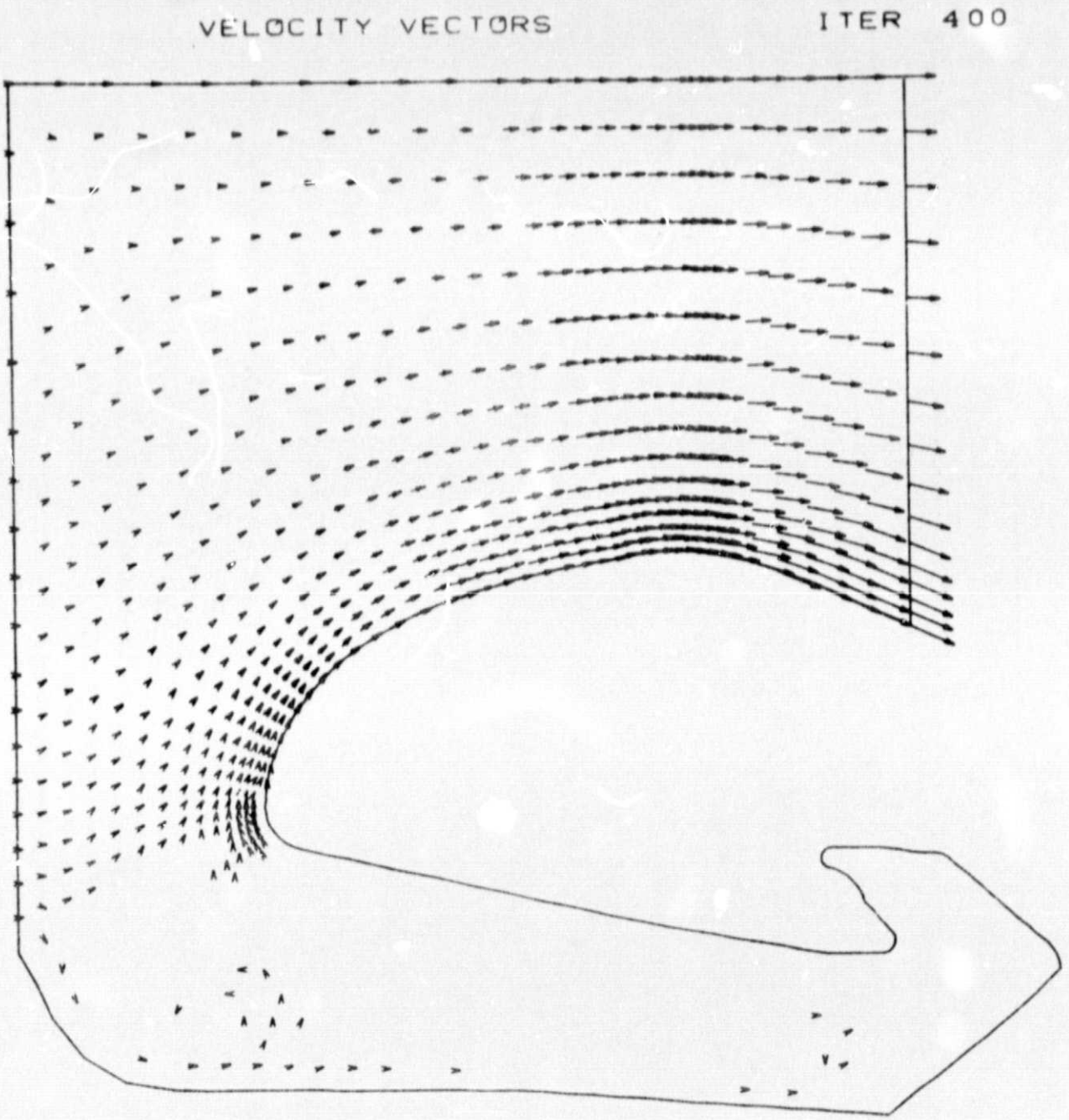

Fig. 20 - SRM Aft Closure Gasdynamic Analysis, Velocity Vector Map (Iteration 400)

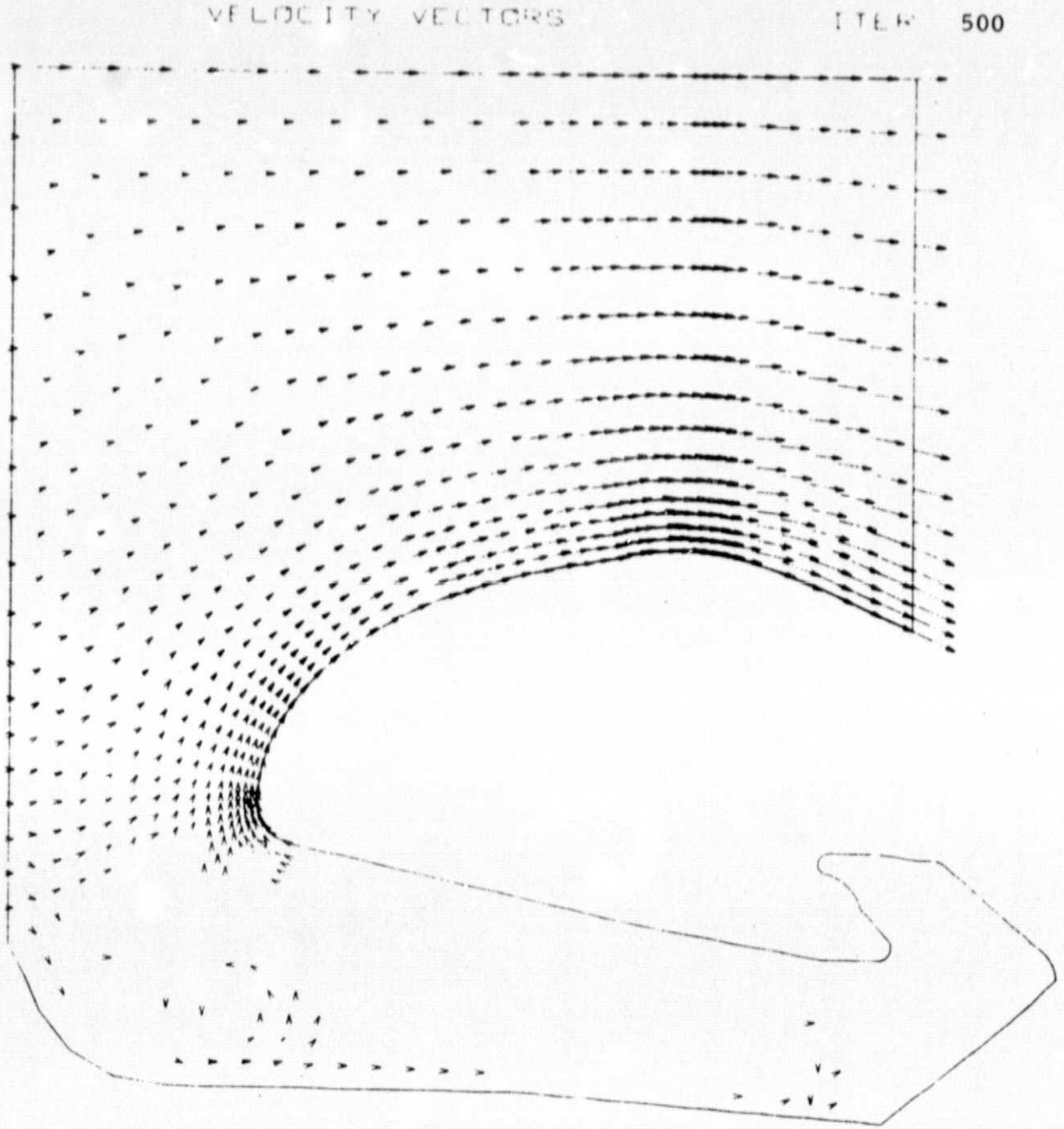

Fig. 21 - SRM Aft Closure Gasdynamic Analysis, Velocity Vector Map (Iteration 500)

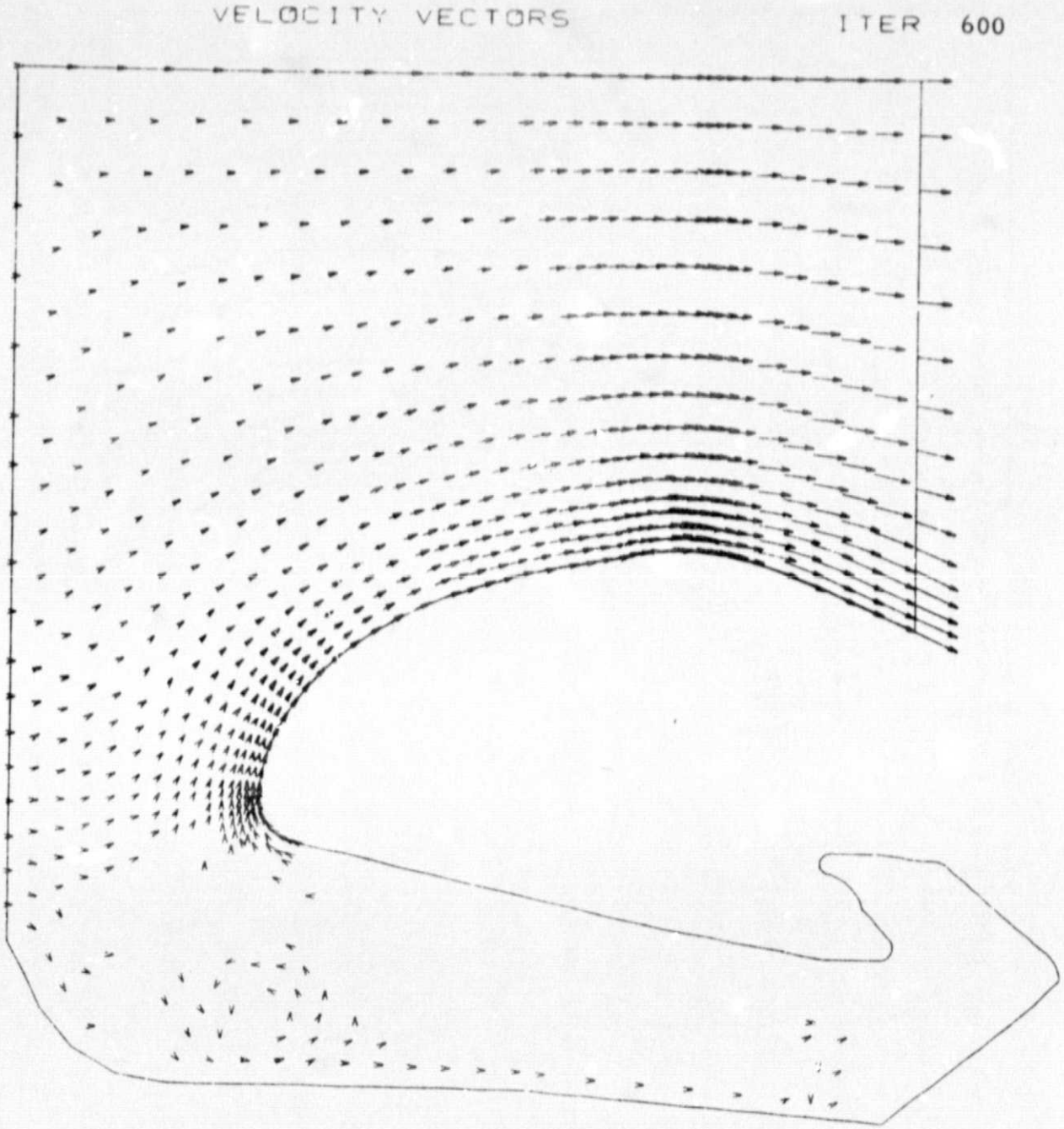

Fig. 22 - SRM Aft Closure Gasdynamic Analysis, Velocity Vector Map (Iteration 600)

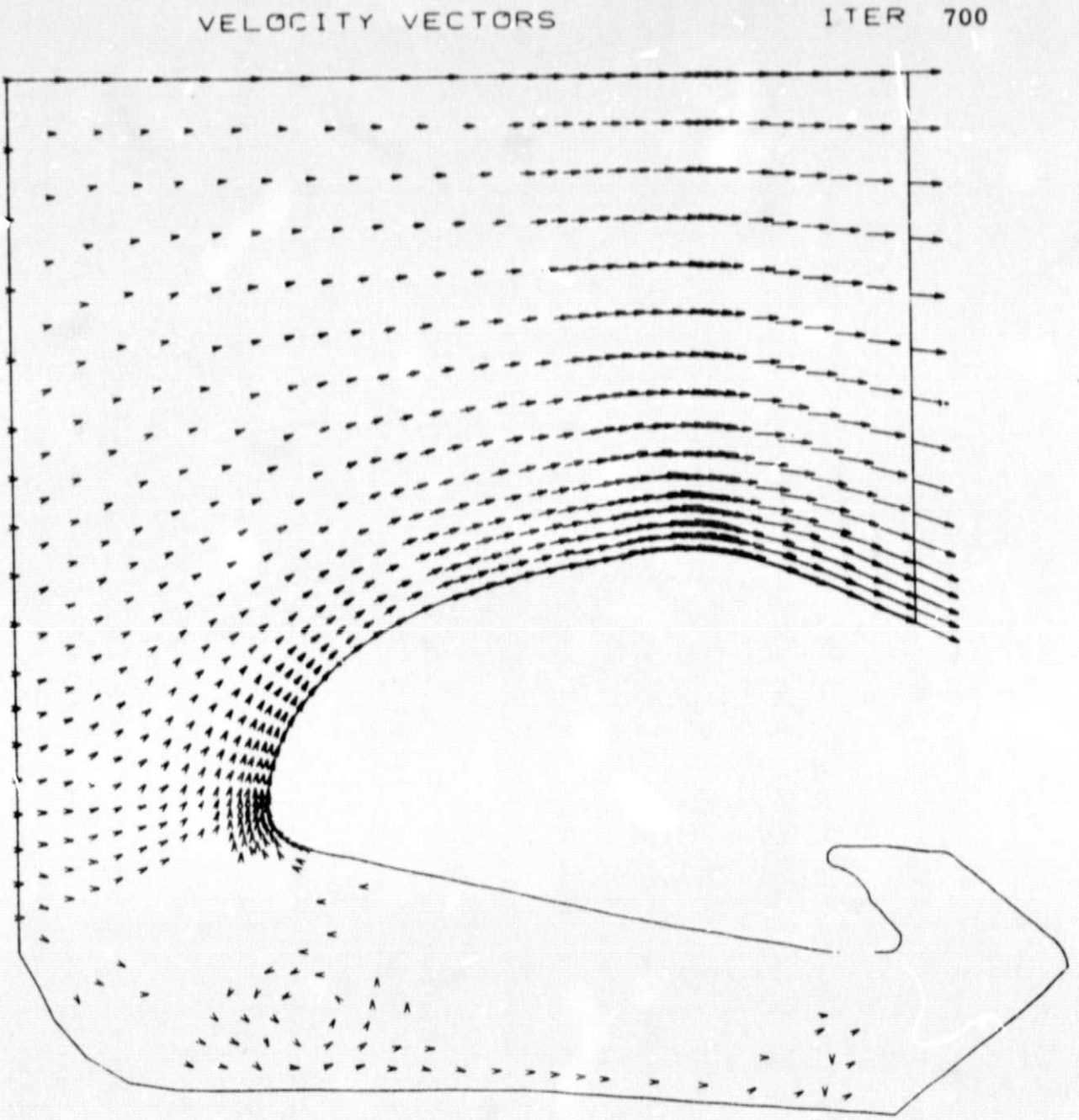

Fig. 23 - SRM Aft Closure Gasdynamic Analysis, Velocity Vector Map (Iteration 700)

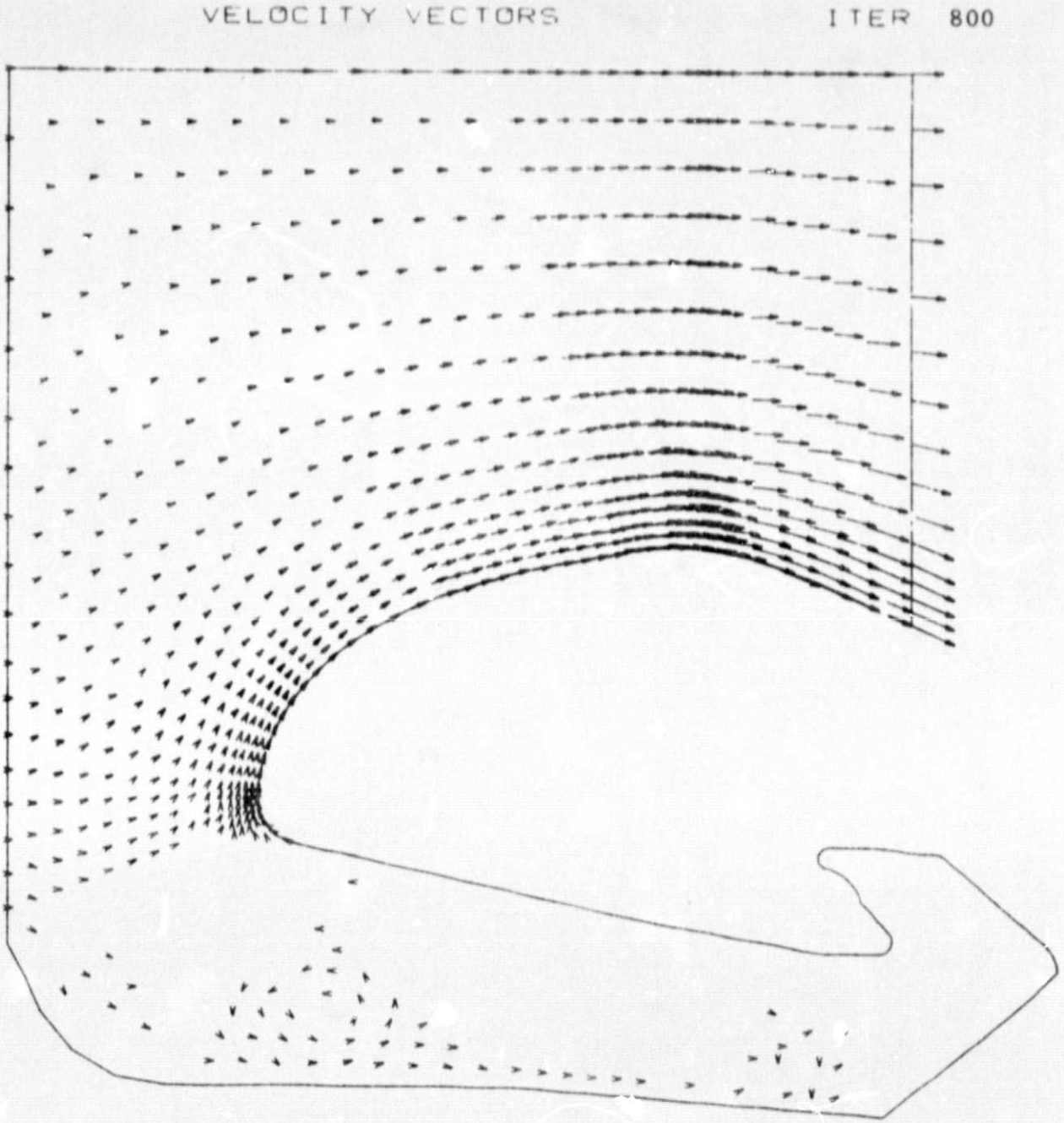

Fig. 24 - SRM Aft Closure Gasdynamic Analysis, Velocity Vector Map (Iteration 800

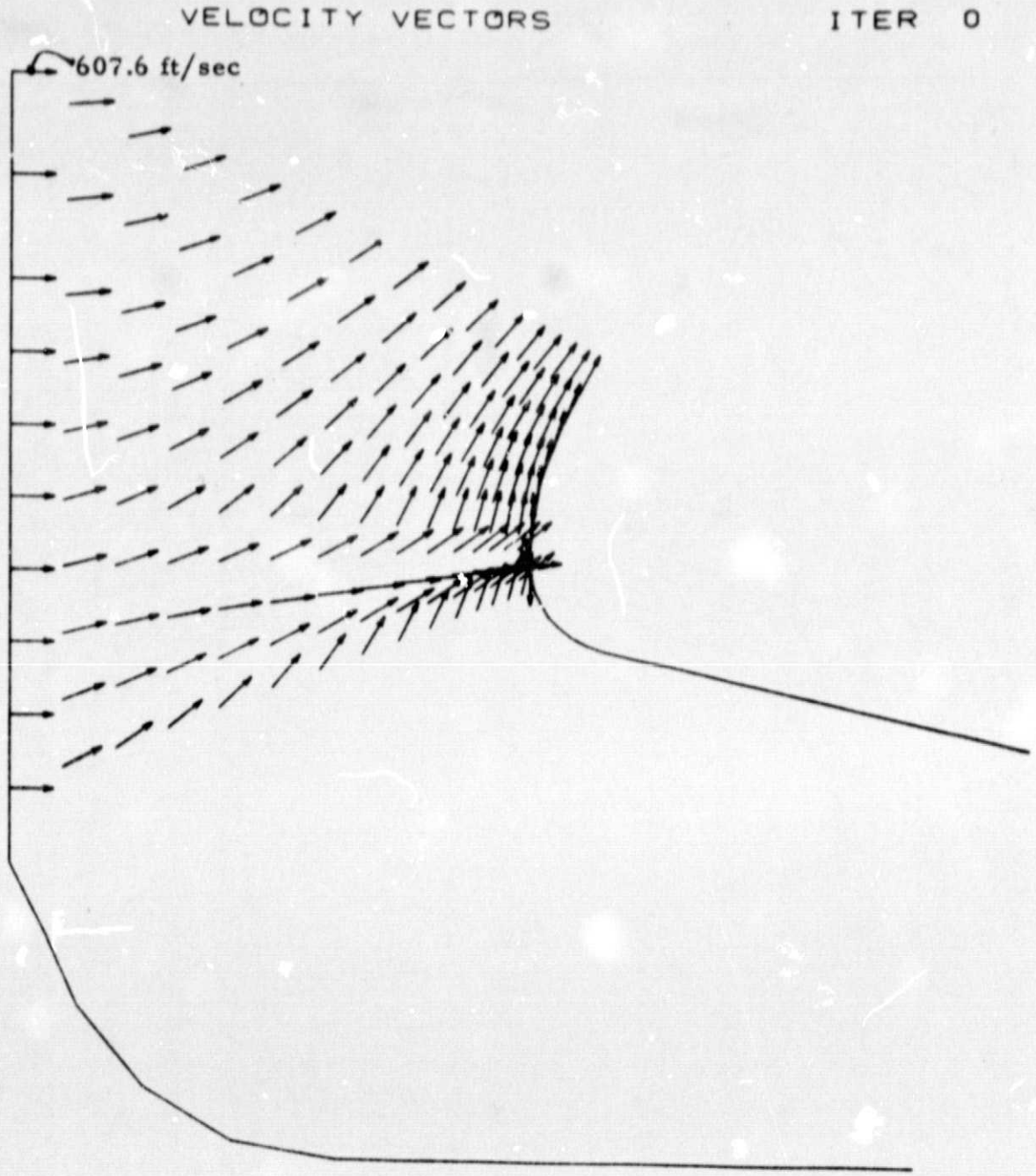

Fig. 25 - SRM Aft Closure Gasdynamic Analysis, Velocity Vector Map, Nose Region (Iteration 0)

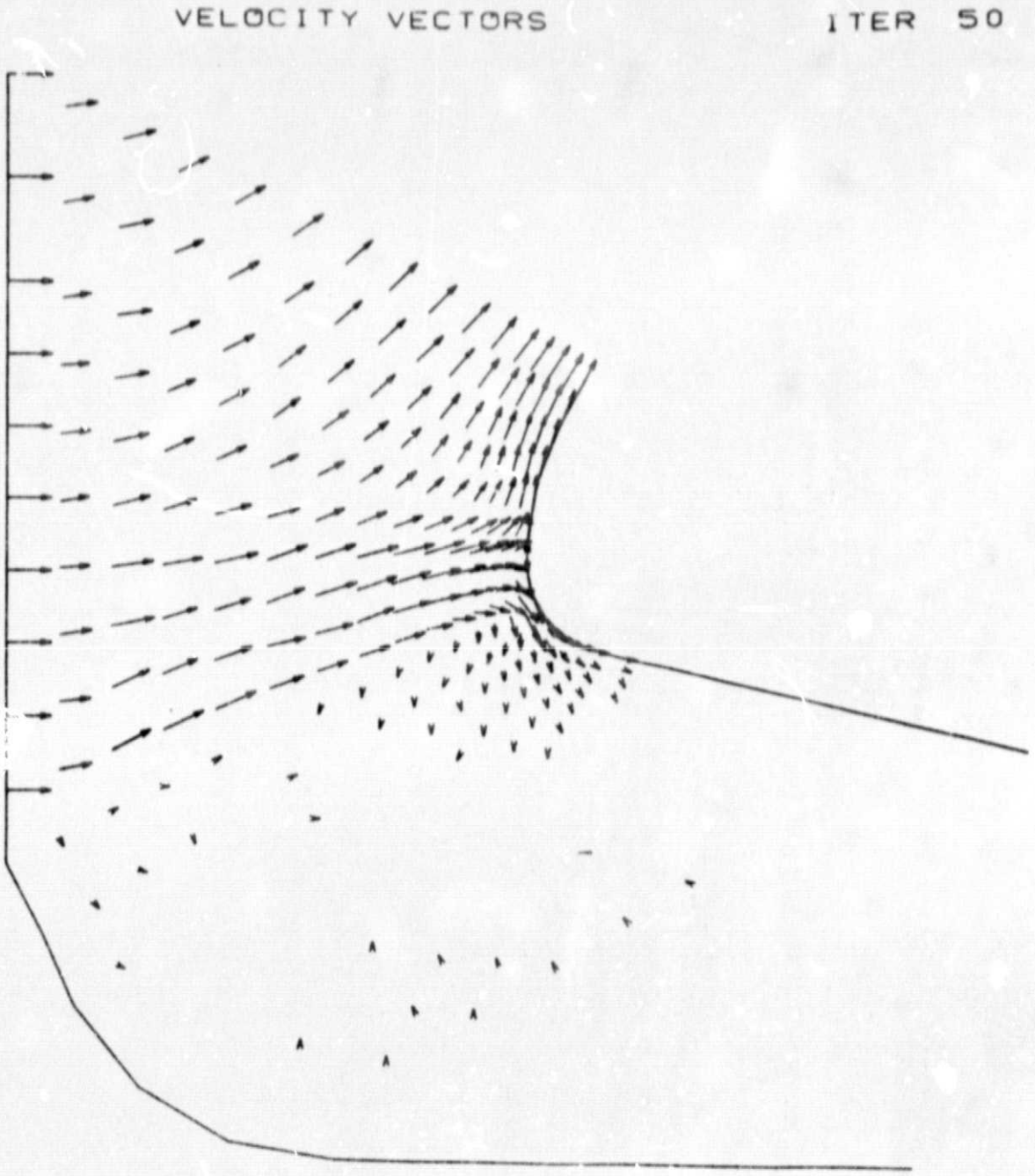

Fig. 26 - SRM Aft Closure Gasdynamic Analysis, Velocity Vector Map, Nose Region (Iteration 50)

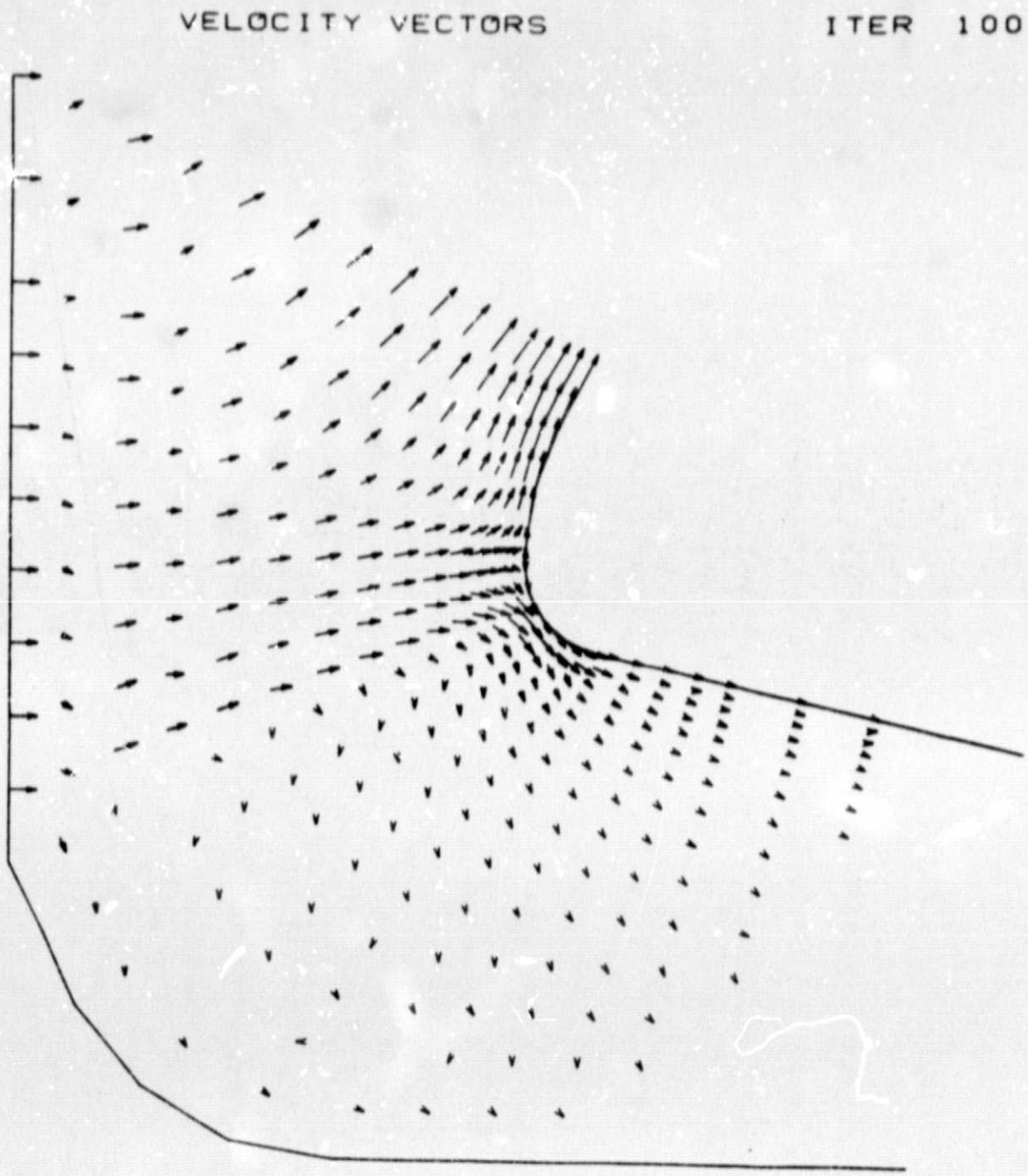

Fig. 27 - SRM Aft Closure Gasdynamic Analysis, Velocity Vector Map, Nose Region (Iteration 100)

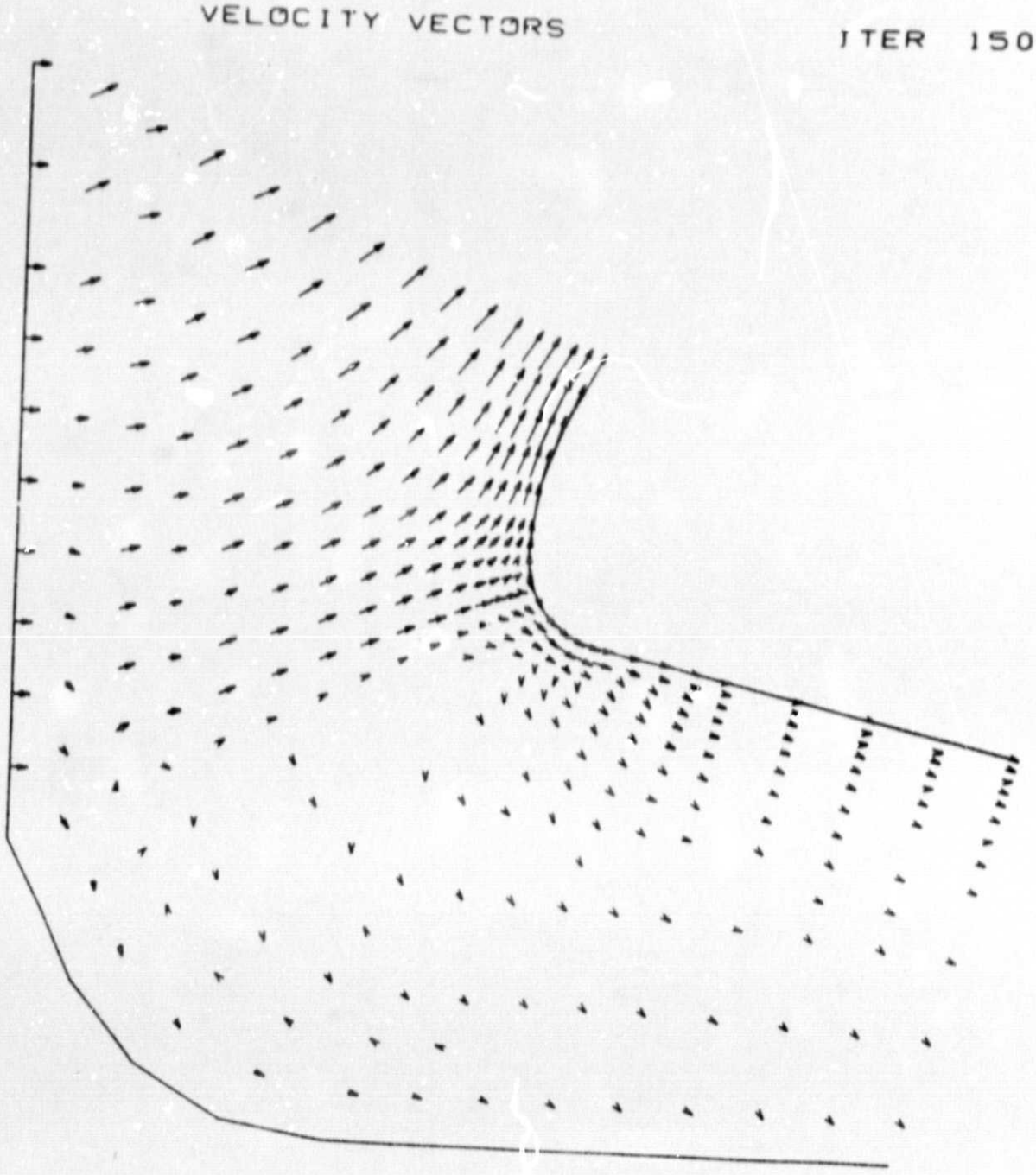

Fig. 28 - SRM Aft Closure Gasdynamic Analysis, Velocity Vector Map, Nose Region (Iteration 150)

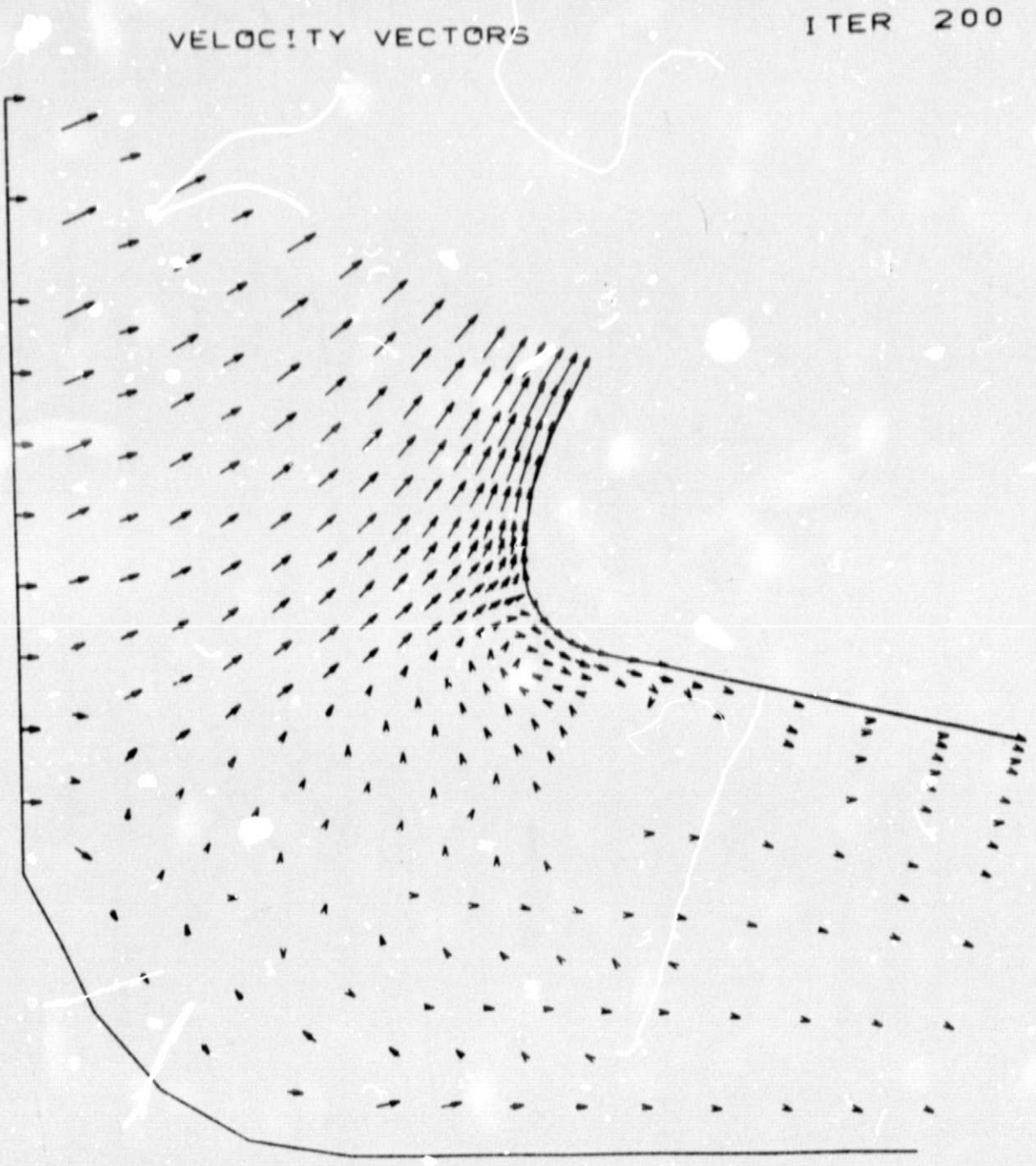

Fig. 29 - SRM Aft Closure Gasdynamic Analysis, Velocity Vector Map, Nose Region (Iteration 200)

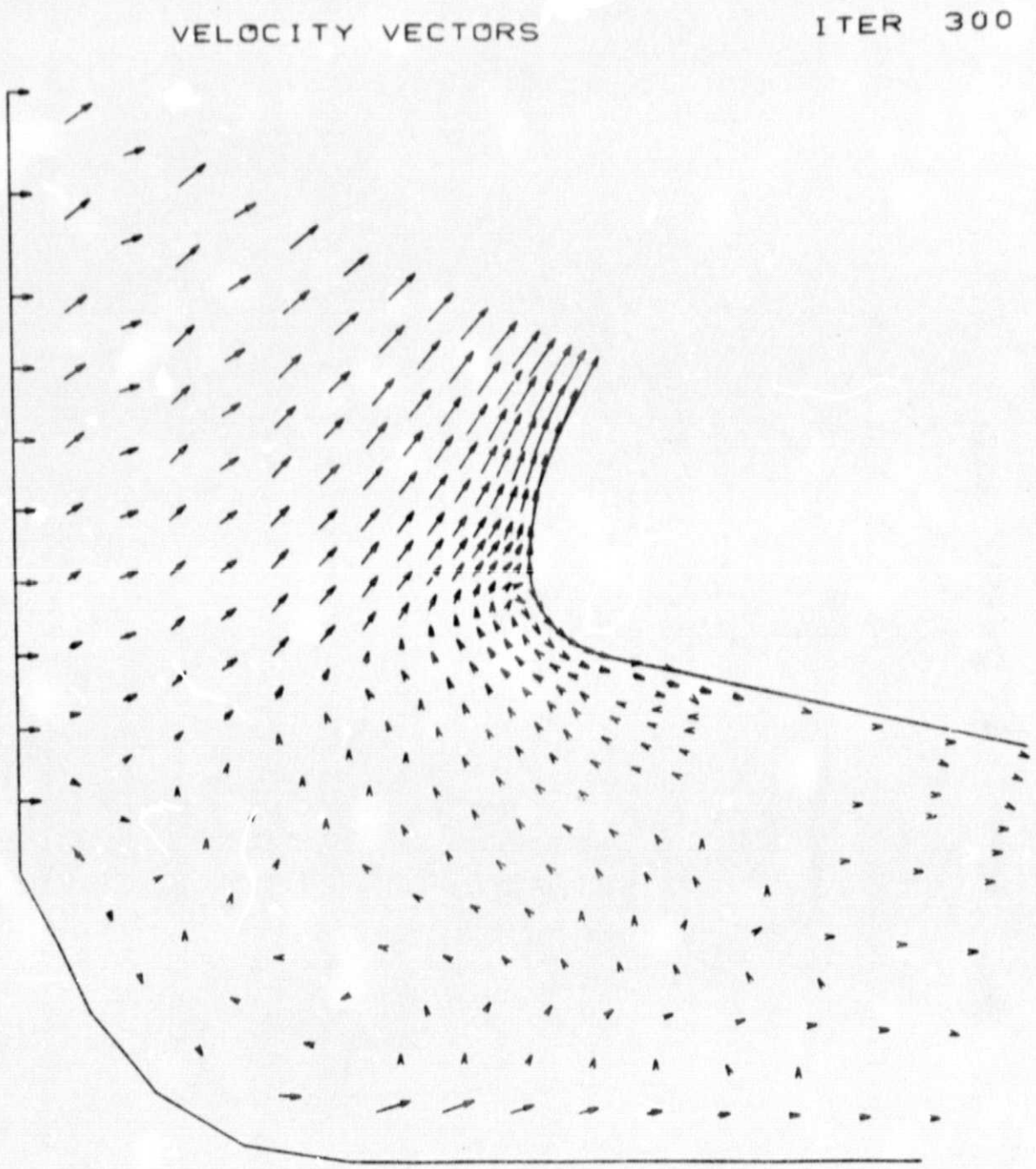

Fig. 30 - SRM Aft Closure Gasdynamic Analysis, Velocity Vector Map, Nose Region (Iteration 300)

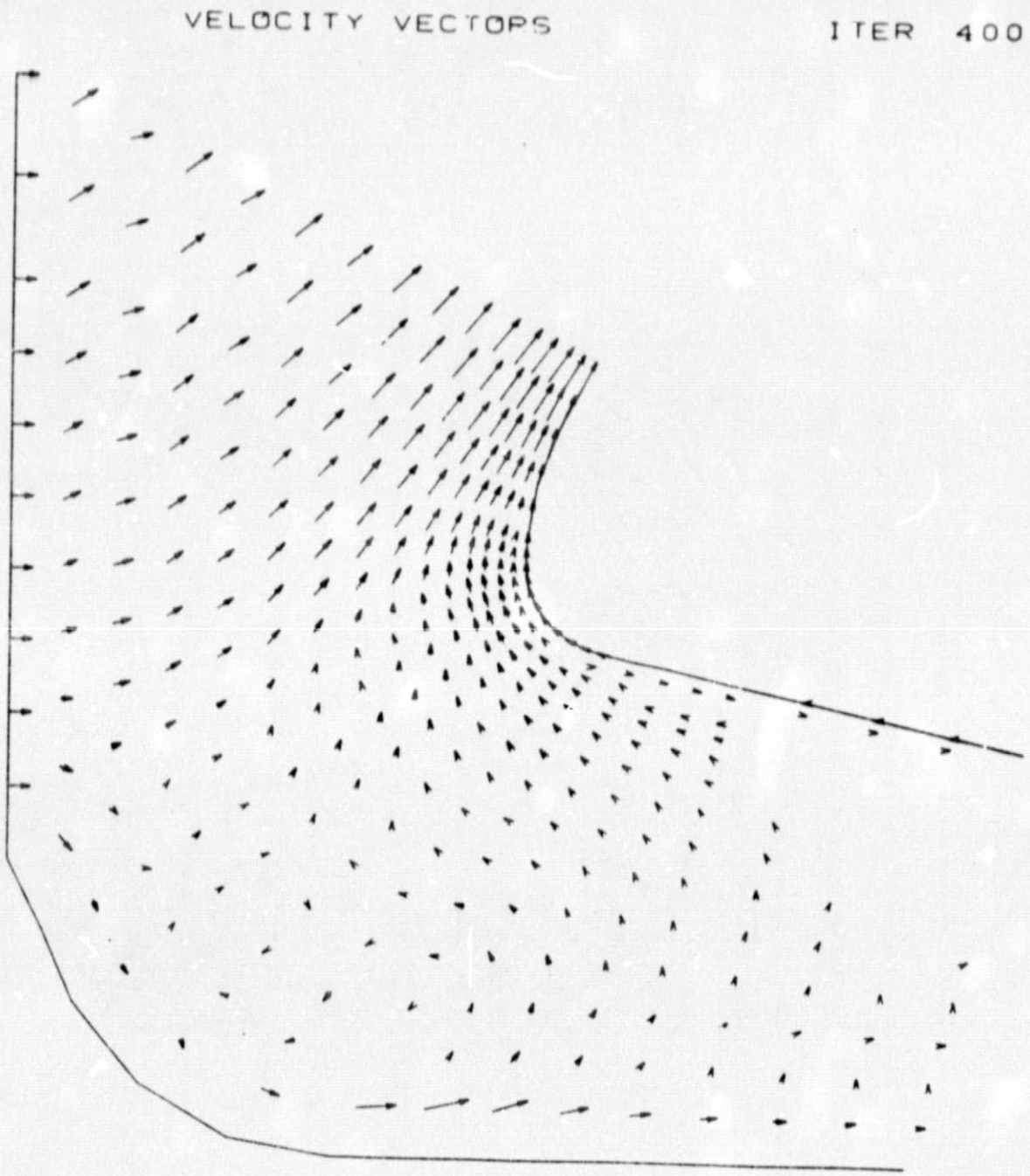

Fig. 31 - SRM Aft Closure Gasdynamic Analysis, Velocity Vector Map, Nose Region (Iteration 400)

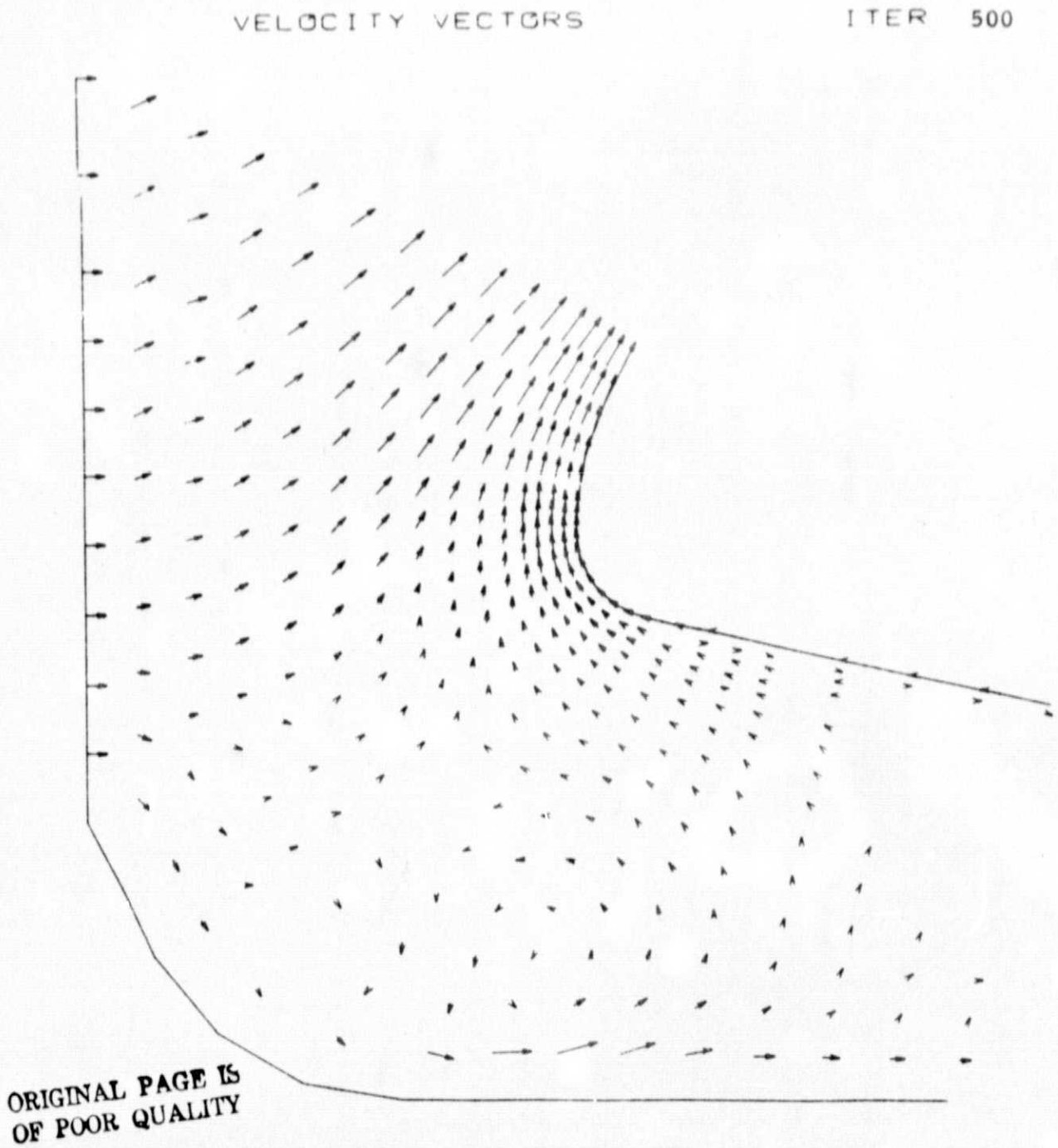

Fig. 32 - SRM Aft Closure Gasdynamic Analysis, Velocity Vector Map, Nose Region (Iteration 500)

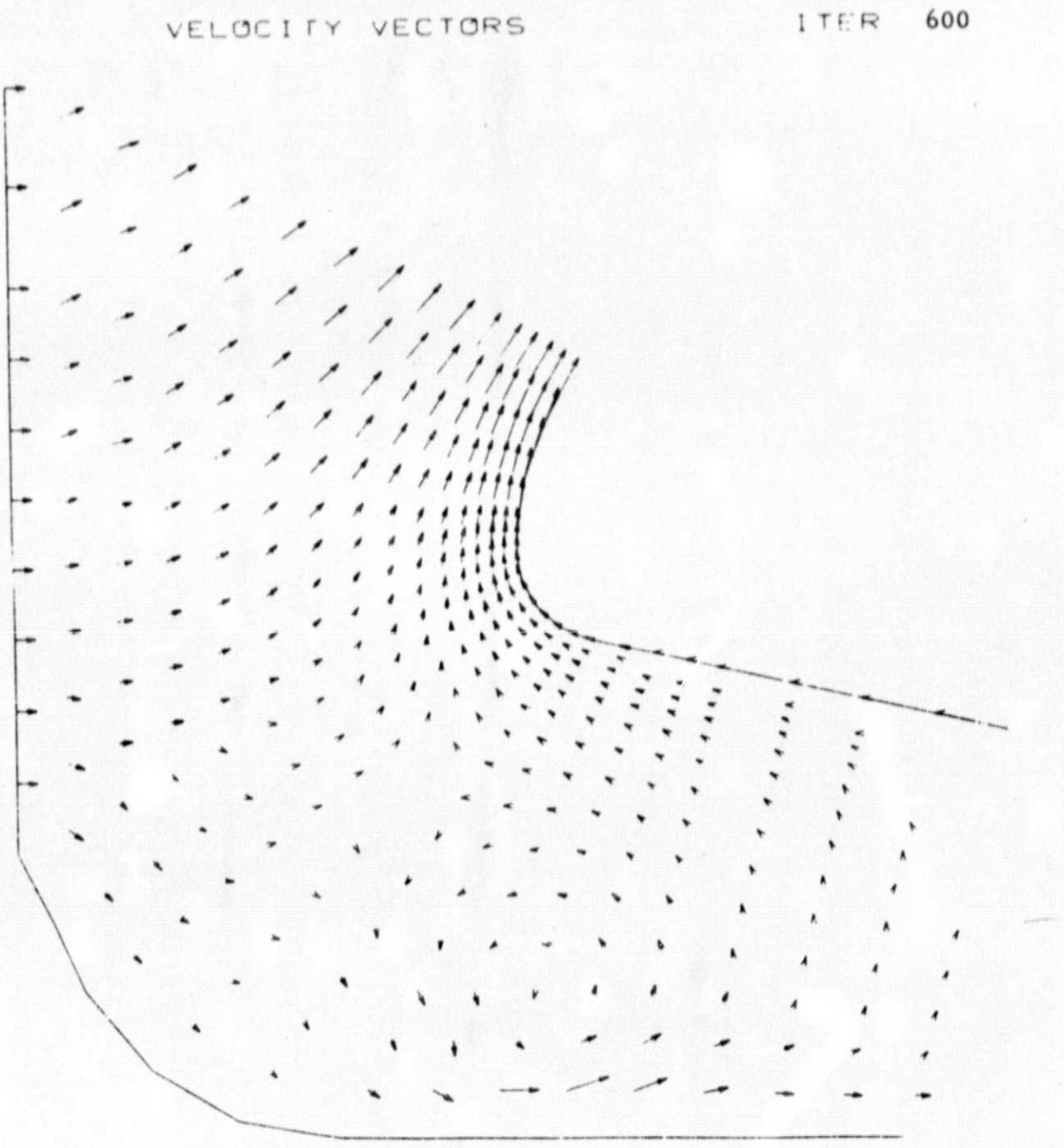

Fig. 33 - SRM Aft Closure Gasdynamic Analysis, Velocity Vector Map, Nose Region (Iteration 600)

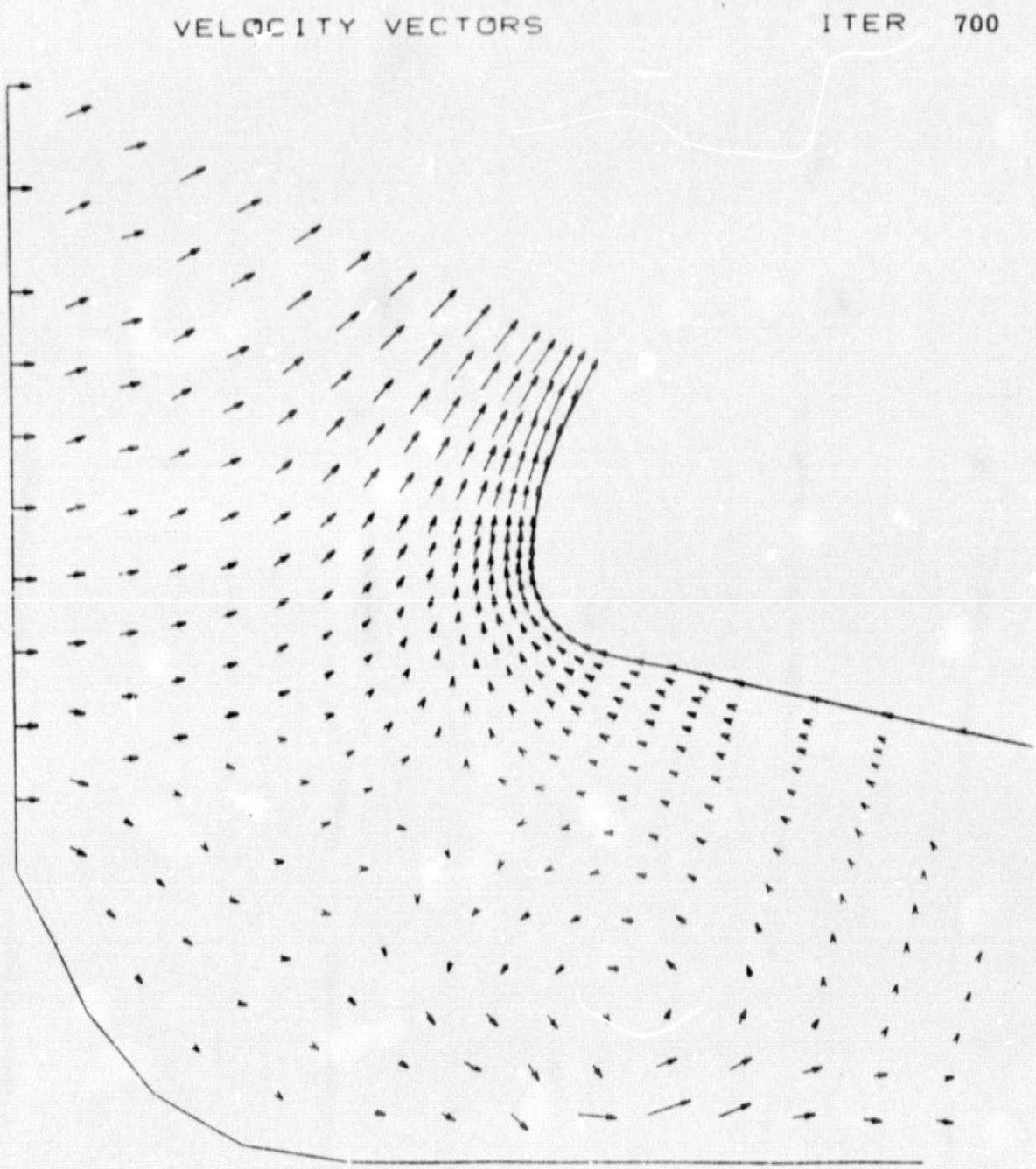

Fig. 34 - SRM Aft Closure Gasdynamic Analysis, Velocity Vector Map, Nose Region (Iteration 700)

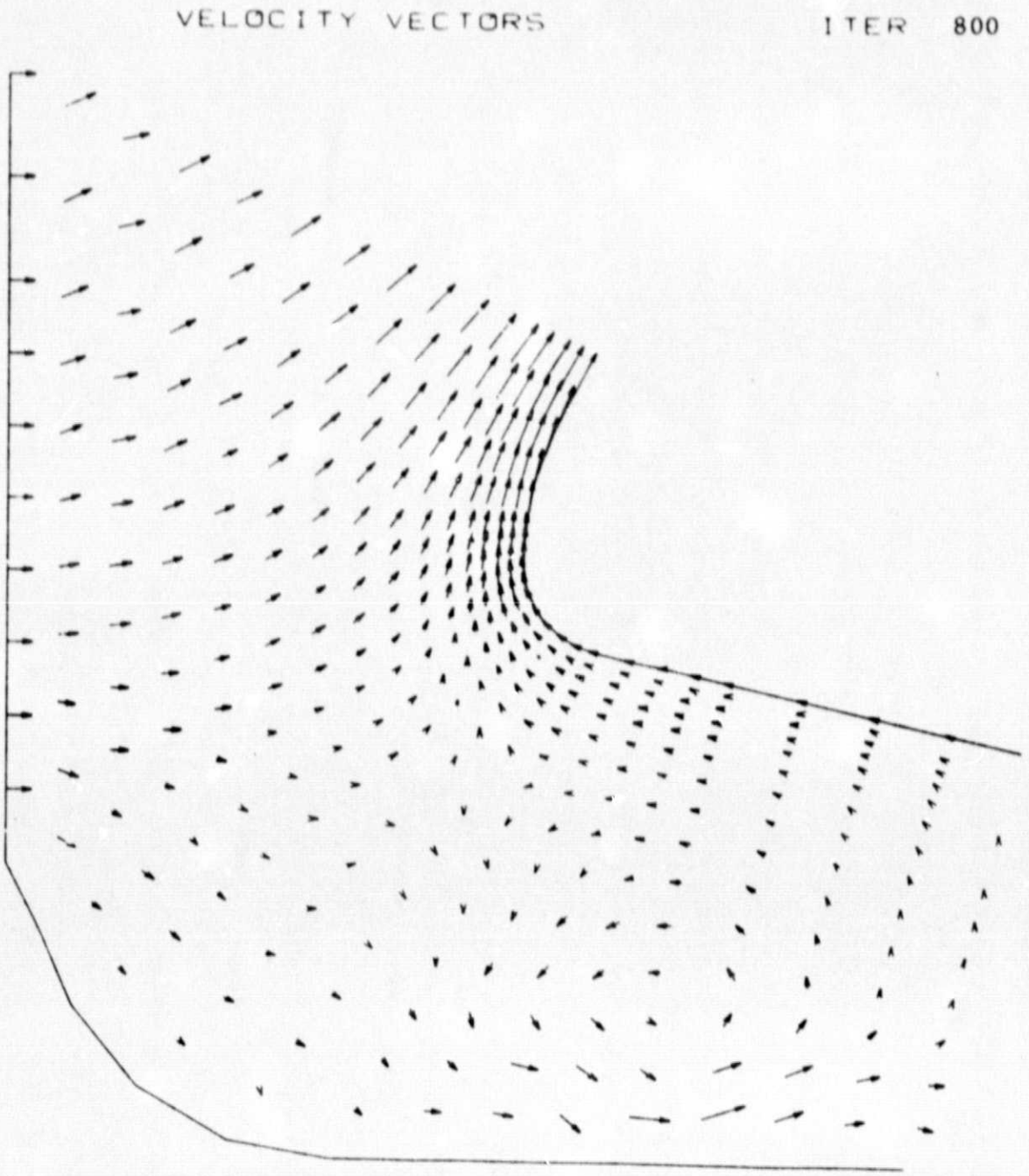

Fig. 35 - SRM Aft Closure Gasdynamic Analysis, Velocity Vector Map, Nose Region (Iteration 800)

C. Flowfield Solution Including the Boot Region

In this portion of the flow field (regions 2 and 3) both inviscid and viscous analyses were employed to provide a steady state solution. Since the top half of the problem (region 1) had reached a steady state solution by 800 iterations, this region was held fixed at the 800th iteration conditions and regions 2 and 3 were allowed to relax. The boundary between regions 1 and 2 was moved to the line connecting nodes 1056 and 1041 (Fig. 7) so that the influence of the boot region solution on the nose region solution could be observed.

1) Inviscid Boot and Nose Region Flowfield Solution Iterations 800 to 1600. The initial conditions for the boot portion (region 3) of the flow field were zero velocity at each node in the region and 98% of the stagnation pressure. Also nodes 1 through 145 were eliminated from the solution because of problems with the mesh construction in this area. The boundary conditions were no-slip or zero-velocity along the walls, and input conditions at the junction of regions 2 and 3 as established at iteration 800 of the solution to regions 1 and 2. The reasoning behind these initial conditions and boundary conditions is to let the flow fill the boot region and allow the GIM to establish the flow directions.

The velocity vector maps for the nose underside region of the flow field for iterations 800 to 1600 are shown in Figs. 36 through 44. Note that the location of the recirculation region is relatively constant. Also the mass flux into the boot region is generally axial and in the positive X direction (Fig. 44).

The velocity vector maps for the boot region for iterations 800 to 1600 are shown in Figs. 45 through 53. In the boot region there is essentially no flow and a slightly lower pressure (98%) than exists at the upstream boundary. Consequently, the flow must first fill up this region and then find a path back out. This is what happens and by iteration 1600 (Fig. 53), the flow has established a direction which is into the region. The remaining part of the analysis is the relaxation of the boot region flow field to provide a means for mass to enter and exit this region.

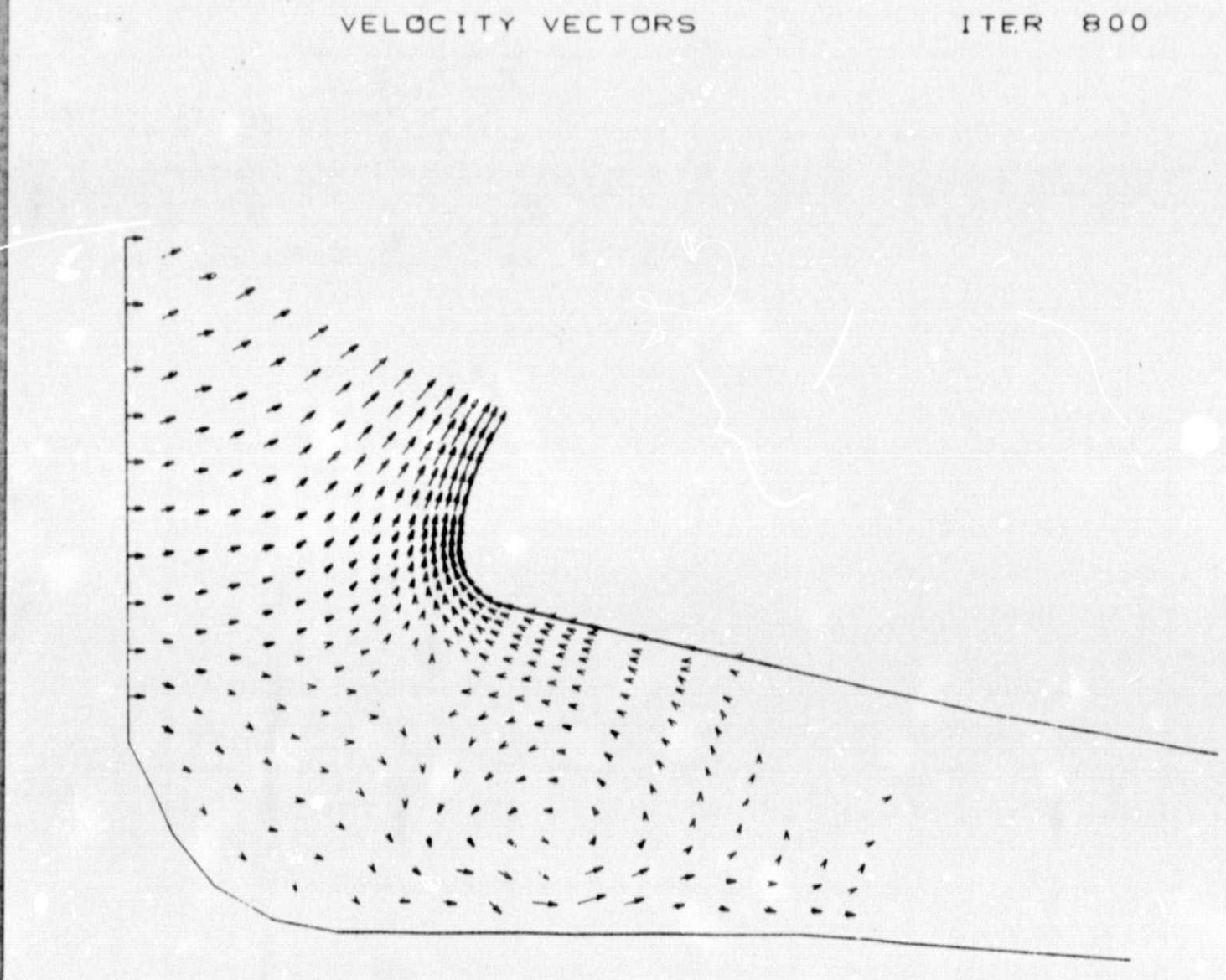

Fig. 36 - SRM Aft Closure Gasdynamic Analysis, Velocity Vector Map, Nose Underside Region (Iteration 800)

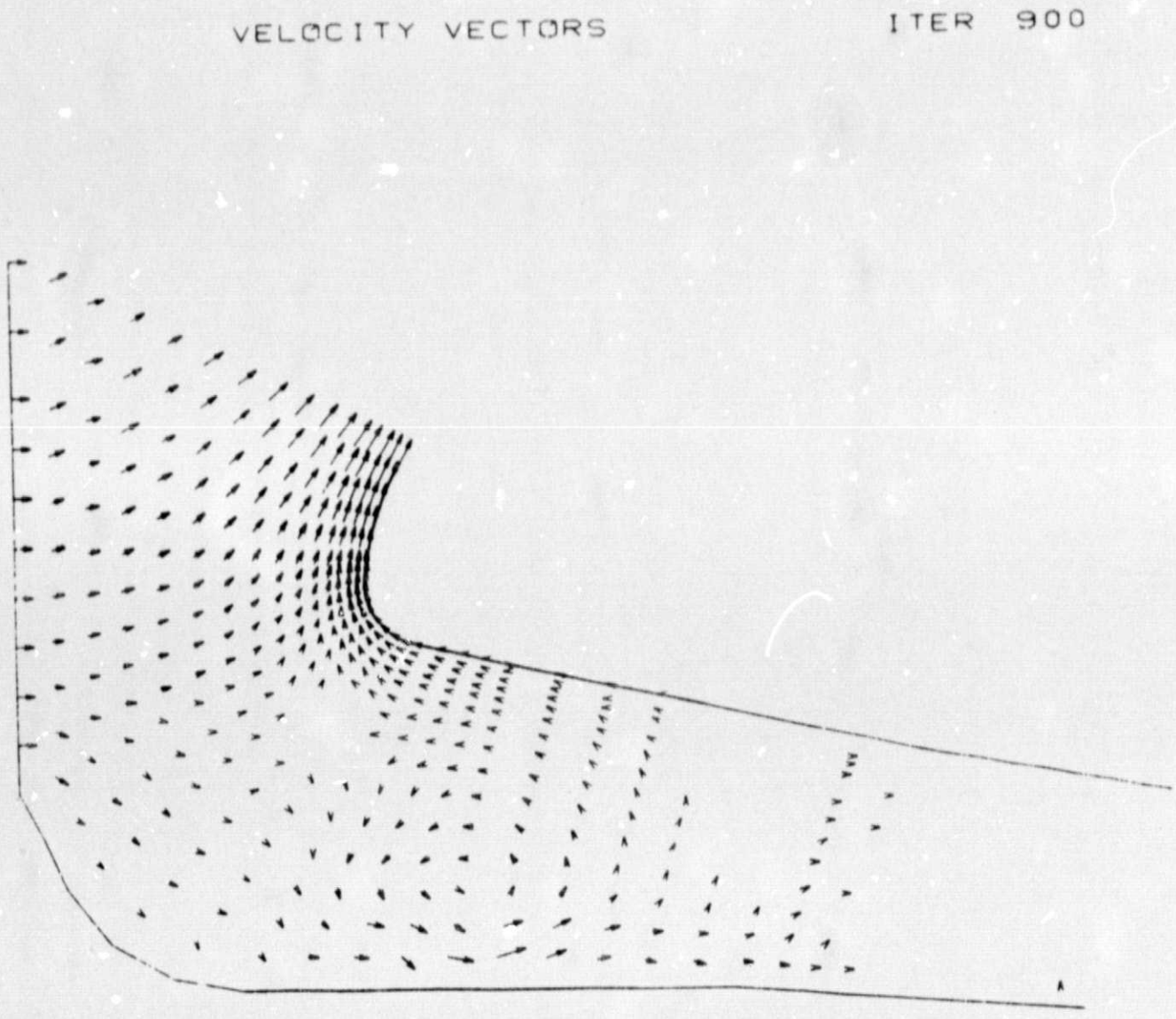

Fig. 37 - SRM Aft Closure Gasdynamic Analysis, Velocity Vector Map, Nose Underside Region (Iteration 900)

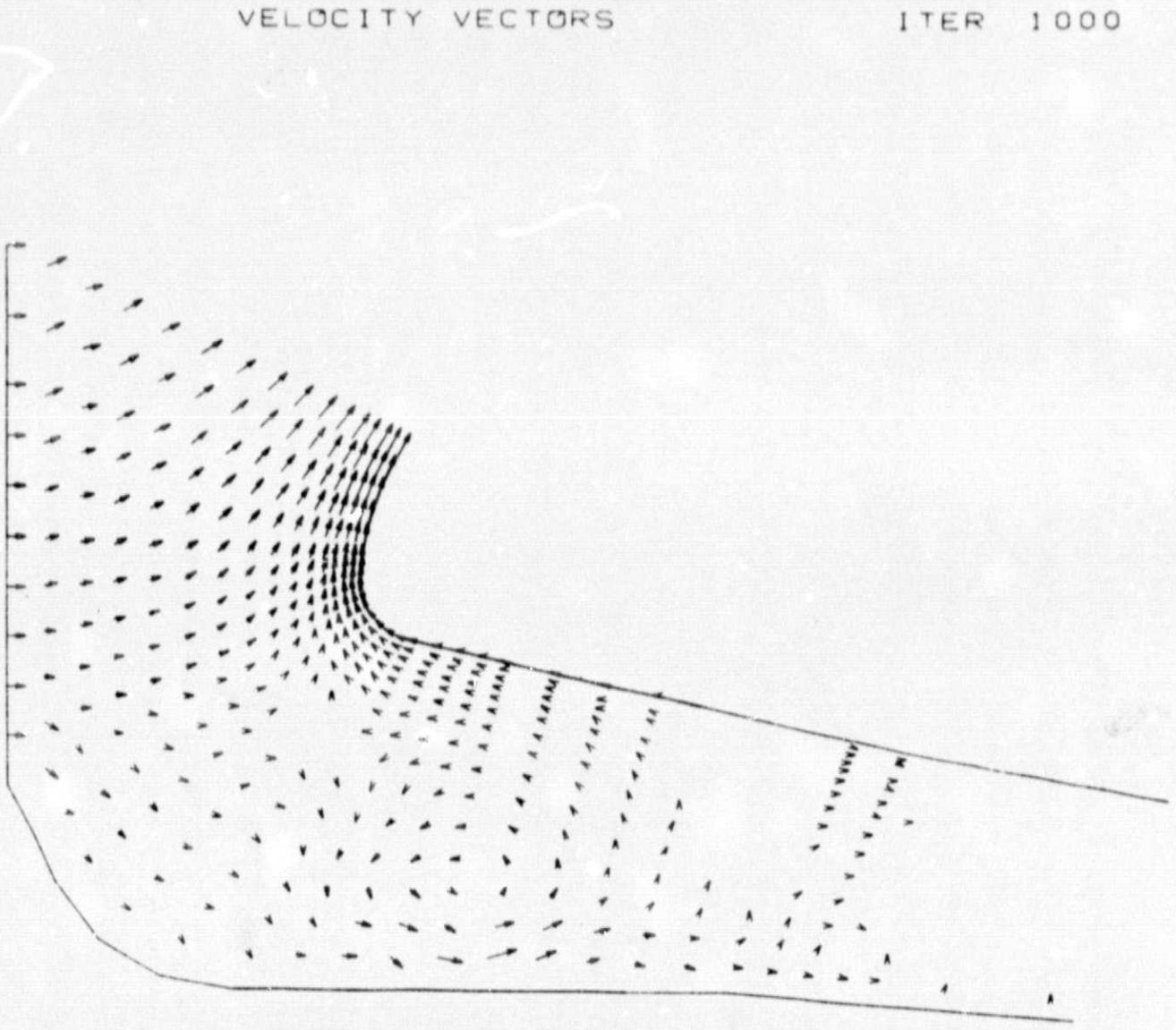

Fig. 38 - SRM Aft Closure Gasdynamic Analysis, Velocity Vector Map, Nose Underside Region (Iteration 1000)

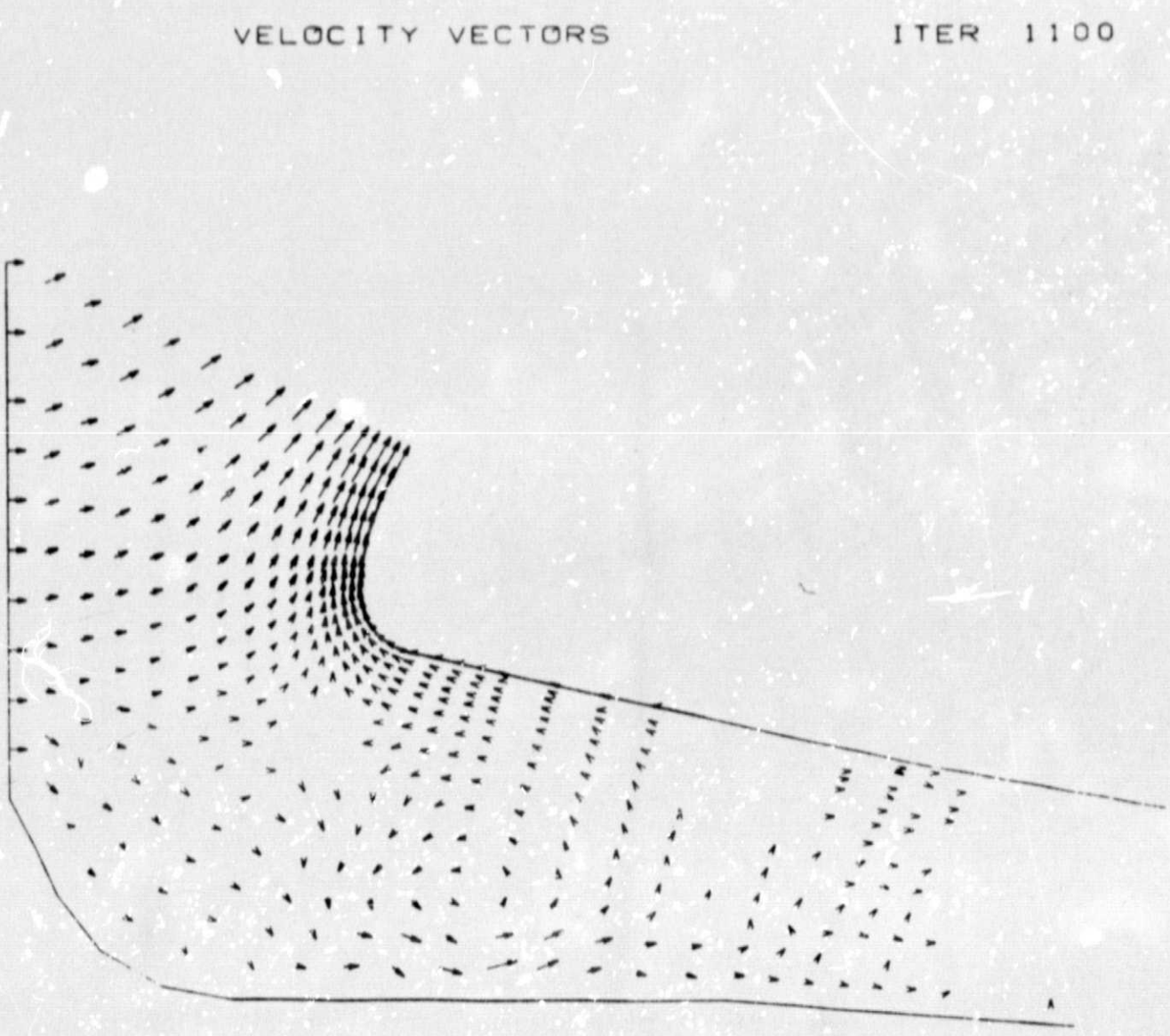

Fig. 39 - SRM Aft Closure Gasdynamic Analysis, Velocity Vector Map, Nose Underside Region (Iteration 1100)

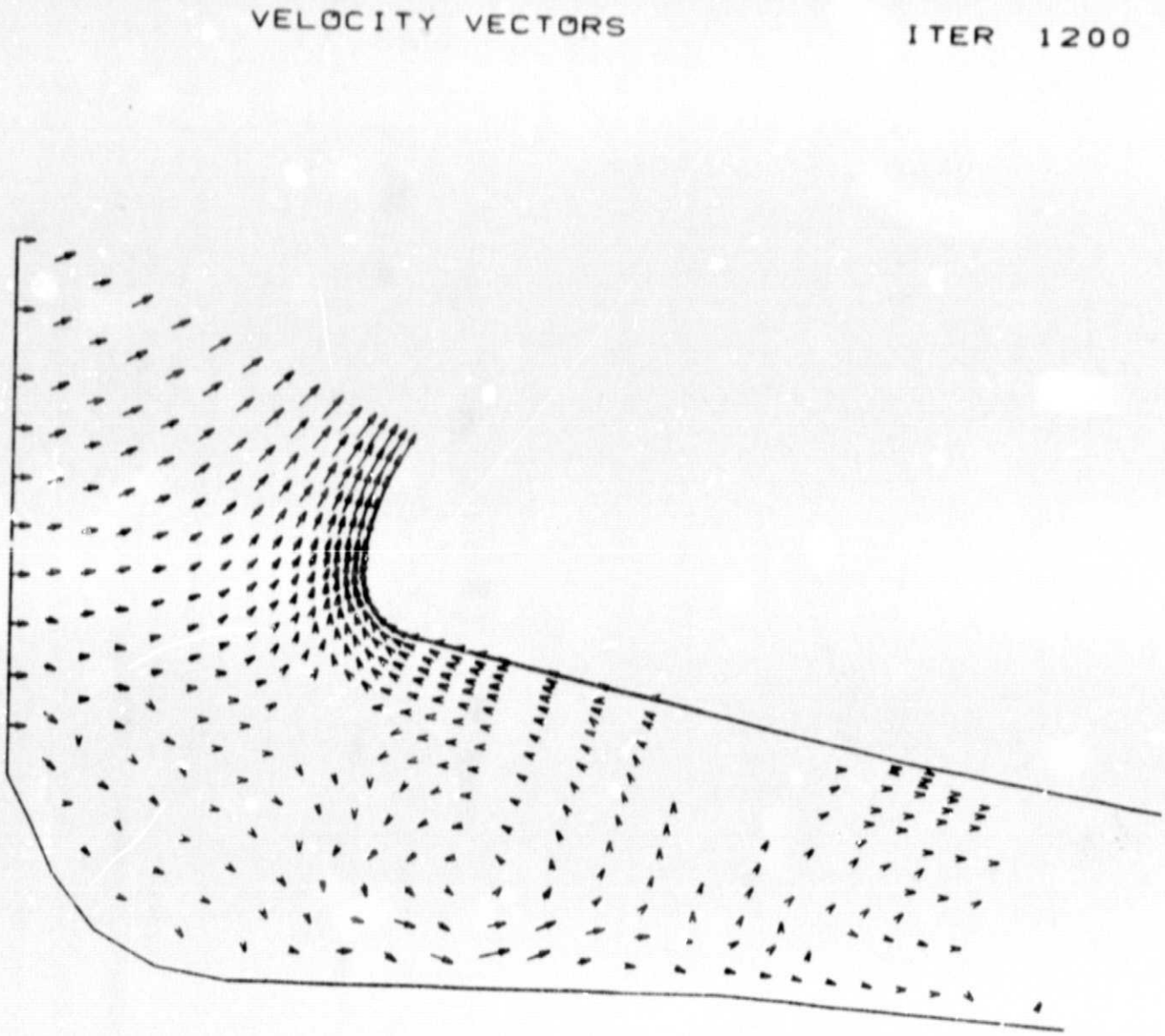

Fig. 40 - SRM Aft Closure Gasdynamic Analysis, Velocity Vector Map, Nose Underside Region (Iteration 1200)

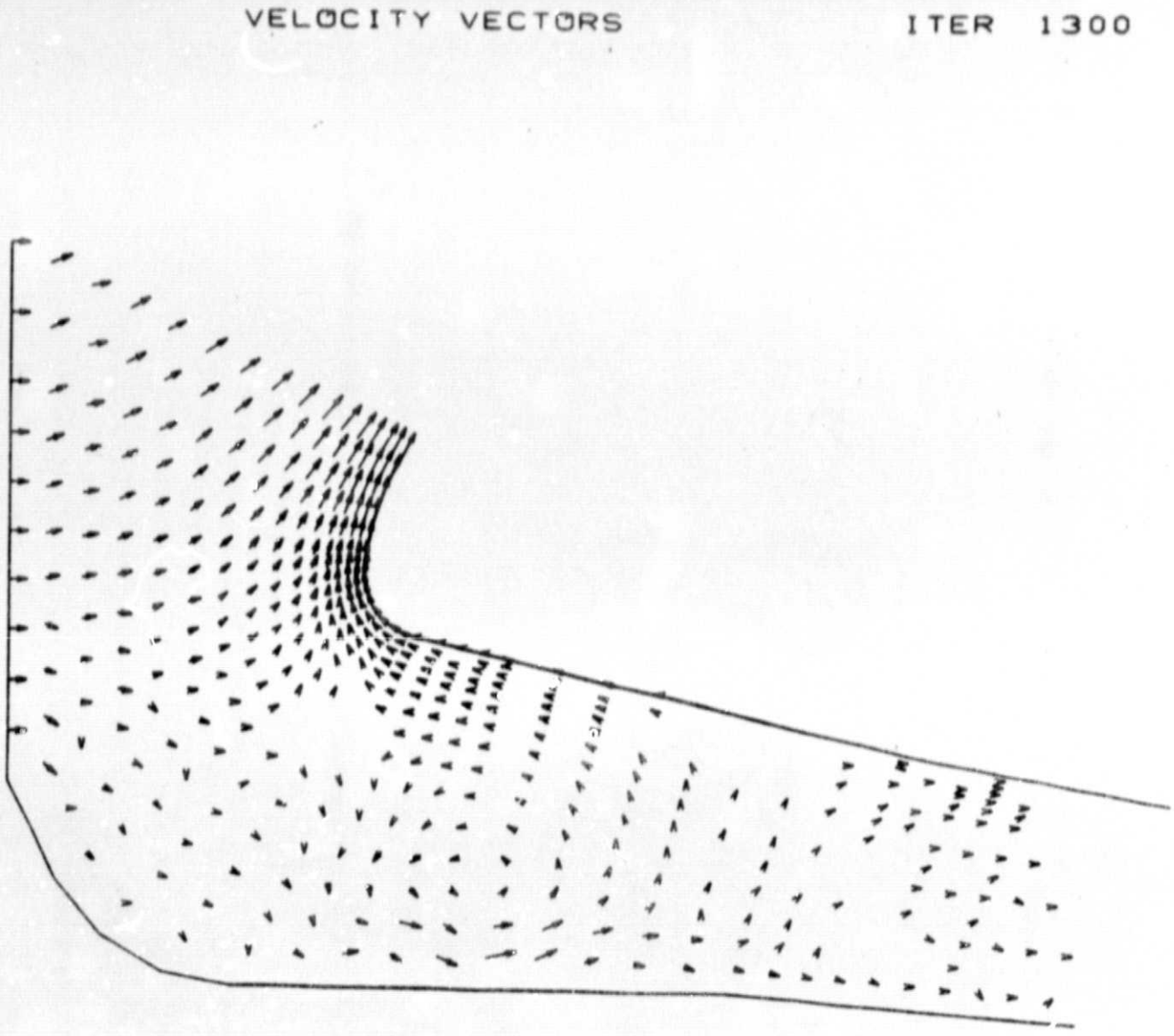

Fig. 41 - SRM Aft Closure Gasdynamic Analysis, Velocity Vector Map, Nose Underside Region (Iteration 1300)

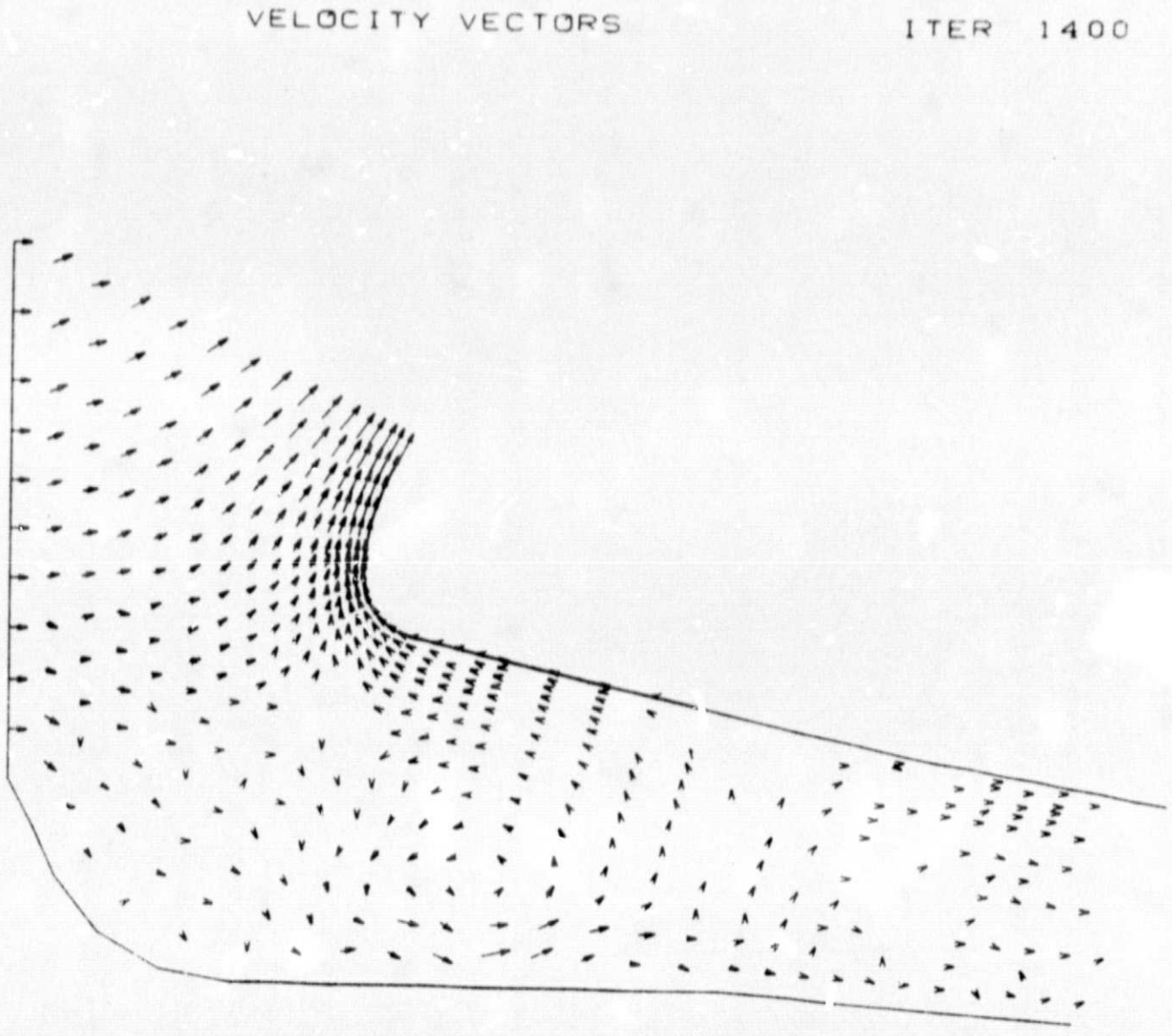

Fig. 42 - SRM Aft Closure Gasdynamic Analysis, Velocity Vector Map, Nose Underside Region (Iteration 1400)

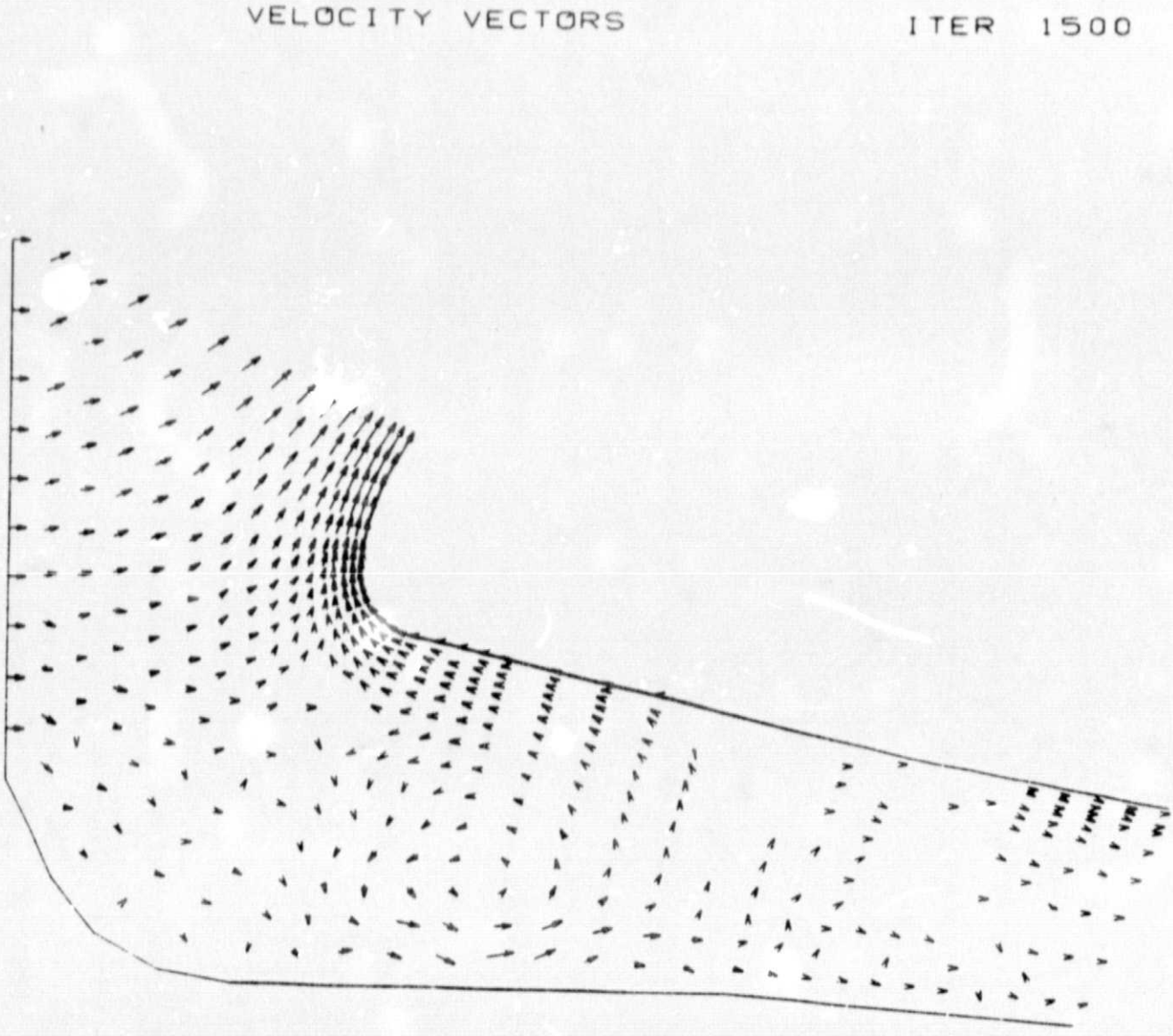

Fig. 43 - SRM Aft Closure Gasdynamic Analysis, Velocity Vector Map, Nose Underside Region (Iteration 1500)

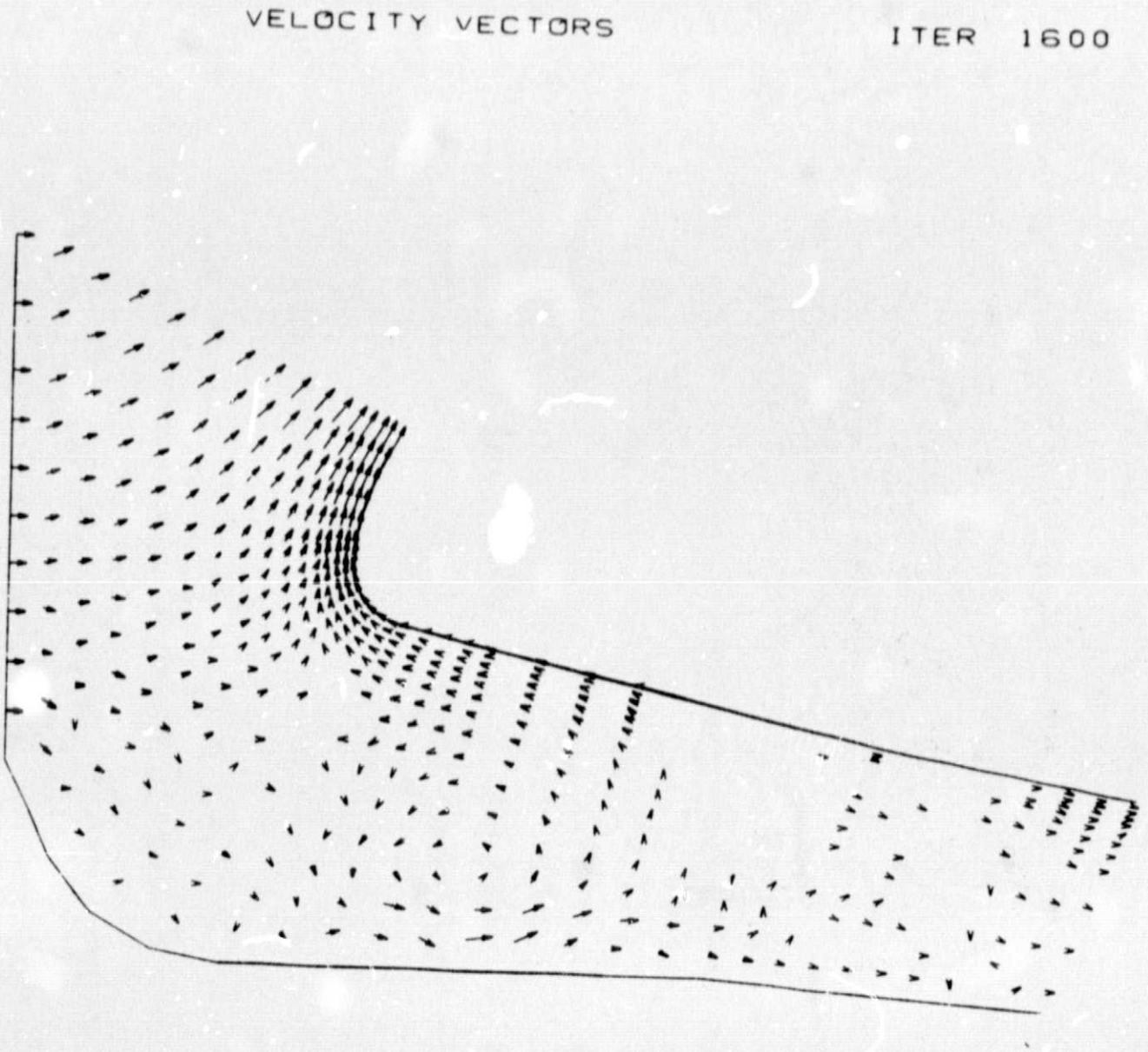

Fig. 44 - SRM Aft Closure Gasdynamic Analysis, Velocity Vector Map, Nose Underside Region (Iteration 1600)

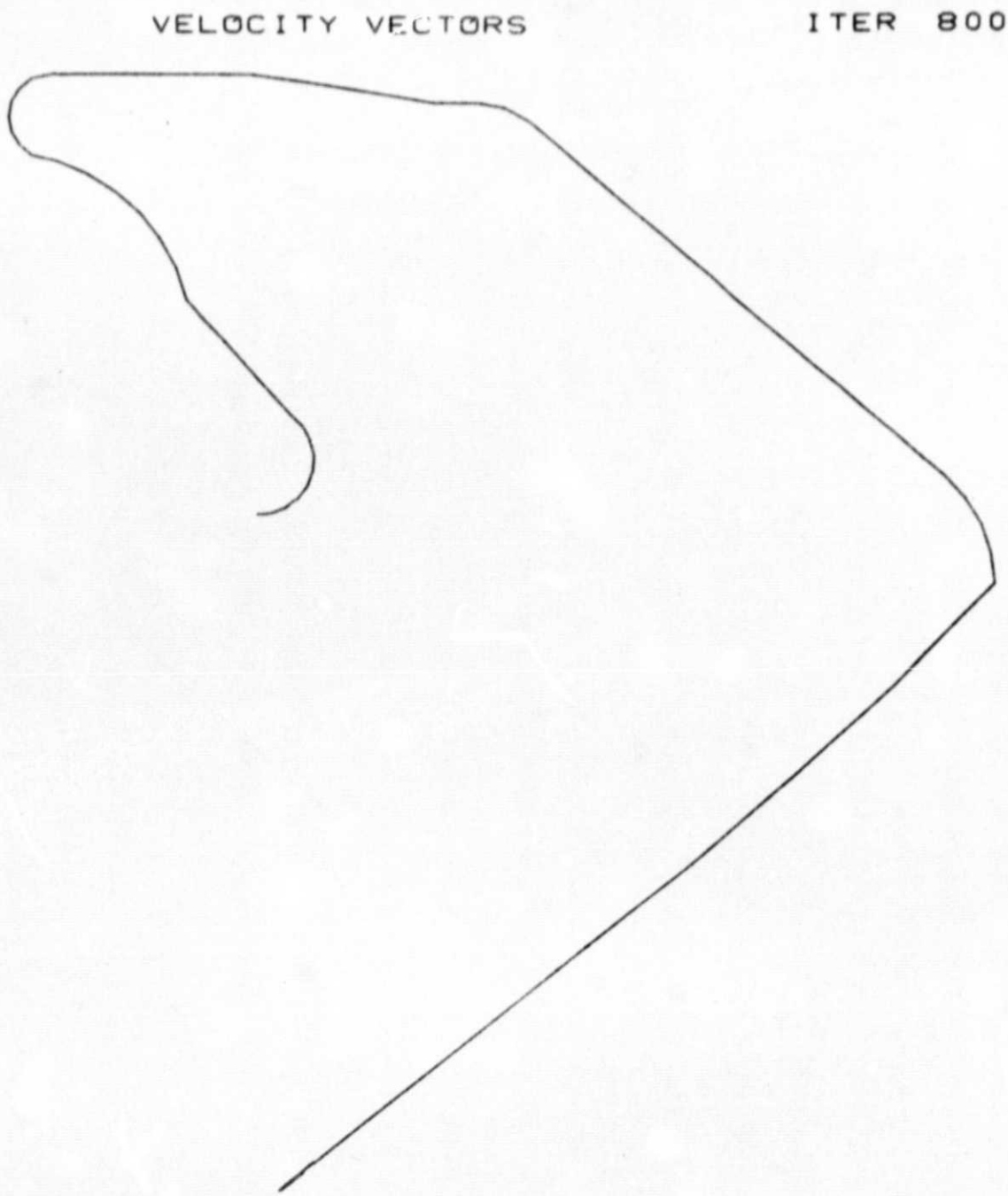

Fig. 45 - SRM Aft Closure Gasdynamic Analysis, Velocity Vector Map, Boot Region (Iteration 800)

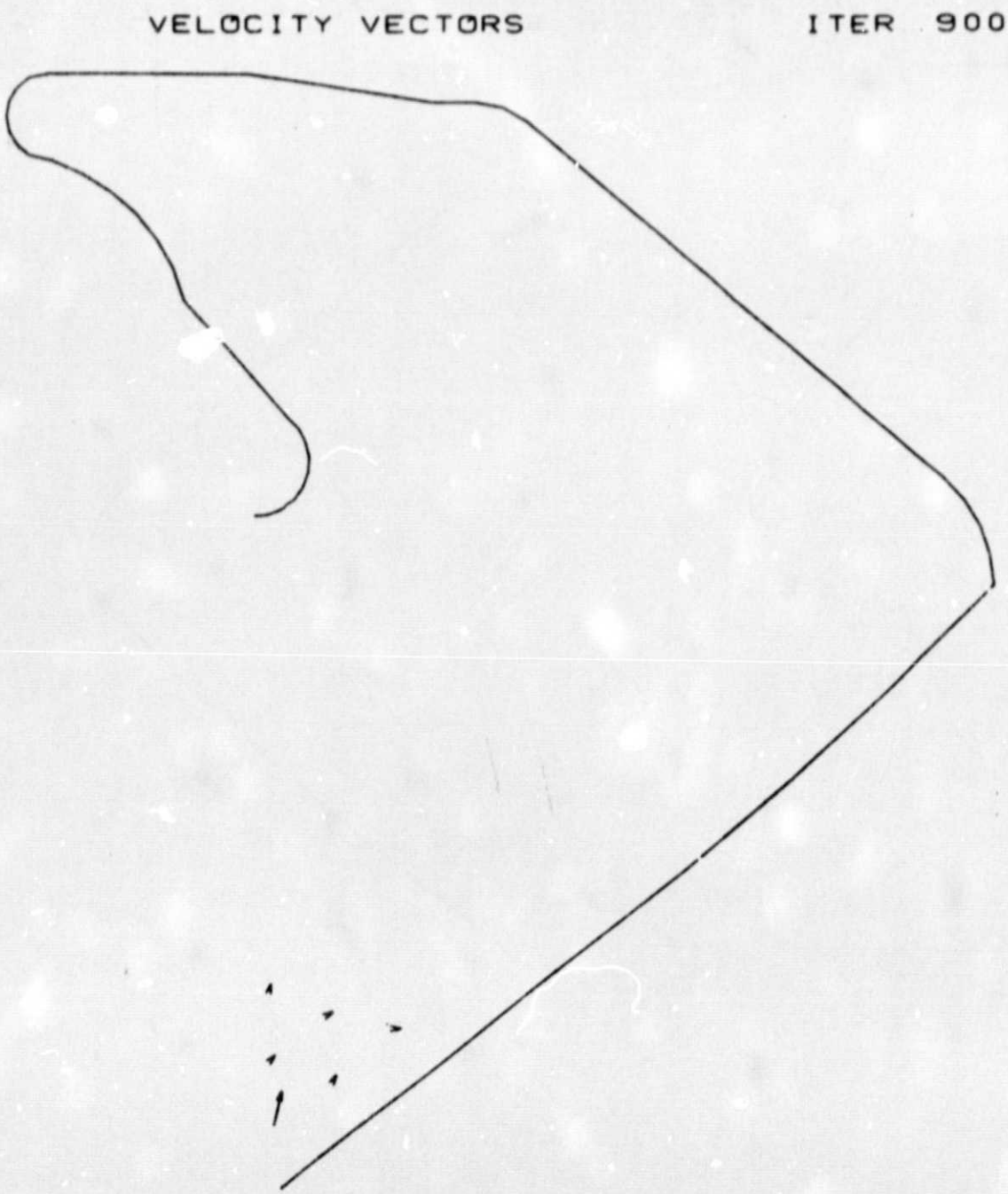

Fig. 46 - SRM Aft Closure Gasdynamic Analysis, Velocity Vector Map, Boot Region (Iteration 900)

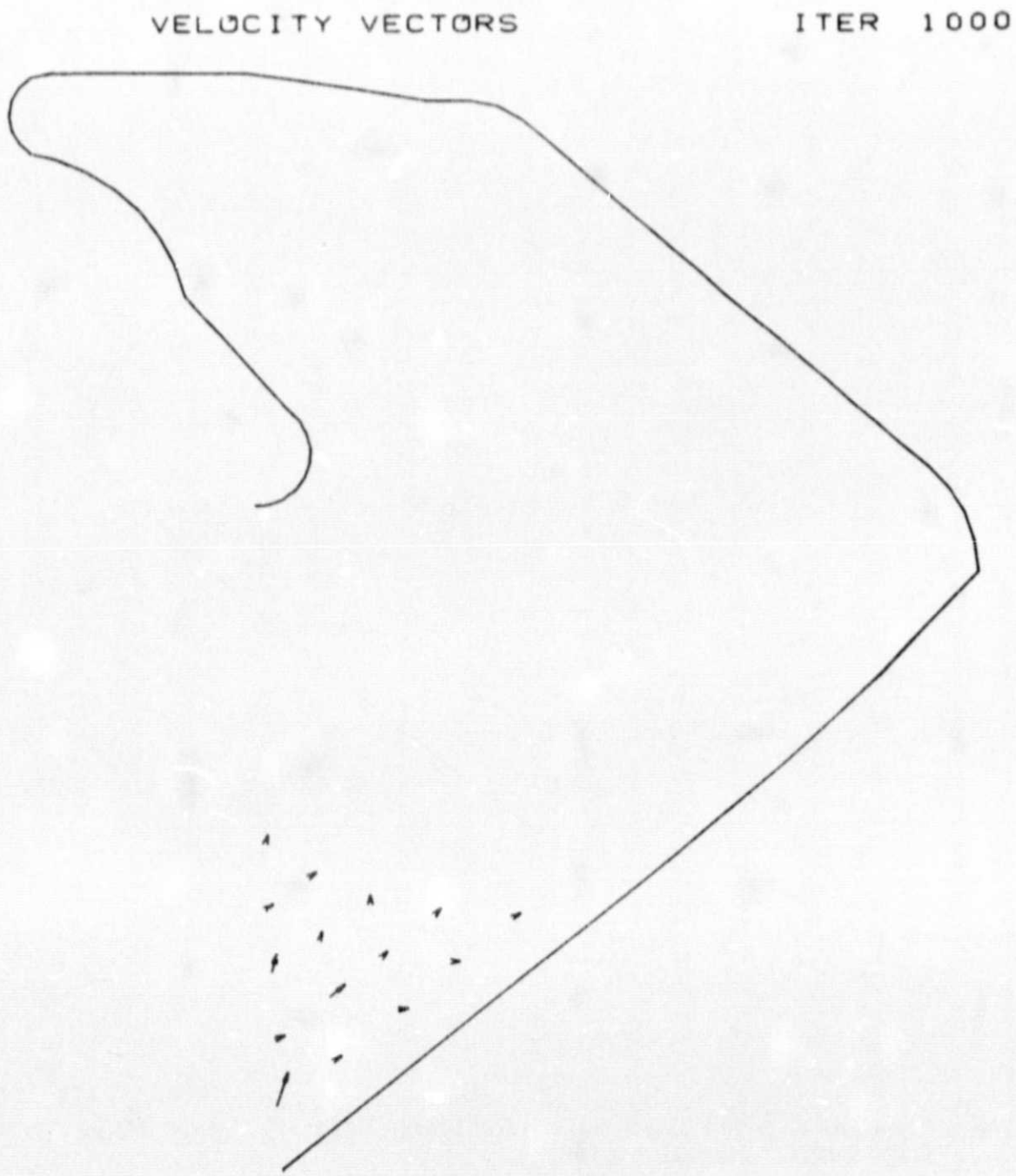

Fig. 47 - SRM Aft Closure Gasdynamic Analysis, Velocity Vector Map, Boot Region (Iteration 1000)

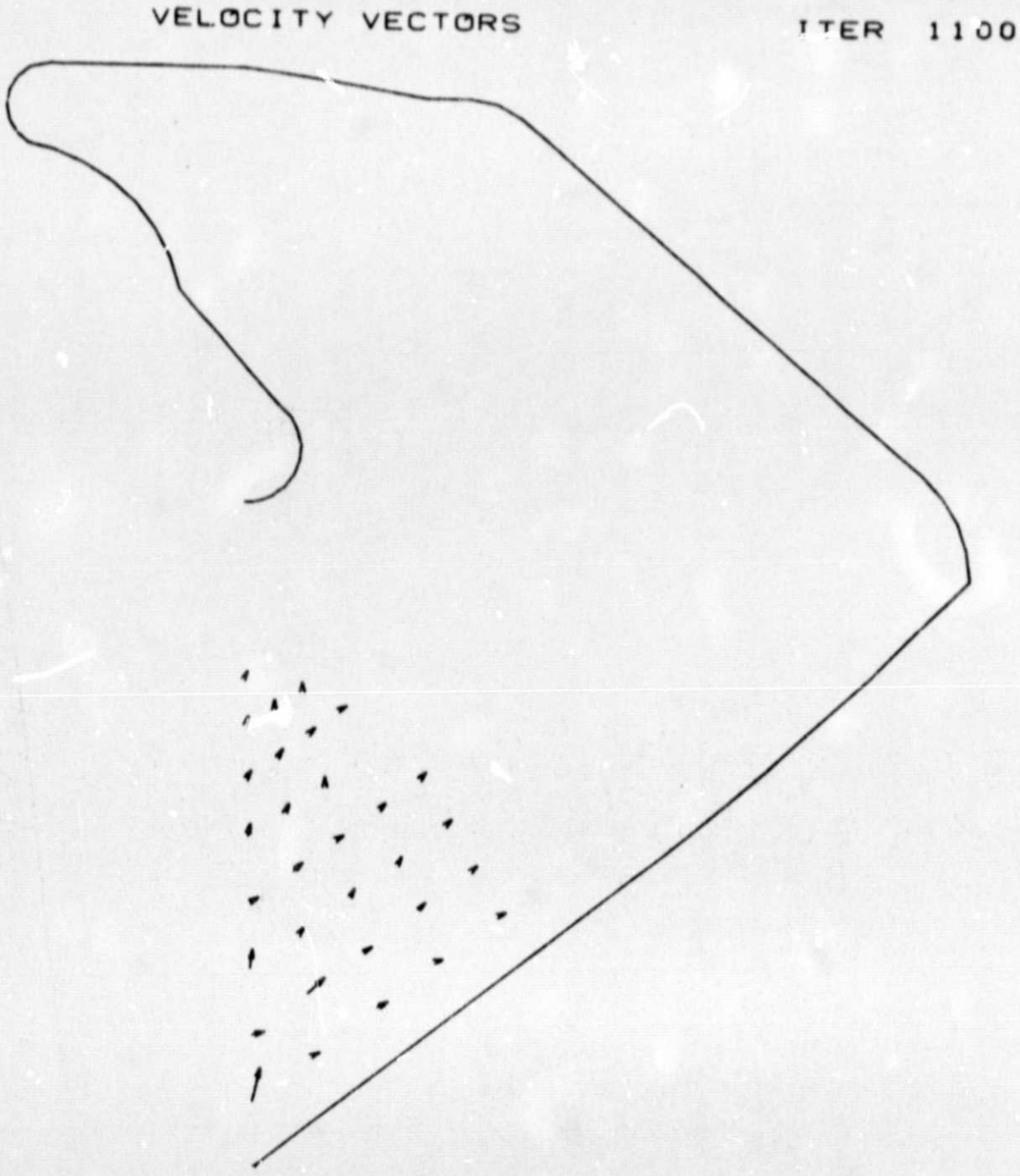

Fig. 48 - SRM Aft Closure Gasdynamic Analysis, Velocity Vector Map, Boot Region (Iteration 1100)

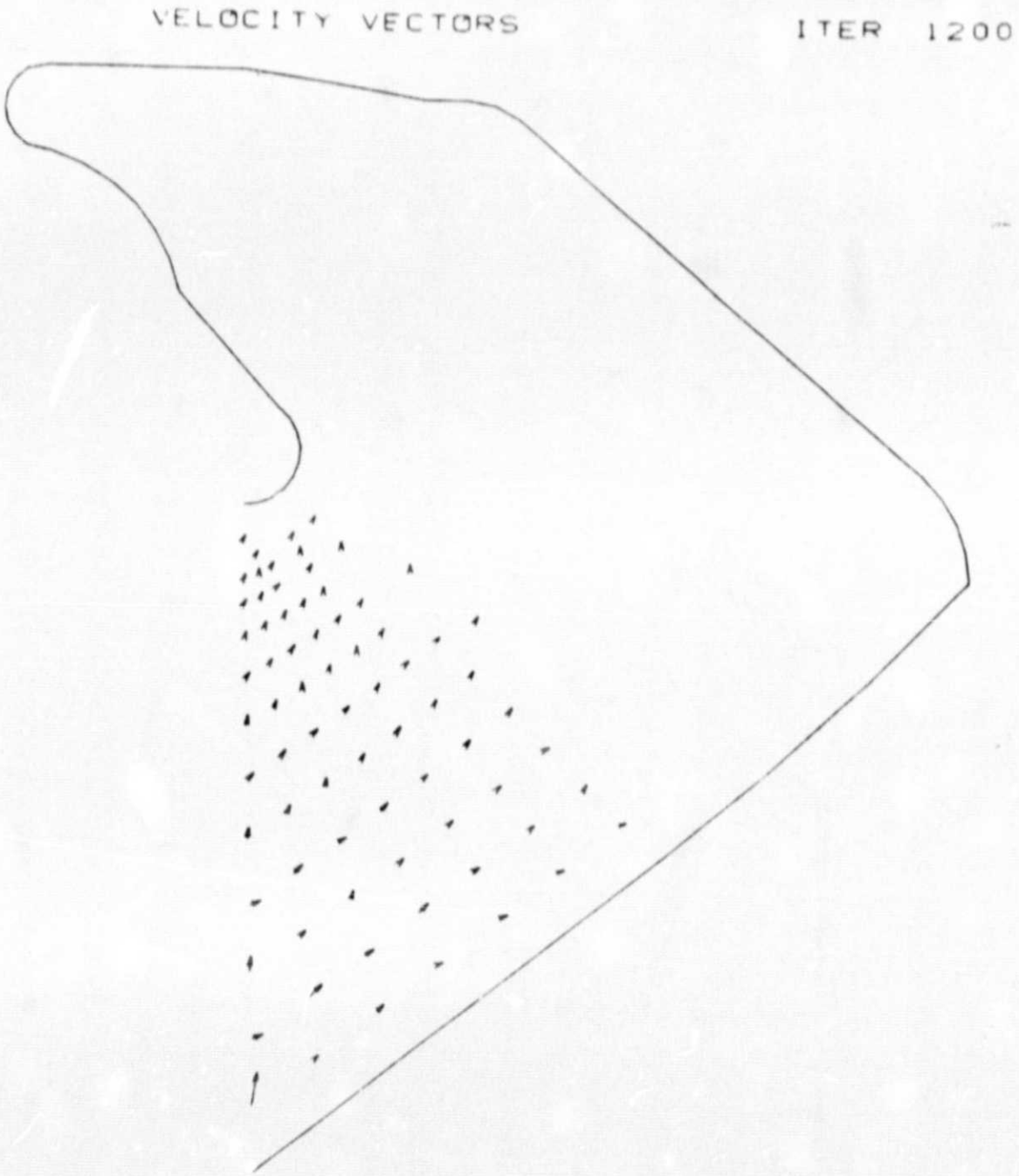

Fig. 49 - SRM Aft Closure Gasdynamic Analysis, Velocity Vector Map, Boot Region (Iteration 1200)

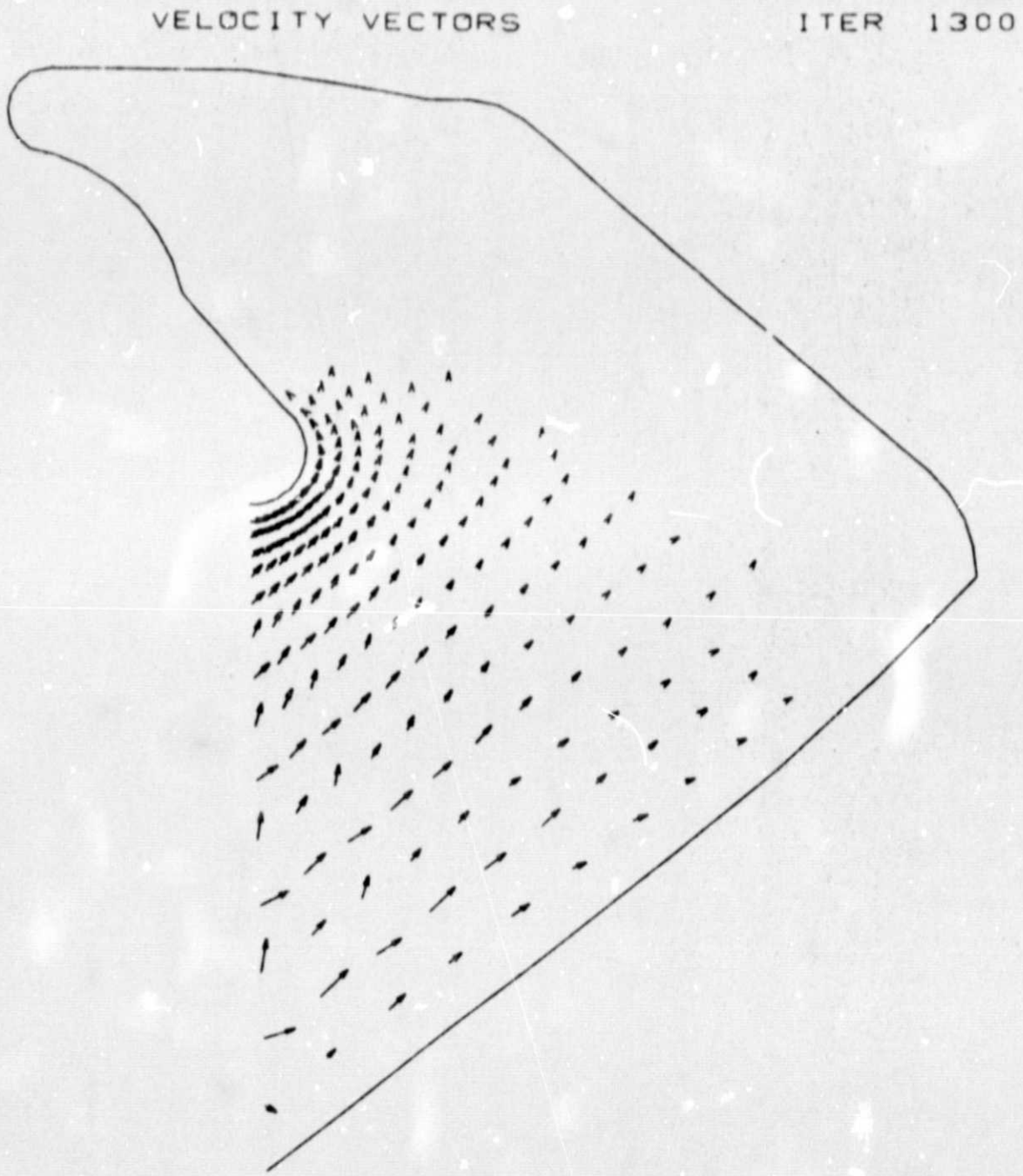

Fig. 50 - SRM Aft Closure Gasdynamic Analysis, Velocity Vector Map, Boot Region (Iteration 1300)

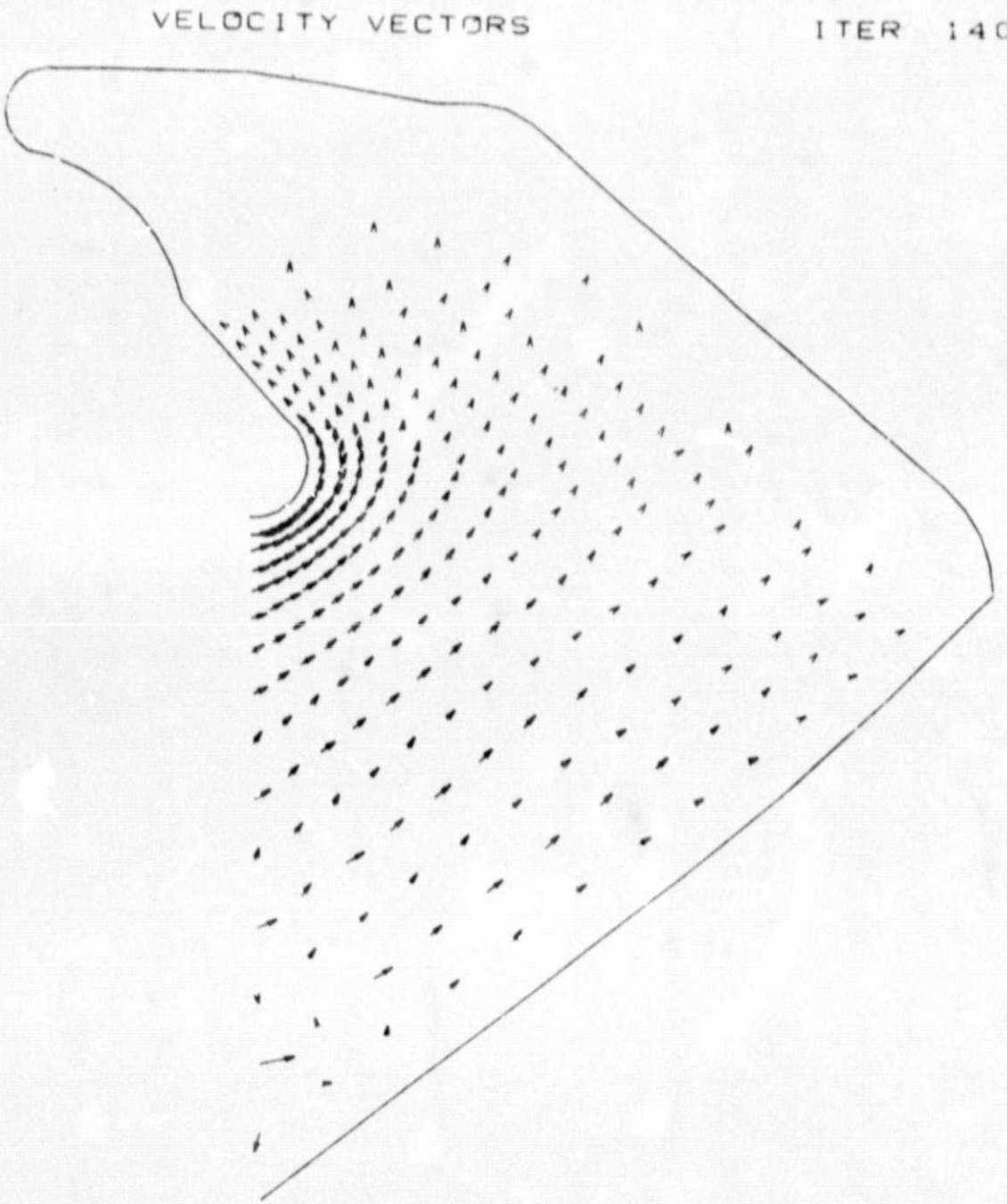

Fig. 51 - SRM Aft Closure Gasdynamic Analysis, Velocity Vector Map, Boot Region (Iteration 1400)

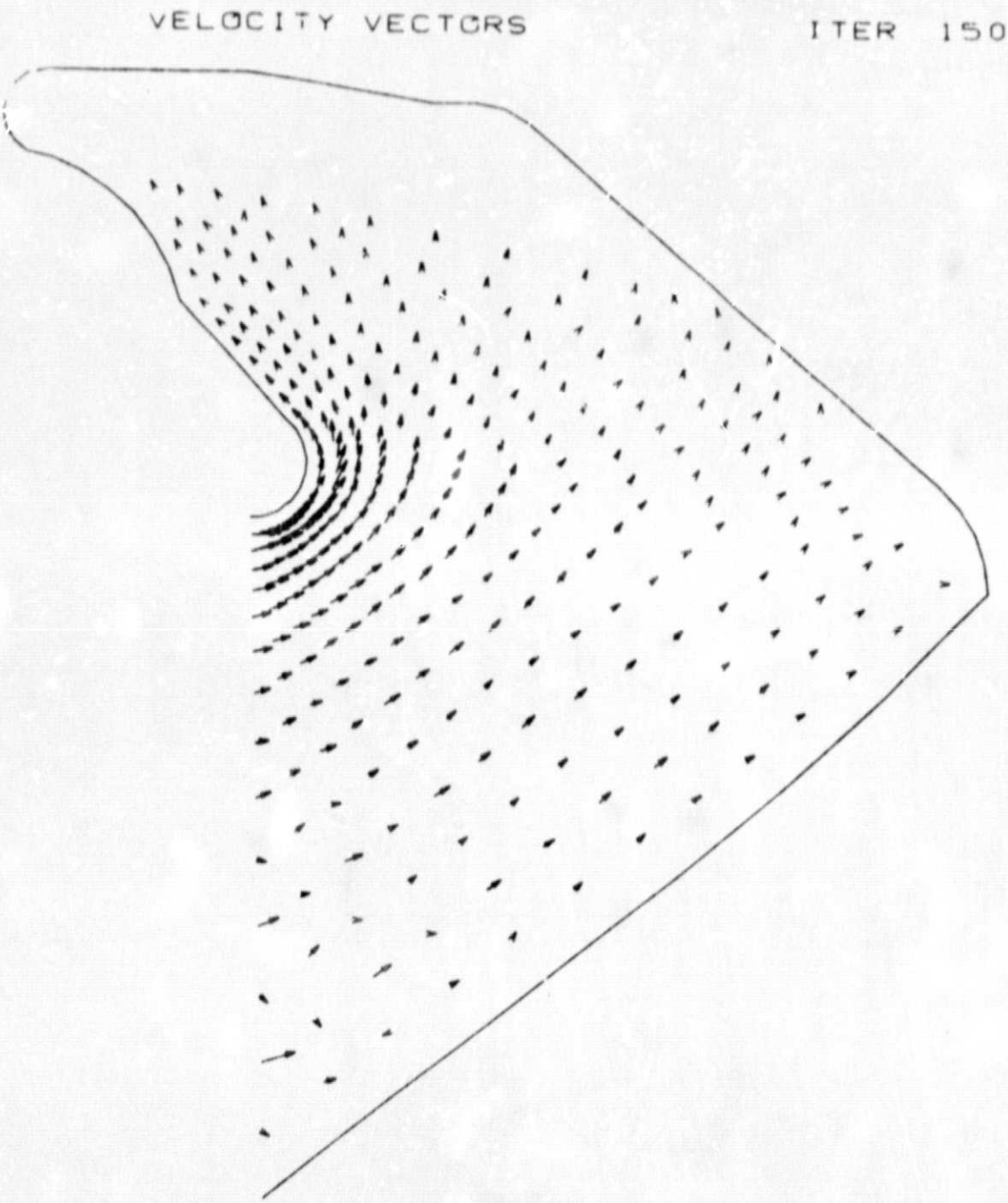

Fig. 52 - SRM Aft Closure Gasdynamic Analysis, Velocity Vector Map, Boot Region (Iteration 1500)

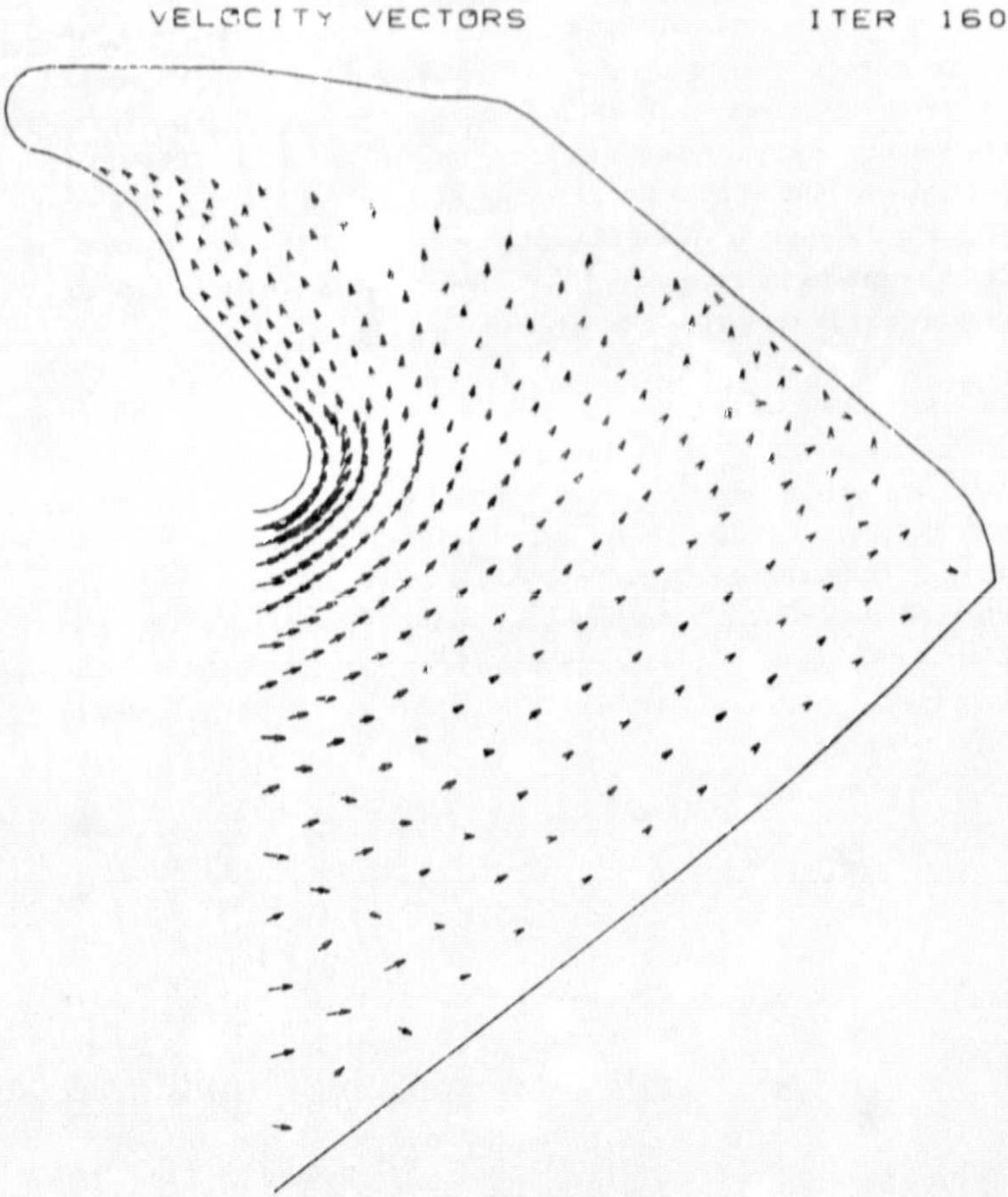

Fig. 53 - SRM Aft Closure Gasdynamic Analysis, Velocity Vector Map, Boot Region (Iteration 1600)

2) Viscous Boot and Nose Region Flowfield Solution iterations 1600 to 2000: Viscosity was added to solution for iterations 1600 to 2000. The viscous terms damp the solution and generally improve the chances of reaching a steady state solution for the boot region of the flow field. The velocity vector maps for the nose underside region of the flow field for iterations 1600 to 2000 are shown in Figs. 54 through 58. Note that in these figures the solution is not changing a great deal and that the recirculation region is relatively stationary. Also the mass flux is basically into the boot region and in the positive X direction.

The velocity vector maps for the boot region of the flow field iterations 1600 to 2000 are shown in Figs. 59 through 63. In these figures the solution is not changing greatly. The mass flux is generally into the region through the left side boundary and the path for the mass to exit the region has not been clearly established. By iteration 2000 the solution for the boot region has not reached steady state. Perhaps by utilizing a boundary condition at the left side of this region which allows mass input along the bottom and mass output along the top of the boundary would allow the boot region solution to relax to steady state.

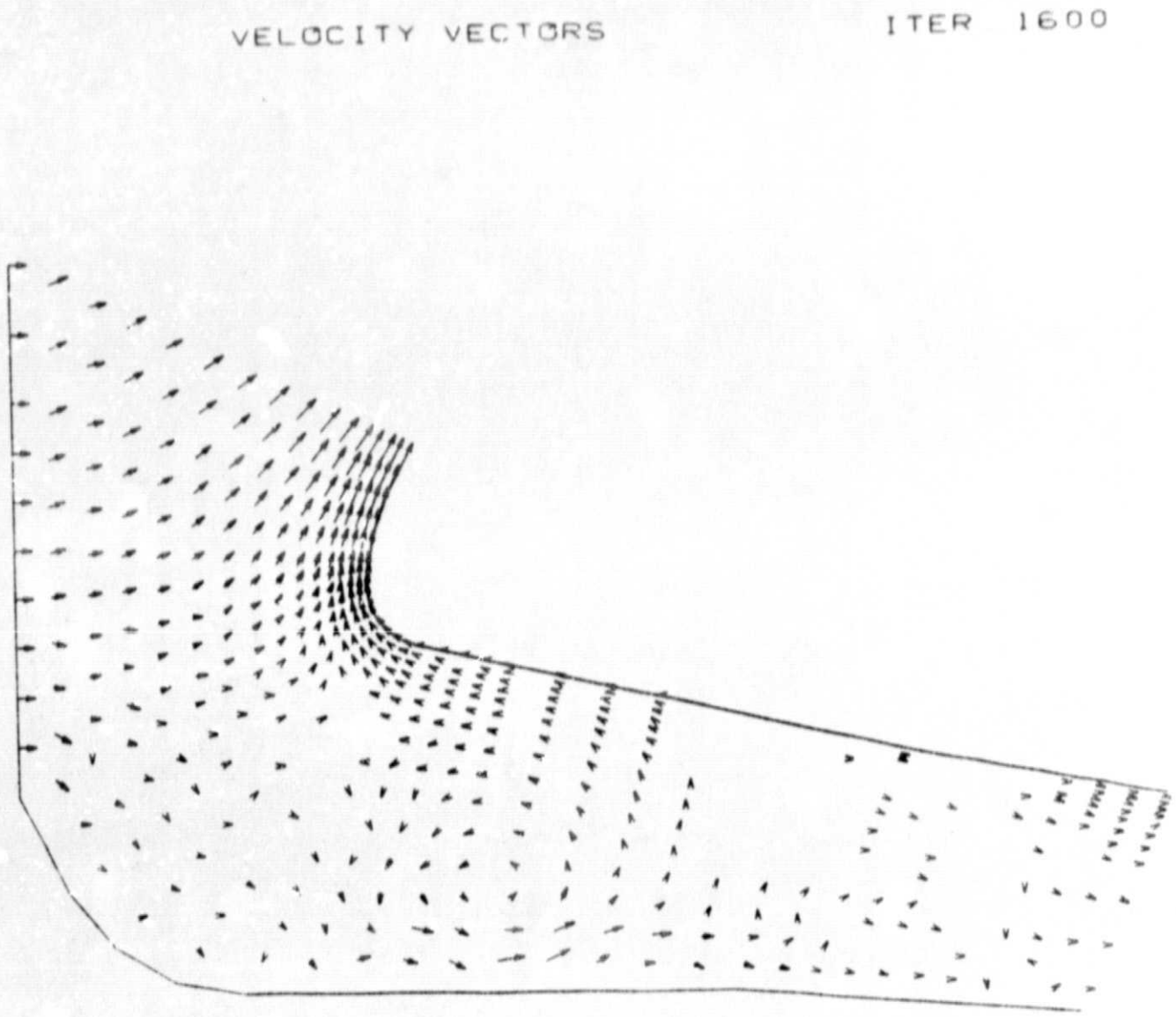

Fig. 54 - SRM Aft Closure Gasdynamic Analysis, Velocity Vector Map, Nose Underside Region (Iteration 1600)

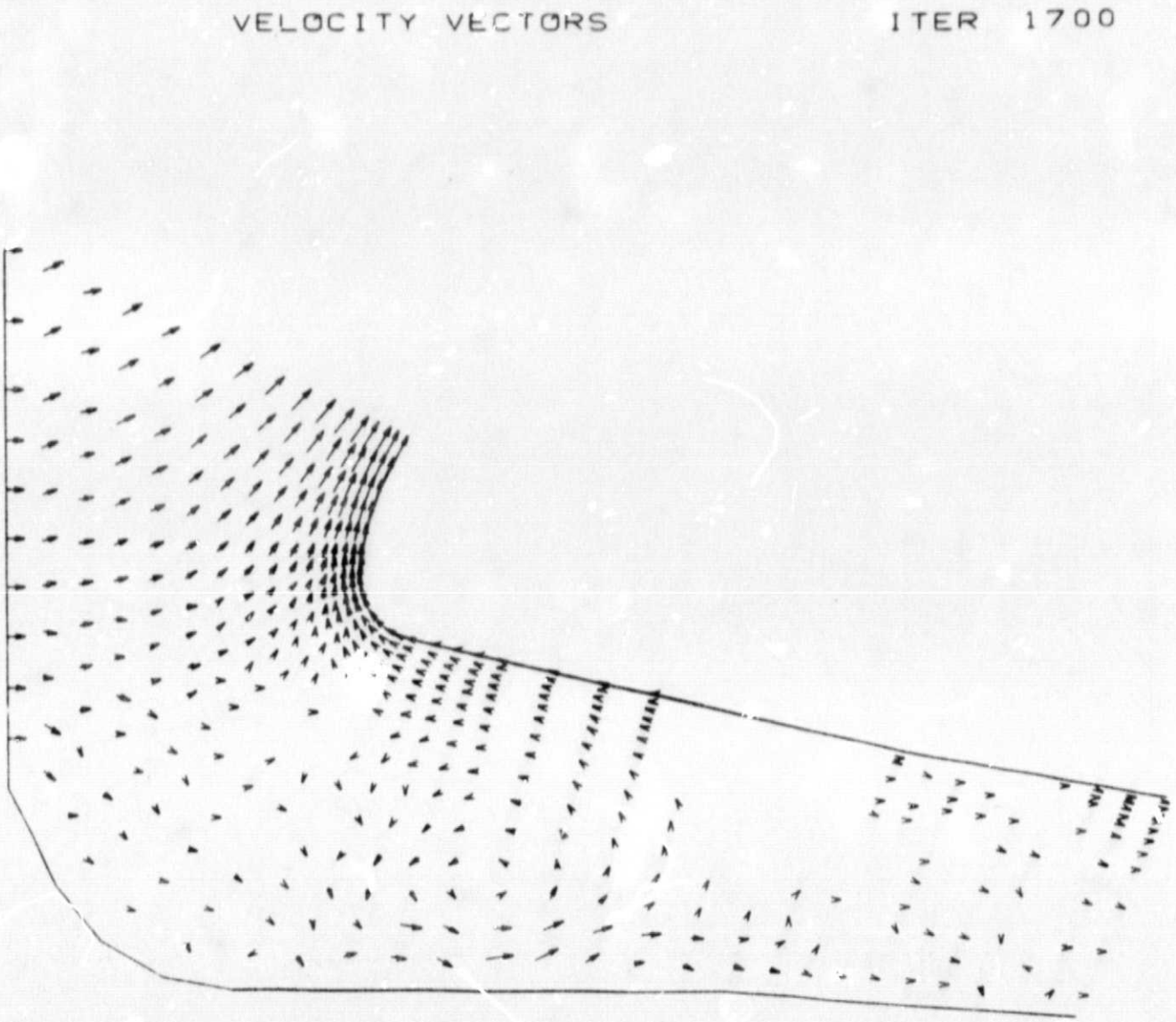

Fig. 55 - SRM Aft Closure Gasdynamic Analysis, Velocity Vector Map, Nose Underside Region (Iteration 1700)

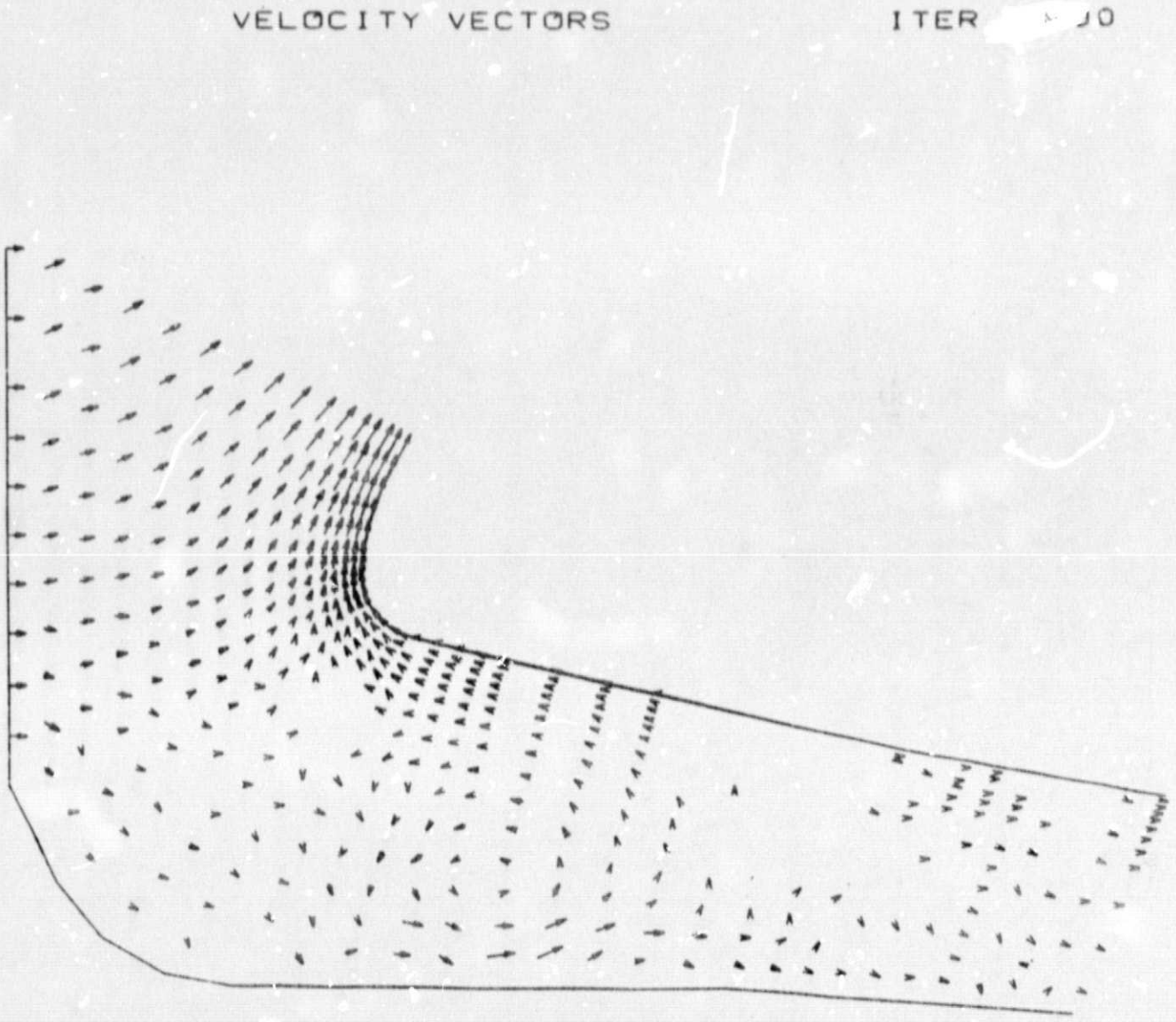

Fig. 56 - SRM Aft Closure Gasdynamic Analysis, Velocity Vector Map, Nose Underside Region (Iteration 1800)

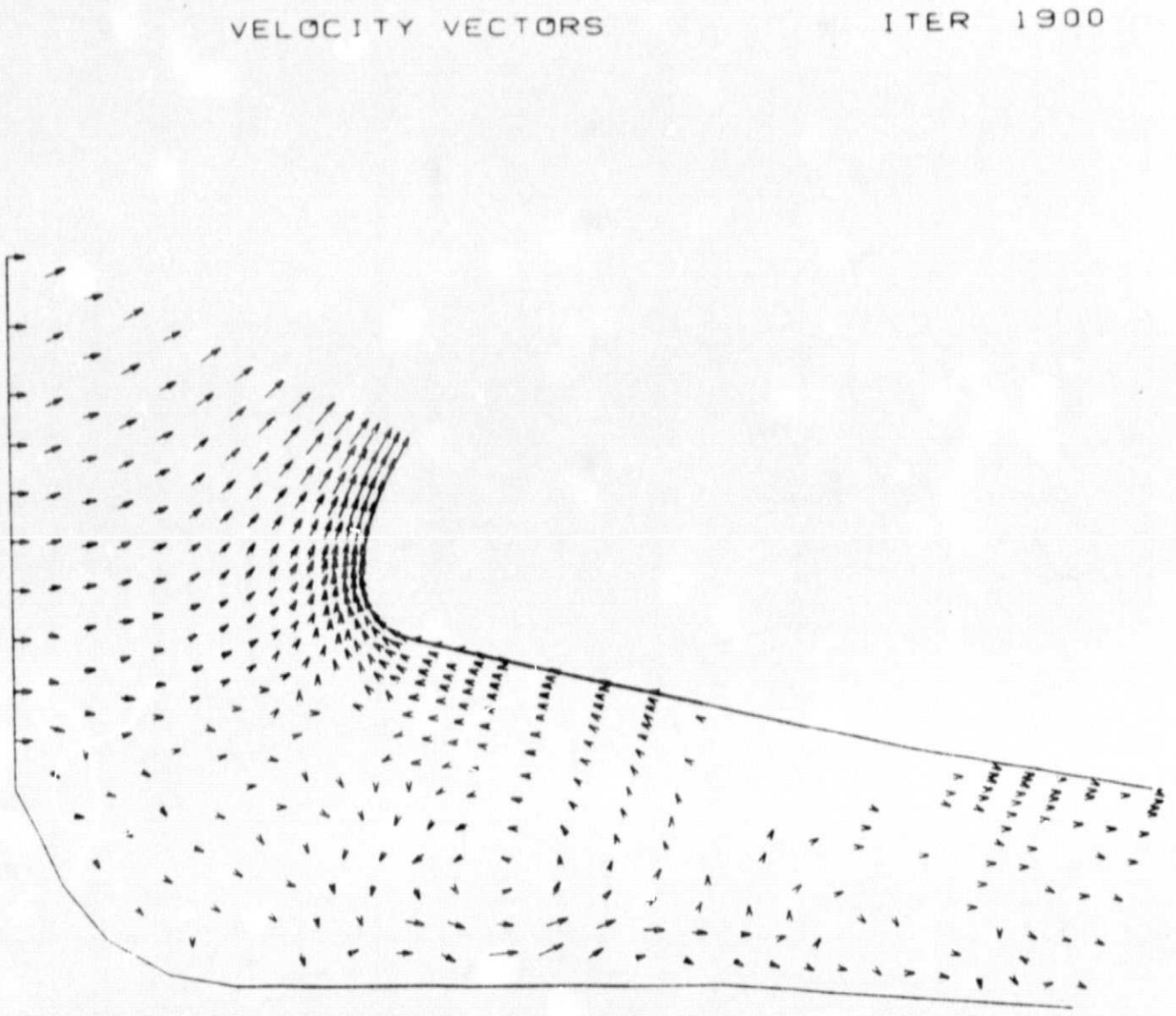

Fig. 57 - SRM Aft Closure Gasdynamic Analysis, Velocity Vector Map, Nose Underside Region (Iteration 1900)

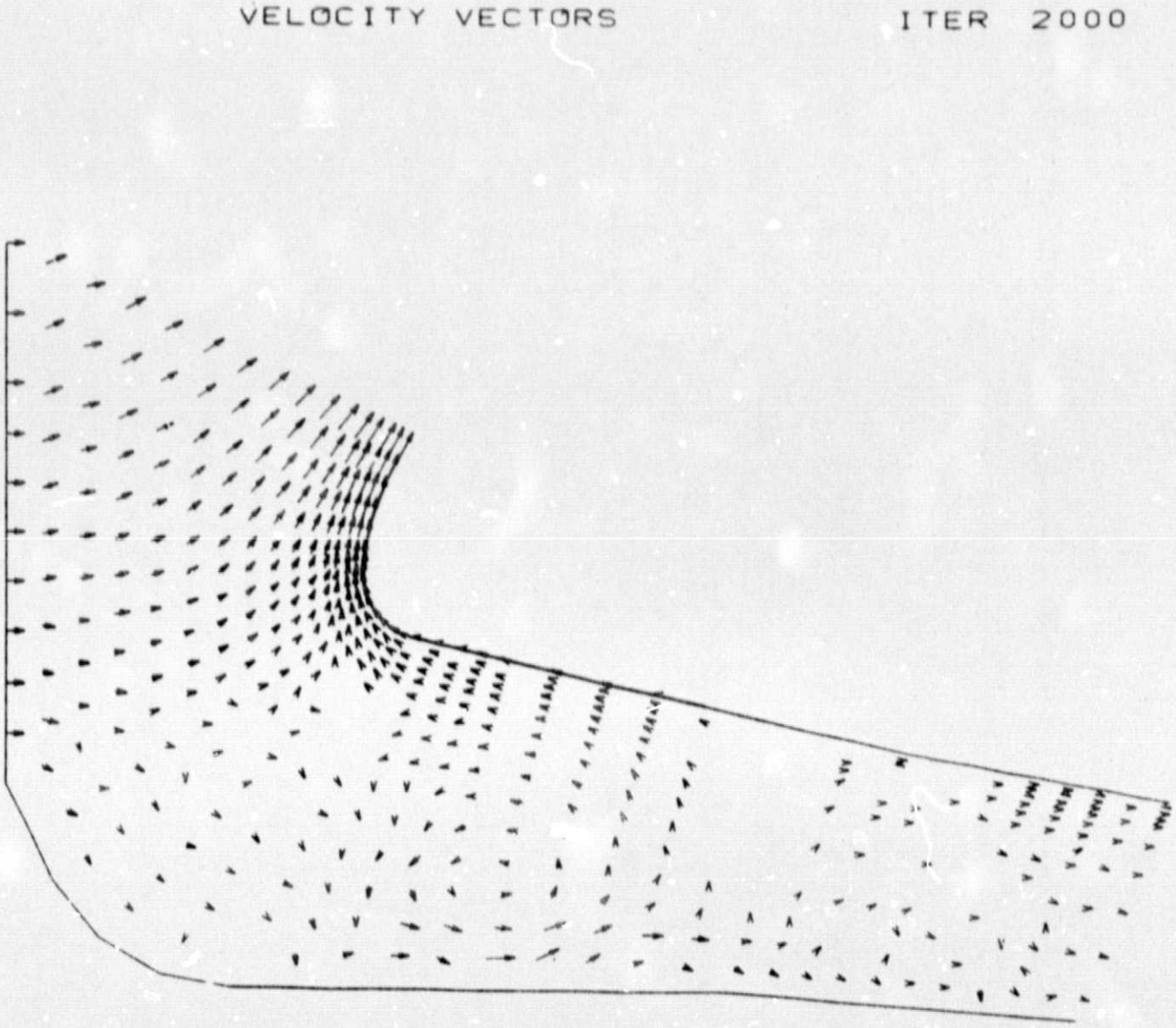

Fig. 58 - SKM Aft Closure Gasdynamic Analysis, Velocity Vector Map, Nose Underside Region (Iteration 2000)

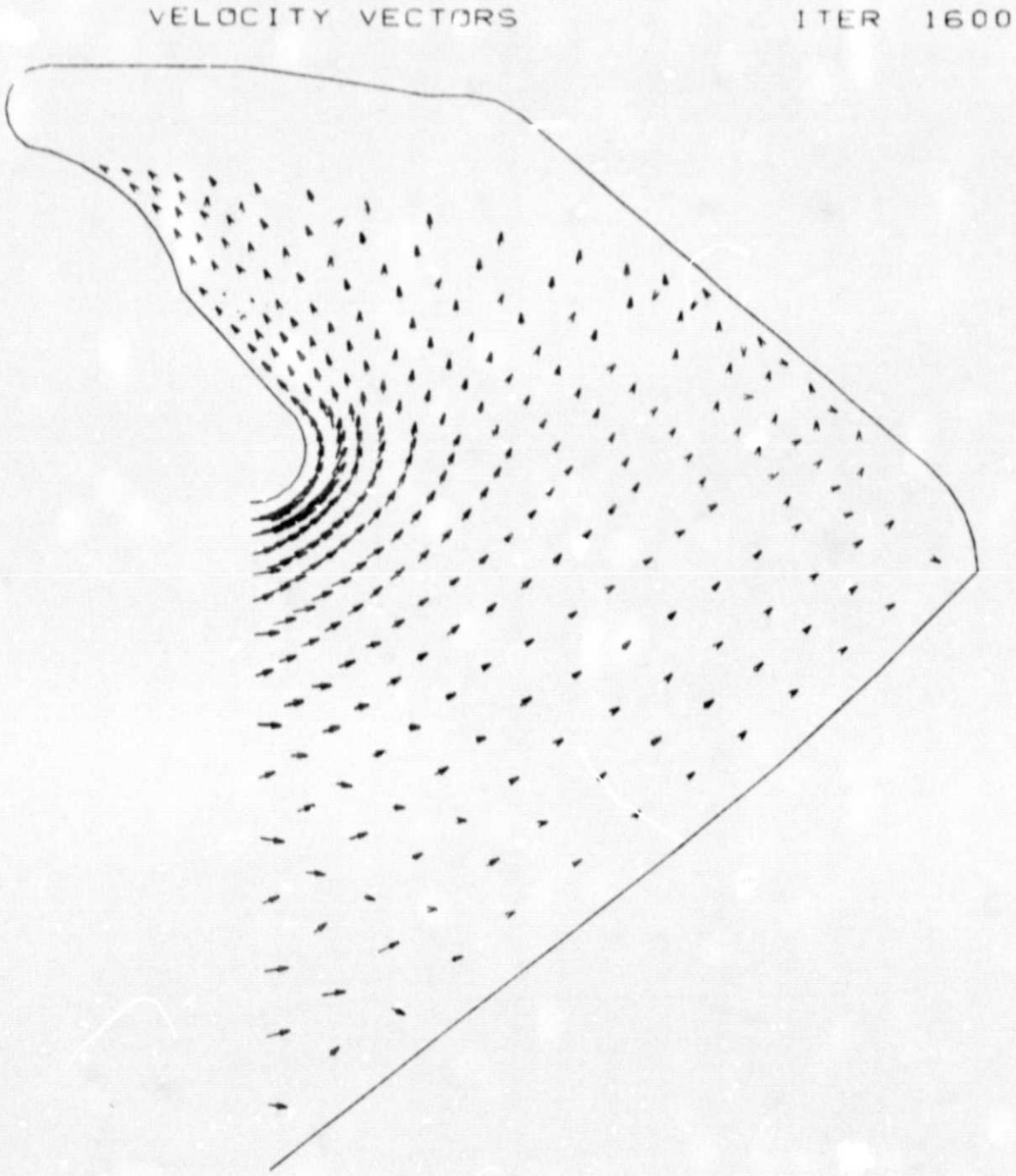

Fig. 59 - SRM Aft Closure Gasdynamic Analysis, Velocity Vector Map, Boot Region (Iteration 1600)

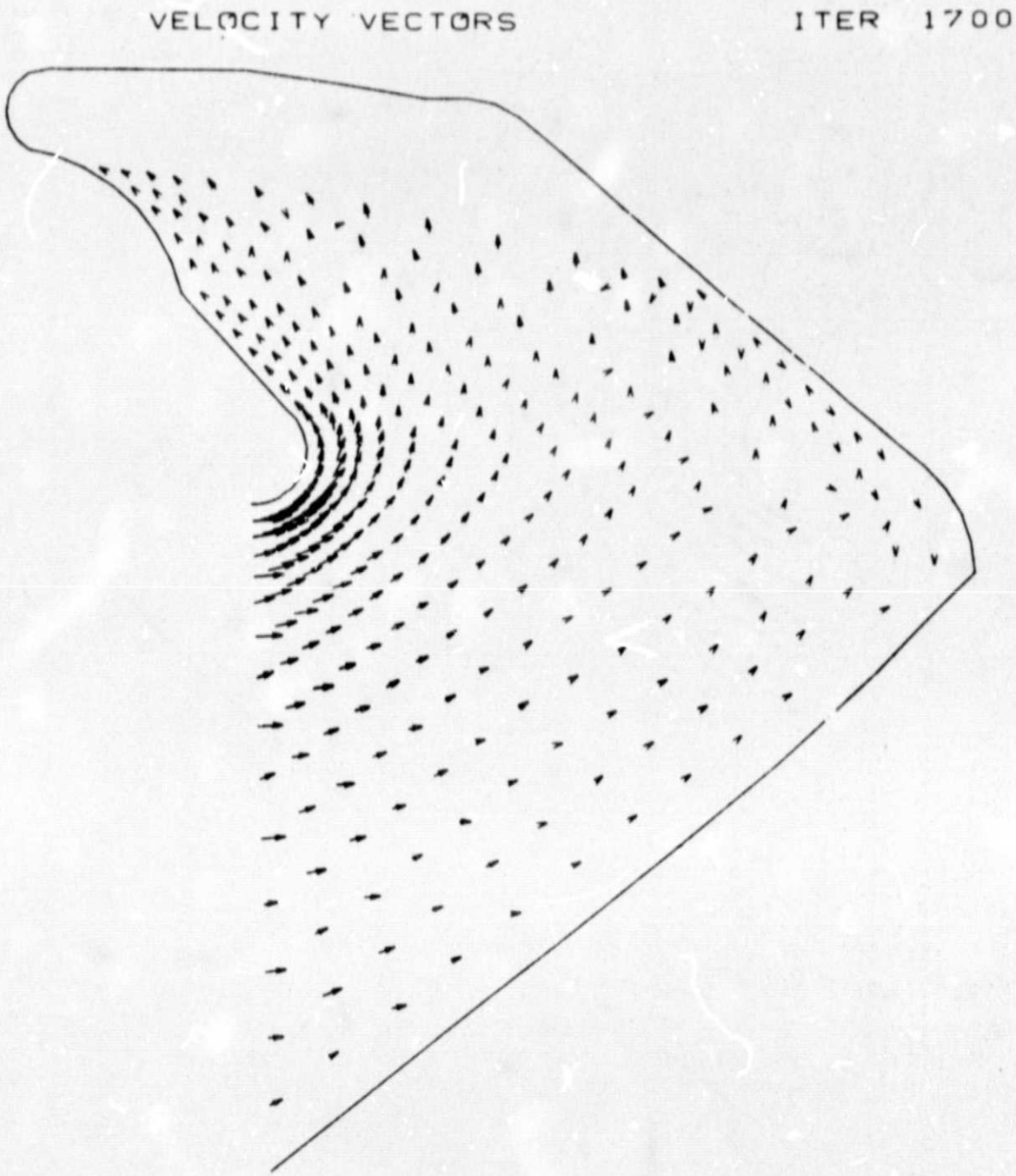

Fig. 60 - SRM Aft Closure Gasdynamic Analysis, Velocity Vector Map, Boot Region (Iteration 1700)

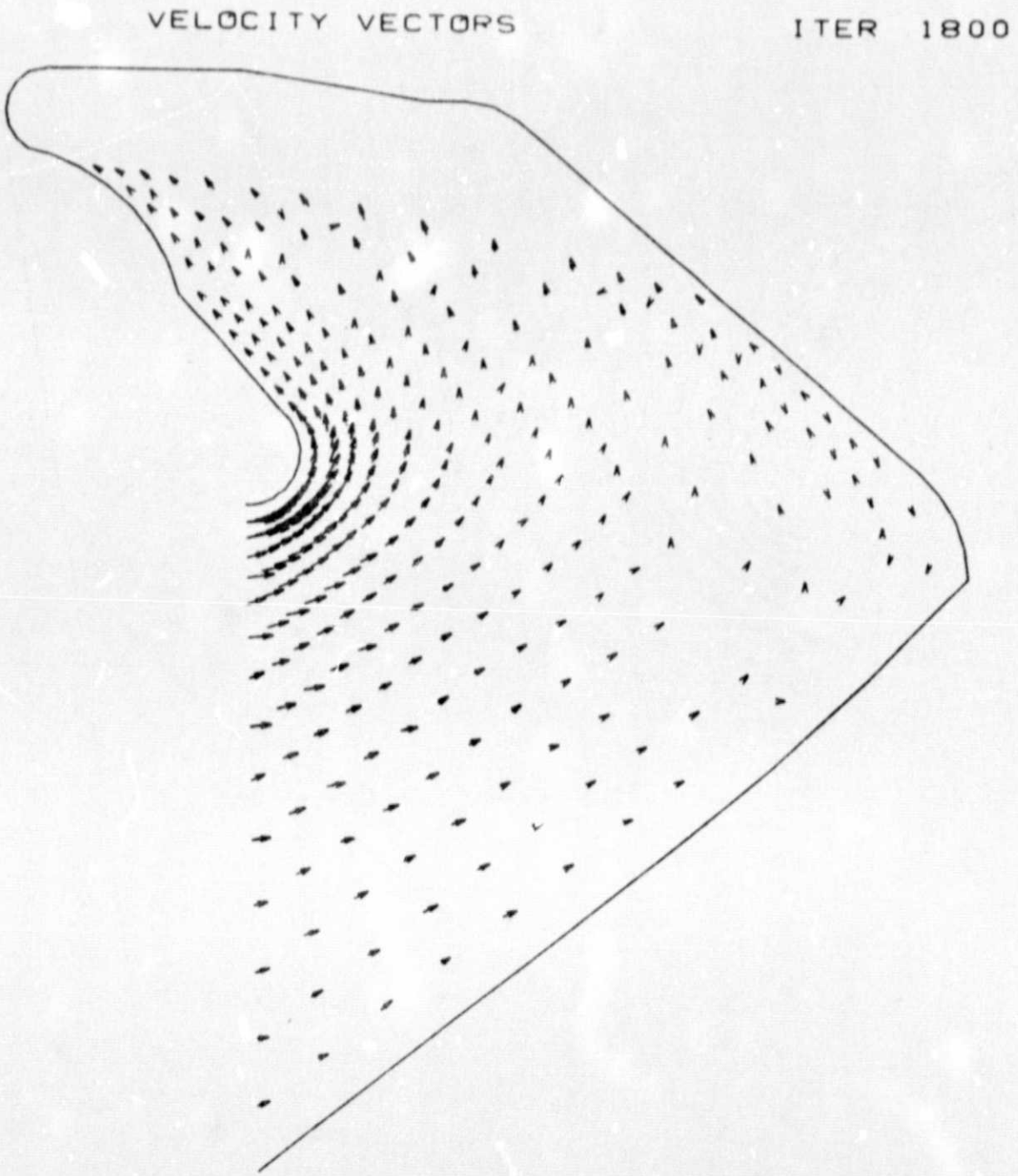

Fig. 61 - SRM Aft Closure Gasdynamic Analysis, Velocity Vector Map, Boot Region (Iteration 1800)

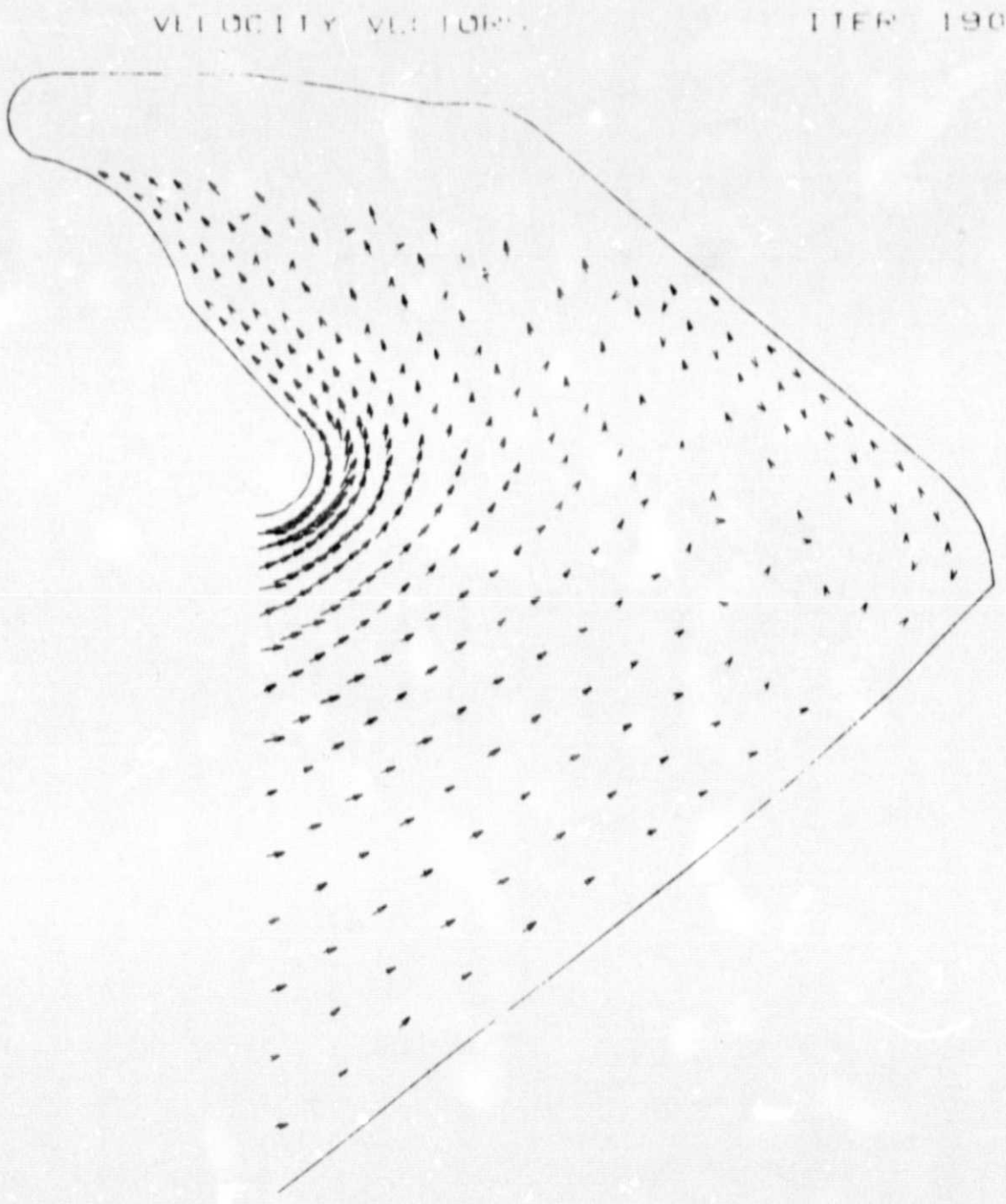

Fig. 62 - SRM Aft Closure Gasdynamic Analysis, Velocity Vector Map, Boot Region (Iteration 1900)

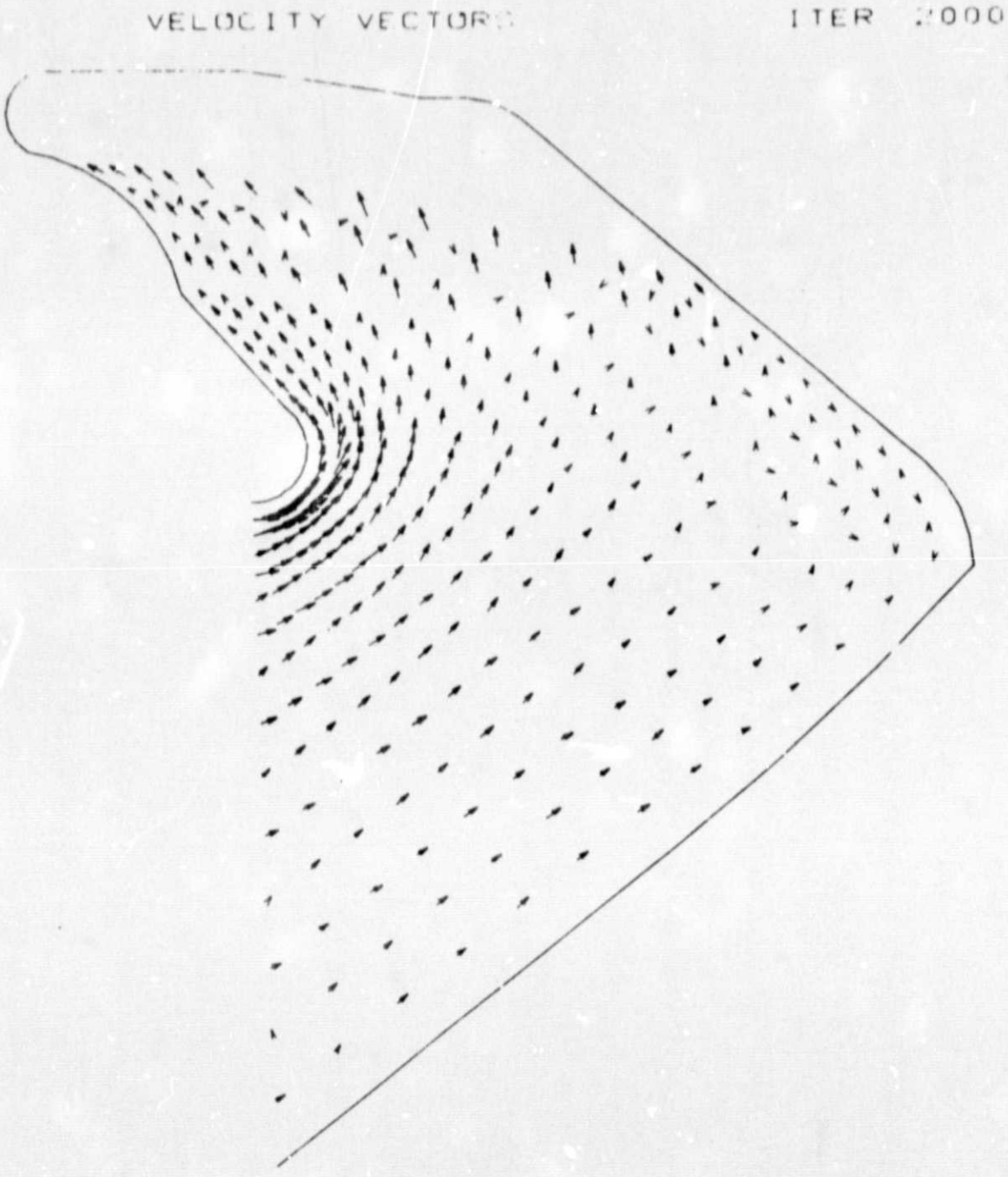

Fig. 63 - SRM Aft Closure Gasdynamic Analysis, Velocity Vector Map, Boot Region (Iteration 2000)

Chapter 3. SRM AFT CLOSURE GASDYNAMIC ANALYSIS CONCLUSIONS AND RECOMMENDATIONS

I. CONCLUSIONS

A two-dimensional axisymmetric solid rocket motor submerged nozzle gasdynamic analysis capability has been developed and demonstrated. This perfect gas analysis technique is not limited by the geometrical complexity of the motor submerged nozzle, or nozzle radii of curvature ratios. The demonstration case, the SRM aft closure region, provides a rigorous test of the technique due to the complex geometry involved. In summary, a steady state solution for the SRM submerged nozzle nose region was obtained using an inviscid analysis in 800 iterations. This solution indicates the development of an area gas flow recirculation near the lower propellant burning surface boundary and in the region of the underside of the nozzle nose. This recirculation region remains spatially fixed for successive iterations (greater than 800) of the solution.

A steady state solution was not obtained for the most complex region (the boot, fixed housing, aft dome region) in 2000 iterations. Further analysis of this region is warranted. A solution for the region can probably be obtained by the correct choice of upstream boundary conditions, i.e., an upstream boundary condition that allows mass to both enter and exit the region.

A two-dimensional solid rocket motor submerged nozzle/aft closure gasdynamic analysis capability has been developed, demonstrated, and delivered to NASA-MSFC. The technique can provide the solid motor designer with gasdynamic environment analyses of the aft closure region which are otherwise unobtainable. Further work on the technique is justified and the steps leading to a comprehensive solid motor aft closure gasdynamic analysis are described below.

II. RECOMMENDATIONS

The two-dimensional, perfect gas solid motor submerged nozzle/aft closure gasdynamic analysis which has been developed can be extended to yield a comprehensive design and analysis analytical tool. The steps leading to such a tool are outlined below.

A. Three-Dimensional Perfect Gas Submerged Nozzle/Aft Closure Gasdynamic Analysis

The need for a three-dimensional analysis capability is obvious. A three-dimensional capability would provide assessment of the impact on the gasdynamic environment of nozzle gimbaling. This capability already exists as the current two-dimensional GIM analysis was derived from a fully three-dimensional GIM analysis. All that remains is to demonstrate a three-dimensional solution for an appropriate case, perhaps the Space Shuttle DM-2 SRM static firing where the nozzle gimbal cycle was more pronounced than on the DM-1 static firing.

B. Three-Dimensional Two-Phase Submerged Nozzle/Aft Closure Gasdynamic Analysis

The final step leading to a comprehensive submerged nozzle/aft closure gasdynamic analysis methodology is the development and inclusion into the analysis of a two-phase flow capability. The effect of particles on the gaseous flow field should be analytically determined. The expandable sets in the GIM formulation allow the inclusion of the required two-phase equations. This task is formidable but Lockheed-Huntsville has the experience to produce such a technique. We have previously developed a two-dimensional two-phase unsteady nozzle flowfield solution. The task is to add the two-phase equations to the three-dimensional perfect gas GIM technique.

REFERENCES

1. Freeman, J. A., "Engineering Analysis of Selected Advanced Propulsion Concepts — IV,, Volume II., Technical Report TK-CR-77-5, U.S. Army Missile Research and Development Command, Redstone Arsenal, Ala., August 1977.

2. Gordon, W. J., and C. A. Hall, "Construction of Curvilinear Coordinate Systems and Application to Mesh Generation," J. Numerical Math., Vol. 1, 1973, pp. 461-477.

3. Spradley, L. W., "The General Interpolants Method (GIM): A Procedure for Numerical Solution of the Partial Differential Equations Governing the Behavior of Continuous Media," LMSC-HREC TB D497112-A, Lockheed Missiles & Space Company, Huntsville, Ala., September 1977.

4. Shackelford, B. W., Jr., Informal communication, "NASA-MSFC Solid Motor Branch Space Shuttle DRM DM-1 Post-Test Static Firing Internal Ballistics Analysis, October 1977.